1-1-2014

Development of a Pressure Swing Adsorption Process for CO2 Capture from Flue Gas Using Solid Amine Sorbents

Anahita Abdollahi Govar
University of South Carolina - Columbia

DEVELOPMENT OF A PRESSURE SWING ADSORPTION PROCESS FOR CO_2 CAPTURE FROM FLUE GAS USING SOLID AMINE SORBENTS

by

Anahita Abdollahi Govar

Bachelor of Science
Sharif University of Technology, 2005

Master of Science
Sharif University of Technology, 2007

Submitted in Partial Fulfillment of the Requirements

For the Degree of Doctor of Philosophy in

Chemical Engineering

College of Engineering and Computing

University of South Carolina

2014

Accepted by:

James A. Ritter, Major Professor

Armin D. Ebner, Committee Member

Miao Yu, Committee Member

Jamil Khan, Committee Member

John Weidner, Committee Member

Lacy Ford, Vice Provost and Dean of Graduate Studies

DEDICATION

To my brilliant, loving and supportive husband Mohsen Nikkhoo

ACKNOWLEDGEMENTS

I want to express my deepest appreciation to my advisor Dr. James A. Ritter, for being a tremendous mentor for me. Without his guidance and encouragement this dissertation would have not been possible. I would particularly like to thank my second advisor Dr. Armin D. Ebner for his insightful comments and suggestions and teaching me the art of problem solving. Many thanks to my committee members, Dr. Miao Yu, Dr. Jamil Khan, and Dr. John Weidner for their time, and guidance.

I am grateful to Dr. Marjorie Nicholson for all her help in carrying out my experiments. I would also like to express my thanks to all my previous and present research group mates, Dr. Hai du, Dr. Amal Mehrotra, Dr. Jan Mangual, Dr. Shubhra Bhadra, Dr. Fan Wu, Mohammad Iftekhar Hossain, Atikur Rahman, Nima Mohammadi, Lutfi Erden and Hanife Erden.

I would like to offer my special thanks to my husband Mohsen Nikkhoo, for his unconditional love and endless support. I owe much gratitude to my hard working parents Aghdas Shariatmadar and Akbar Abdollahi Govar for all the sacrifices they made, their love and care. Special thanks also to my sister Armita Abdollahi Govar for being my best friend and always believing in me. I also want to extend special thanks to my in-laws, Nahid Ansari and Hassan Nikkhoo for their constant support and encouragement.

ABSTRACT

Solid amines are comprised of adsorbent materials, like silica gel, that contain amine based organic compounds, either physically or chemically, attached within their pores. The major characteristic of these sorbents that makes them interesting for CO_2 capture from flue gas is that unlike zeolites they are not negatively affected by the presence of water. The current work has been focusing on the development of a novel PSA cycle for CO_2 capture from flue gas using a solid-amine sorbent composed of PEI physically immobilized on a commercial silica substrate. The goal was to achieve > 90% recovery and > 95 vol. % purity of CO_2 at reasonable throughputs and operating cost.

A non-equilibrium kinetic model was developed to describe the reversible adsorption and desorption of CO_2 on this material over a wide range of industrial relevant conditions. Effect of water on adsorption and desorption of CO_2 was studied at various temperatures and pressures of CO_2 using TGA. Considering the adsorption of water on this particular material and utilizing the developed model for CO_2-solid amine, a series of simulations were carried out for two PSA cycles under different operating conditions for both dry and humid feeds.

In this dissertation the key results regarding the use of solid amines for post combustion CO_2 capture from flue gas by PSA are presented. The effects of different parameters on the performance of the PSA process in terms of recovery and purity of CO_2 and the required energy are discussed. The process conditions under which the separation goal is achievable are provided. The role of water in the PSA process

performance is explored. Finally two hypothetical sorbents are proposed. The use of these sorbents can improve the performance of the PSA process in terms of water recovery in the CO_2-enriched product.

TABLE OF CONTENTS

LIST OF TABLES

LIST OF FIGURES

LIST OF SYMBOLS

A	Area (m^2)
b^0_{1,H_2O}	Pre-exponential constant for temperature dependence of b_{1,H_2O} (kPa^{-1})
b^0_{1,N_2}	Pre-exponential constant for temperature dependence of b_{1,N_2} (kPa^{-1})
b^0_{2,H_2O}	Pre-exponential constant for temperature dependence of b_{2,H_2O} (kPa^{-1})
b^0_{2,N_2}	Pre-exponential constant for temperature dependence of b_{2,N_2} (kPa^{-1})
b_{1,H_2O}	Constant in Dual Process Langmuir isotherm for water (kPa^{-1})
b_{1,N_2}	Constant in Dual Process Langmuir isotherm for Nitrogen (kPa^{-1})
b_{2,H_2O}	Constant in Dual Process Langmuir isotherm for water (kPa^{-1})
b_{2,N_2}	Constant in Dual Process Langmuir isotherm for Nitrogen (kPa^{-1})
B_{1,H_2O}	Energy parameter in for adsorption of water on site 1, (K^{-1})
B_{1,N_2}	Energy parameter in for adsorption of Nitrogen on site 1 (K^{-1})
B_{2,H_2O}	Energy parameter in for adsorption of water on site 2 (K^{-1})
B_{2,N_2}	Energy parameter in for adsorption of Nitrogen on site 2 (K^{-1})
$Cp_{a,j}$	Adsorbed phase heat capacity of component j ($kJ.mol^{-1}.K^{-1}$)
Cp_g	Gas phase heat capacity ($kJ.mol^{-1}.K^{-1}$)
$Cp_{g,j}$	Gas phase heat capacity of component j ($kJ.mol^{-1}.K^{-1}$)
Cp_p	Pellet heat capacity ($kJ.mol^{-1}.K^{-1}$)

C_T Total molar concentration ($mol.m^{-3}$)

c_v Valve coefficient

$E_{k,f}$ Forward activation energy for the CO_2 chemisorption reaction k ($kJ.mol^{-1}$)

$E_{k,b}$ Backward activation energy for the CO_2 chemisorption reaction k ($kJ.mol^{-1}$)

E_{H,H_2O} Energy parameter in the Arrhenius equation for Henry's law constant for water (kPa^{-1})

F Molar flow rate through the valve

h_w Overall heat transfer coefficient ($kW.m^{-2}.K^{-1}$)

k Reaction number

K_{CO_2} Mass transfer coefficient of CO_2 (s^{-1})

$K_{k,e}$ Equilibrium constant for reaction k (kPa^{-1})

$K_{k,0}$ Pre-exponential constant for equilibrium constant of reaction k (kPa^{-1})

$K_{k,f}$ Forward reaction rate constant for reaction k ($kPa^{-1}.min^{-1}$)

$K_{k,b}$ Backward reaction rate constant for reaction k (min^{-1})

$K_{k,b,0}$ Pre-exponential constant for backward reaction k (min^{-1})

$K_{k,f,0}$ Pre-exponential constant for forward reaction k (min^{-1})

k_{H_2O} Mass transfer coefficient of water (s^{-1})

K_{H0,H_2O} Pre-exponential constant in the Arrhenius equation for Henry's law constant for water (kPa^{-1})

K_{H,H_2O} Henry's law constant for water (kPa^{-1})

k_{N_2} Mass transfer coefficient of Nitrogen (s^{-1})

K_p Constant (min^{-1})

K_q Constant ($kg.kPa.K^{-1}.mol^{-1}$)

$K_{k,b,0}$ Pre-exponential constant in Arrhenius eq. for $K_{k,b}$

$K_{k,f,0}$ Pre-exponential constant in Arrhenius eq. for $K_{k,b}$

$K_{1,e}$ Equilibrium constant for reaction between CO_2 and N_1

$K_{2,e}$ Equilibrium constant for reaction between CO_2 and N_2

$K_{3,e}$ Equilibrium constant for reaction between CO_2 and N_3

$K_{4,e}$ Equilibrium constant for reaction between CO_2 and N_4

$K_{5,e}$ Equilibrium constant for reaction between CO_2 and $q_{CO_2,4}$

$K_{1,b}$ Backward reaction rate constant for reaction of CO_2 and N_1 (min^{-1})

$K_{1,f}$ Forward reaction rate constant for reaction of CO_2 and N_1 ($kPa^{-1}.min^{-1}$)

$K_{2,b}$ Backward reaction rate constant for reaction of CO_2 and N_2 (min^{-1})

$K_{2,f}$ Forward reaction rate constant for reaction of CO_2 and N_2 ($kPa^{-1}.min^{-1}$)

$K_{3,b}$ Backward reaction rate constant for reaction of CO_2 and N_3 (min^{-1})

$K_{3,f}$ Forward reaction rate constant for reaction of CO_2 and N_3 ($kPa^{-1}.min^{-1}$)

$K_{4,b}$ Backward reaction rate constant for reaction of CO_2 and N_4 (min^{-1})

$K_{4,f}$ Forward reaction rate constant for reaction of CO_2 and N_4 ($kPa^{-1}.min^{-1}$)

$K_{5,b}$ Backward reaction rate constant for reaction of CO_2 and $q_{CO_2,4}$ (min^{-1})

$K_{5,f}$ Forward reaction rate constant for reaction of CO_2 and $q_{CO_2,4}$ ($kPa^{-1}.min^{-1}$)

L Length of the bed (m)

$M(t)$ Molar flow leaving the bed at time t

M_g Average molecular weight of the gas phase

N Number of components

N_{max} Maximum number of adsorption/reaction sites for CO_2 (mol/kg^{-1})

N_t Total number of adsorption/reaction sites for CO_2 (mol.kg^{-1})

N_1 Number of adsorption/reaction sites which react with CO_2 and form $q_{co_2,1}$ (mol.kg^{-1})

N_2 Number of adsorption/reaction sites which react with CO_2 and form $q_{co_2,2}$ (mol.kg^{-1})

N_3 Number of adsorption/reaction sites which react with CO_2 and form $q_{co_2,3}$ (mol.kg^{-1})

N_4 Number of adsorption/reaction sites which react with CO_2 and form $q_{co_2,4}$ (mol.kg^{-1})

P Pressure (kPa)

P_o Pressure outside the valve (kPa)

P_{CO_2} Partial pressure of CO_2 in the feed gas (kPa)

$P^*_{CO_2}$ Partial pressure of CO_2 in the gas that is in contact with the adsorbent (kPa)

$q_{CO_2,1,e}$ Sites taken from N_1 by CO_2 at equilibrium (mol.kg^{-1})

$q_{CO_2,1}$ Sites taken from N_1 by CO_2 at time t (mol.kg^{-1})

$q_{CO_2,2,e}$ Sites taken from N_2 by CO_2 at equilibrium (mol.kg^{-1})

$q_{CO_2,2}$ Sites taken from N_2 by CO_2 at time t (mol.kg^{-1})

$q_{CO_2 3,e}$ Sites taken from N_3 by CO_2 at equilibrium (mol.kg^{-1})

$q_{CO_2,3}$ Sites taken from N_3 by CO_2 at time t (mol.kg^{-1})

$q_{CO_2,4,e}$ Sites taken from N_4 by CO_2 at 2 at equilibrium (mol.kg^{-1})

$q_{CO_2,4}$ Sites taken from N_4 by CO_2 at time t (mol.kg^{-1})

$q_{CO_2,5,e}$ Sites taken from N_4 by two CO_2s at equilibrium (mol.kg^{-1})

$q_{CO_2,5}$ Sites taken from N_4 by two CO_2s at time t (mol.kg^{-1})

$q_{CO_2,t,e}$ Total CO_2 loading at equilibrium (mol.kg^{-1})

$\bar{q}_{\exp}$ Mean of experimental CO_2 loading over four cycles (mol.kg^{-1})

$q^*_{H_2O}$ Equilibrium adsorbed amount of water (mol.kg^{-1})

q_{H_2O} Loading on water at time t (mol.kg^{-1})

$q_{i,\exp}$ Experimental value for CO_2 loading at time t (mol.kg^{-1})

$q_{i,\mathrm{mod}}$ Model value for CO_2 loading (mol.kg^{-1})

$q^*_{N_2}$ Equilibrium adsorbed amount of Nitrogen (mol.kg^{-1})

q_{N_2} Loading on Nitrogen at time t (mol.kg^{-1})

q^s_{1,H_2O} Maximum possible adsorbed amount of water on site 1 (mol.kg^{-1})

q^s_{2,H_2O} Maximum possible adsorbed amount of water on site 2 (mol.kg^{-1})

q^s_{1,N_2} Maximum possible adsorbed amount of Nitrogen on site 1 (mol.kg^{-1})

q^s_{2,N_2} Maximum possible adsorbed amount of Nitrogen on site 2 (mol.kg^{-1})

R Universal gas constant (J.mol^{-1}.K^{-1})

R^2 Coefficient of determination

$r_{b,i}$ Internal radius of the bed (m)

r_p Radius of the pellet (m)

s Number of energy consuming steps

S_g Specific gravity of the gas relative to air at 1 atm and 21.45°C

t Time

T Temperature (K)

T_o Ambient temperature (K)

T_{FD} Constant in Fermi-Dirac distribution (K)

V Volume of the TGA chamber (m^3)

V_s Adsorbent volume (m^3)

y_i Mole fraction of component *i*

z Column position (m)

α Fraction of total reaction sites that belongs to N_1

β Fraction of total reaction sites that belongs to N_2

κ Fraction of total reaction sites that belongs to N_3

η Fraction of total reaction sites that belongs to N_4

μ_g Gas phase viscosity (Pa.s)

ε_b Bed porosity

ε_p Particle porosity

k_α Constant in Fermi-Dirac distribution

k_α Constant in Fermi-Dirac distribution used for temperature dependency of N_t

$\rho_{a,i}$ Density of adsorbed phase of component *i* ($kg.m^{-3}$)

ρ_p Density of the particle ($kg.m^{-3}$)

ρ_s Adsorbent density ($kg.m^{-3}$)

$\Delta H_{CO_2,k}$ Effective heat of adsorption/reaction for reaction k ($kJ.mol^{-1}$)

ΔH_i Effective heat of adsorption/reaction for component i ($kJ.mol^{-1}$)

δ Efficiency of compressor

ω Fraction of gas stream leaving the bed during the feed step light reflux that is recycled to the bed undergoing the light reflux step

λ Fraction of gas stream leaving the bed during the light reflux step that is recycled to the bed undergoing the heavy reflux step.

LIST OF ABBREVIATIONS

CBSA ..... Carbon-Based Solid Amine

CGSA ..... CARiACT G10 Solid Amine

CMB ..... Component Mass Balance

CnD ..... Counter- Current Depressurization

CoD ..... Co-Current Depressurization

EB ..... Energy Balance

Eq ..... Equalization-down

Eq' ..... Equalization-up

HCBSA ..... Hydrophobic Carbon-Based Solid Amine

HR ..... Heavy Reflux

KM ..... Kinetic Model

LDFE ..... Linear Driving Force Equation

LPP ..... Light Product Pressurization

LR ..... Light Reflux

OMB ..... Overall Mass Balance

PSA ..... Pressure Swing Adsorption

TGA ..... Thermogravimetric Analyzer

VE. ..... Valve Equation

CHAPTER 1

SEMI-EMPIRICAL KINETIC MODEL THAT DESCRIBES THE REVERSIBLE ADSORPTION AND DESORPTION OF CO_2 IN A SOLID AMINE SORBENT

1.1 Summary

Five semi-empirical, temperature-dependent kinetic models were studied to describe the reversible adsorption of CO_2 in a solid amine sorbent composed of poly (ethyleneimine) immobilized in to a CARiACT® G10 support at 28 conditions; four temperatures (40, 60, 80 and 100°C) and eight concentrations of CO_2 (1.2, 4.8, 14.5, 32.8, 56.1, 69.8, and 88.6 vol. % in Nitrogen). At each condition experimental data was obtained for 4 cycles of 40 minutes adsorption followed by 40 minutes desorption using thermogravimetric analyzer. Model parameters were determined by fitting the first two cycles at 20 conditions; 1.2, 4.8, 14.5, 56.1, and 88.6 vol. % in Nitrogen at all temperatures. The following cycles (3^{rd} and 4^{th} cycles) and also the cycling data at other eight conditions were then predicted using the same parameters, to evaluate interpolation and extrapolation capabilities of each model. The goodness of fit of models was then compared based on their predicted results for all four cycles considering all the 28 conditions. The model which best represented the kinetic was consisted of three parallel reactions. It also gave a good fit for the periodic state working capacities and the equilibrium loadings at higher temperatures. Considering the wide range of conditions, there was a very good agreement between the model results and experimental data.

Therefore this model can be used in dynamic adsorption process simulator to investigate the performance of a PSA process using this sorbent for CO_2 capture from flue gas.

1.2 Introduction

Carbon dioxide is one of the primary greenhouse gases existing in the atmosphere. Increasing amounts of these gases because of human activities have led to global warming in recent years which will result in changes in climate like longer and stronger heat waves, reduced snowpack, increased evaporation, and other changes which will affect human and wildlife health.[1] Fossil fuel power plants are a major source for CO_2 emissions. Capturing CO_2 from the flue gas before releasing it to the atmosphere is an option that is being considered in order to reduce the CO_2 amount that is emitted by these plants.

One promising technology for separating the CO_2 from flue gas is pressure swing adsorption (PSA). An appropriate sorbent is an essential part of an efficient PSA process. When it comes to capturing CO_2 from flue gas, specific characteristics of the adsorbent should be taken into account; having a good working capacity for CO_2 and being water tolerant. Several sorbents have been studied for CO_2 capture like zeolites Y and 13X, and activated carbon at ambient temperature and HTLcs at high temperatures (302°C).[2] Another group of sorbents that are being considered for post combustion CO_2 capture are solid amine sorbents that have been reported to have adequate working capacity for CO_2 even in the presence of water.[3-37] In these sorbents amine functional groups are chemically attached or physically immobilized on the surface of a porous support like silica.[3] The main characteristic of these sorbents is that unlike zeolites 13X which is the

mostly used sorbent for CO_2 capture, the adsorption of CO_2 in these sorbents is not negatively affected by the presence of water.[3] Suitability of solid amine sorbents for CO_2 capture from flue gas by pressure swing adsorption (PSA) has been studied by Ebner et al.[3] and Belmakhout and Sayari[4]. Yet the performance of a PSA process using these sorbents have not been reported in the literature. In order to simulate and study the performance of the PSA process with solid amines, a kinetic model which can describe the reversible adsorption and desorption of CO_2 in these sorbents is needed.

Reaction between CO_2 and liquid alkanolamines have been extensively studied.[38] Three mechanisms have been provided to describe CO_2-Alkanolamine reactions; zwitterian, termolecular and base catalyzed mechanisms; zwitterion has been mostly used for reaction with primary, secondary and sterically hindered amines whereas base-catalyzed hydration of CO_2 has been used for reaction with tertiary amines.[38] However none of these reactions have been used to model the kinetics of adsorption and desorption of CO_2 in a solid amine sorbent.

Yousef Belmabkhout and Abdelhamid Sayyari used linear driving force (LDF) to fit the adsorption of CO_2 on a series of amine modified silica sorbents.[5, 6] Still they only studied the kinetics of adsorption and they did not provide any data or model on desorption. Rodrigo Serna-Guerrero et al. proposed an equilibrium model to describe the CO_2 adsorption isotherms on amine-grafted mesoporous silica.[7] In their model adsorption of CO_2 was occurred through two independent mechanisms: 1. chemisorption on amine functional groups and 2. physisorption on the surface of the adsorbent. Subsequently the total equilibrium loading was sum of the equilibrium physisorbed loading and the equilibrium chemisorbed loading. Each loading was represented by using Toth model.

This equilibrium model was then used in another work by their group where they used a series of Lagergen's pseudo-first and pseudo-second order and Avrami kinetic models to model adsorption of CO_2 on amine functionalized mesoporous silica.[8] Then again no data related to desorption kinetics was provided. Ebner et al. provided a reversible mechanism for the kinetic of chemisorption and developed a Langmuir-type expression for equilibrium loading of CO_2 on CARiACT® G10 solid amine[3] but no kinetic data fitting was shown.

To our knowledge a mechanism that clearly describes the reversible adsorption and desorption of CO_2 on solid amines is lacking. Therefore the aim of this study was to develop a kinetic model which could predict the adsorption and desorption of CO_2 in a solid amine, composed of poly (ethyleneimine) (PEI) supported on a commercial silica substrate. This sorbent has been reported by Ebner et al.[3] to be suitable to be used in a PSA process to capture CO_2. Starting from a one site-one reaction model, five models were studied in order to describe the adsorption and desorption of CO_2 on this material at 28 conditions. These models included various combinations of reactions taking place in parallel and/or in series with each other. Also an empirical equation has been utilized to capture the particular temperature dependency of the kinetics caused by rheological changes of the PEI in this material with temperature. The kinetic model developed here can be used in a dynamic adsorption process simulator to study the performance of a PSA process.

1.3 Experimental

The solid amine used here is comprised of 40 wt. % polyethylenimine physically immobilized on a silica support. Details of the method are given elsewhere.[3, 9, 10, 11] The adsorption and desorption of CO_2 at various industrial relevant conditions was measured using a Perkin Elmer TGA-7 thermogravimetric. Every experimental run was consisted of 80 minutes activation of around 20 mg of the sorbent in pure Nitrogen (UHP Grade, Airgas) at 100°C and 4 cycles of adsorption of CO_2 (Coleman Grade, Airgas) mixture followed by desorption in pure Nitrogen, each for 40 minutes. The adjustment of temperature from 100°C to the desired temperature was carried out using a 20°C/min ramp. The gas flow was set to 60 (cm^3/min) at 1 atm. Experiments were carried out for CO_2 concentrations from 1 to 88.9 vol. % and temperatures from 40 to 100°C. The experimental setup and the details of the method is thoroughly explained by Ebner et al.[3]

1.4 Kinetic Model Development

Five models were studied to predict the reversible adsorption of CO_2 in CARiACT® G10 solid amine sorbent. Models studied in this work are consisted of different combinations of reactions shown below.

$$1) P_{CO_2} + N_1 \leftrightarrow q_{CO_2,1}$$

$$2) P_{CO_2} + N_2 \leftrightarrow q_{CO_2,2}$$

$$3) P_{CO_2} + N_3 \leftrightarrow q_{CO_2,3}$$

$$4) P_{CO_2} + N_4 \leftrightarrow q_{CO_2,4} + P_{CO_2} \leftrightarrow q_{CO_2,5}$$

In these reactions, P_{CO_2} is the partial pressure of CO_2, N_1-N_4 are different adsorption/reaction sites in the sorbent. $q_{CO_2,1}$, $q_{CO_2,2}$, and $q_{CO_2,3}$ are the reaction sites taken by CO_2 from N_1, N_2, and N_3 respectively.. $q_{CO_2,4}$ represents the reaction sites taken from N_4 with one CO_2 per site, while $q_{CO_2,5}$ shows the reaction sites taken from N_4 with two CO_2s per site.

Table 1.1 shows the reactions present in each model. There is only one type of reaction site in model I (N_1). Each reaction site reacts with one CO_2. In model II, there are two types of reaction sites (N_1 and N_2) that react with CO_2 via two parallel reactions. In model III, there are three types of reaction sites (N_1, N_2 and N_3) that react with CO_2 through three parallel reactions. Model IV is consisted of two reactions in series with one type of reaction site (N_4). Each reaction site can take two CO_2s. A mechanism similar to model IV has been provided by Planas et al., for adsorption of CO_2 in an alkylamine-functionalized metal-organic framework.[39] In their proposed mechanism, two amine sites adsorb two CO_2s, but this happens in a series of reactions. Although in their mechanism, each reaction sites, takes only one CO_2, the second CO_2 reacts with the amine sites only after the first one has been adsorbed. Two types of reaction sites (N_1 and N_4) are present in model V; one adsorbs one CO_2 per site, the other adsorbs two CO_2s per site. Reactions of CO_2 with these two types are in parallel. Equations describing the above reactions are shown in equations 1-10. Equation 11 which is a form of Fermi-Dirac distribution was used to explain the temperature dependency of the amine sites.

$$\frac{dq_{CO_2,1}}{dt} = K_{1,f} P_{CO_2}, (N_1 - q_{CO_2,1}) - k_{1,b} q_{CO_2,1} \quad (1)$$

$$\frac{dq_{CO_2,2}}{dt} = K_{2,f} P_{CO_2} (N_2 - q_{CO_2,2}) - k_{2,b} q_{CO_2,2} \quad (2)$$

$$\frac{dq_{CO_2,3}}{dt} = K_{3,f} P_{CO_2} (N_3 - q_{CO_2,3}) - k_{3,b} q_{CO_2,3} \quad (3)$$

$$\frac{dq_{CO_2,4}}{dt} = K_{4,f} P_{CO_2} (N_4 - q_{CO_2,4} - q_{CO_2,5}) - k_{5,b} q_{CO_2,5} - \frac{dq_{CO_2,5}}{dt} \quad (4)$$

$$\frac{dq_{CO_2,5}}{dt} = K_{5,f} q_{CO_2,4} P_{CO_2} - k_{5,b} q_{CO_2,5} \quad (5)$$

$$q_{CO_2,1} + q_{CO_2,2} + q_{CO_2,3} + q_{CO_2,4} + 2q_{CO_2,5} = q_{CO_2,t} \quad (6)$$

$$N_1 = \alpha N_t \quad (7)$$

$$N_2 = \beta N_t \quad (8)$$

$$N_3 = \kappa N_t \quad (9)$$

$$N_4 = \eta N_t = (1 - \alpha - \beta - \kappa) N_t \quad (10)$$

$$N_t = \frac{N_{\max}}{1 + \exp(-k_\alpha (T - T_{FD}))} \quad (11)$$

In equations 1-11, $K_{1,f}$, $K_{2,f}$, $K_{3,f}$, $K_{4,f}$, and $K_{5,f}$ are forward reaction constants and $K_{1,b}$, $K_{2,b}$, $K_{3,b}$, $K_{4,b}$, and $K_{5,b}$ are backward reaction constants for formation of q_1, q_2, q_3, q_4, and q_5, respectively. q_t is the total CO_2 loading. α, β, γ and η show the fractions of N_t that belong to N_1, N_2, N_3, and N_4 respectively. These fractions were assumed to be constant. N_{max}, k_α and T_0 are constants in Fermi-Dirac equation. The amines in the solid amine studied here, is a mixture of linear and branched primary, secondary and tertiary

amines.[3, 11] The fact that different amine types are present in the sorbent and also the way that each amine group is located on the support may result in different adsorption/reaction sites in the sorbent. Models II to V were studied in order to count for these different sites if exist. Moreover the flexibility of PEI changes with temperature, which leads to the changes in the accessibility of the amine sites for CO_2 with temperature.[12, 13] Since PEI is more flexible at higher temperatures, more amines are available for CO_2 to react with, whereas at lower temperatures, some may become unavailable due to the rigidity of the PEI. To capture the possible morphological changes with temperature, equation 11 was considered; it was assumed that the number of each kind of reaction sites, which could participate in the chemisorption of CO_2, was a function of temperature.

Temperature dependence of reaction constants was expressed by Arrhenius equation:

$$K_{k,f} = K_{k,f,0} \exp(\frac{-E_{k,f}}{RT}) ; k = 1, 2, 3, 4, 5 \quad (12)$$

$$K_{k,b} = K_{k,b,0} \exp(\frac{-E_{k,b}}{RT}) ; k = 1, 2, 3, 4, 5 \quad (13)$$

At equilibrium the forward reaction rate is equal to the backward reaction rate and we have:

$$\frac{dq_{CO_2,1}}{dt} = \frac{dq_{CO_2,2}}{dt} = \frac{dq_{CO_2,3}}{dt} = \frac{dq_{CO_2,4}}{dt} = \frac{dq_{CO_2,5}}{dt} = 0 \quad (14)$$

Equilibrium loadings and heat of reactions are shown in equations 15-23.

$$q_{CO_2,1,e} = \frac{K_{1,e} P_{CO_2} N_1}{1 + K_{1,e} P_{CO_2}} \quad (15)$$

$$q_{CO_2,2,e} = \frac{K_{2,e} P_{CO_2} N_2}{1 + K_{2,e} P_{CO_2}} \tag{16}$$

$$q_{CO_2 3,e} = \frac{K_{3,e} P_{CO_2} N_3}{1 + K_{3,e} P_{CO_2}} \tag{17}$$

$$q_{CO_2,4,e} = \frac{K_{4,e} P_{CO_2} N_4}{1 + K_{4,e} P_{CO_2} + K_{5,e} K_{4,e} P_{CO_2}^2} \tag{18}$$

$$q_{CO_2,5,e} = \frac{K_{5,e} K_{4,e} P_{CO_2}^2 N_4}{1 + K_{4,e} P_{CO_2} + K_{5,e} K_{4,e} P_{CO_2}^2} \tag{19}$$

$$q_{CO_2,1,e} + q_{CO_2,2,e} + q_{CO_2,3,e} + q_{CO_2,4,e} + 2q_{CO_2,5,e} = q_{CO_2,t,e} \tag{20}$$

$$K_{k,e} = \frac{K_{k,f}}{K_{k,b}} = K_{k,0} \exp(-\frac{\Delta H_{CO_2,k}}{RT}) \; ; k = 1, 2, 3, 4, 5 \tag{21}$$

$$K_{k,0} = \frac{K_{k,f,0}}{K_{k,b,0}} ; k = 1, 2, 3, 4, 5 \tag{22}$$

$$\Delta H_{CO_2,k} = E_{k,f} - E_{k,b} ; k = 1, 2, 3, 4, 5 \tag{23}$$

In equations 12-23, $K_{k,f,0}$, $K_{k,b,0}$, $E_{k,f}$ and $E_{k,b}$ show the pre-exponential constants and activation energies in Arrhenius equations for forward and backward reactions $K_{k,e}$ shows the equilibrium constant for reaction k. $q_{CO_2,1,e}$, $q_{CO_2,2,e}$, $q_{CO_2,3,e}$, $q_{CO_2,4,e}$, and $q_{CO_2,5,e}$ are equilibrium loadings of CO_2 corresponded to N_1, N_2, N_3 and N_4 respectively. $q_{CO_2,t,e}$ is the total equilibrium loading of CO_2 and $\Delta H_{CO_2,k}$ represents the effective heat of reaction for reaction k.

1.5 Results and discussion

In each cycle, at the beginning of adsorption and desorption, the feed gas replaces the gas exists in the TGA chamber from previous step. Therefore partial pressure of CO_2 does not reach the feed gas partial pressure immediately. In order to consider this effect in the modeling, the mass balance equation for TGA chamber was taken into account which is shown in equation 24:

$$\left(\frac{V^*}{RT}\right)\frac{dP^*_{CO_2}}{dt} = \frac{K_{CO_2}A}{RT}(P_{CO_2} - P^*_{CO_2}) - \rho_s V_s\left(\frac{dq_{CO_2,t}}{dt}\right) \quad (24)$$

In this equation, $P^*_{CO_2}$ is the partial pressure of CO_2 in the gas that is in contact with the sorbent. V^* is the volume of the chamber, K_{CO_2} is the mass transfer coefficient of CO_2, A is the area, P_{CO_2} is the partial pressure of CO_2 in feed gas, ρ_s is the adsorbent density, V_s is the adsorbent volume, $q_{CO_2,t}$ is the total loading, t is time, T is the temperature and R is the universal gas constant. For simplification, equation 24 was rearranged and constants were combined in 2 new constants; shown in equations 25-27. In all previously described models, P should be substituted by $P^*_{CO_2}$. P_{CO_2} is equal to CO_2's partial pressure in adsorption step and is equal to zero in desorption step. "TGA effect" affects both adsorption and desorption, however is more pronounced in adsorption because at a given temperature the initial adsorption rate is relative to pressure of CO_2. Figure 1.1 shows this effect on the results of fitting model III of adsorption in the first cycle at 14.5 vol. % CO_2 and four temperatures. Started from the same time, the model without "TGA effect" does not capture the data during the first 2-3 minutes of adsorption. Similar trends were seen at other conditions.

$$\frac{dP^*_{CO_2}}{dt} = K_p(P_{CO_2} - P^*_{CO_2}) - K_q T\left(\frac{dq_{CO_2,t}}{dt}\right) \quad (25)$$

$$K_P = \frac{K_{CO_2} A}{V^*} \quad (26)$$

$$K_q = \rho_s R \frac{V_s}{V^*} \quad (27)$$

In the proposed models (eq. 1-12 and table 1.1), since adsorption is involved in forward reactions, the activation energies of forward reaction constants ($E_{k,f}$) were allowed to take negative values [40, 41] while other activation energies were forced to be positive. Parameters were obtained by fitting the experimental data (first two cycles) at 40, 60, 80 and 100°C and at 1.2, 4.8, 14.5, 56.1 and 88.6 vol. % CO_2 in Nitrogen by using least-squares method using MS Excel Solver. The values for these parameters for all models are shown in table 1.2. The same parameters were then used to predict the following cycles (3rd and 4th cycles) and also the cycling data at 32.8 and 69.8 vol. %, to evaluate the interpolation and extrapolation capabilities of each model. Goodness of fit of each model was evaluated by considering the following criteria:

- Coefficient of determination (R^2)
- Visual examination of the fitted curves; capability of capturing kinetic features at both low and high temperatures for all 4 cycles.
- Model predictions for working capacity.
- Model predictions for equilibrium loadings at 80 and 100°C.

Model predictions for heat of adsorption/reaction ($\Delta H_{CO_2,k}$) are shown in table 1.3. Due to adsorption and exothermic reaction between amines and CO_2, $\Delta H_{CO_2,k}$ s are

expected to be negative. However $\Delta H_{CO_2,5}$ is positive which cannot be physically true. Hence from now on predictions of model V is not included in the results shown in this work. For other models, obtained values are not far from the values reported in the literature (42.7, [11] 50.03,[3] 63.2,[11] 67, [42] and 94 (±8)[14] (kJ.mol^{-1})) for adsorption of CO_2 on solid amines and not that different from heat of reactions for different amine types and CO_2 that have been reported by Kohl A. et al. cited by Satyapal et al.[14]; primary amines: 84 (kJ.mol^{-1}), secondary amines: 72 (kJ.mol^{-1}) and tertiary amines: 48 (kJ.mol^{-1}). However it should be noted that numbers reported here are not the same as the number Ebner et al. reported for the same material.[3] This inconsistency can be due to the fact that in their work, only equilibrium data at 80 and 100^{o}C were used to determine the heat of adsorption. Also they assumed the total number of sites to be constant.

For each condition, R^2 (coefficient of determination) was calculated using equation 28. In this equation $q_{i,\,exp}$ is the experimental value for CO_2 loading at time t, $q_{i,\mathrm{mod}}$ is model value for CO_2 loading at time t and $\bar{q}_{\exp}$ is mean of experimental CO_2 loading over four cycles. Calculated values are shown in tables 1.4 for those conditions that were included in fitting process and in table 1.5 for those which were not (32.8 and 69.8 vol. % CO_2 in Nitrogen). Also for each condition, the best model which had the maximum R^2 is displayed.

$$R^2 = 1 - \frac{\Sigma (q_{i,\exp} - q_{i,\mathrm{mod}})^2}{\Sigma (q_{i,\exp} - \bar{q}_{\exp})^2} \tag{28}$$

Based on the values of R^2, all models were able to capture the experimental cycling data at 80 and 100^{o}C ($R^2 \geq 0.98$) except for 1.2 vol. % CO_2. Since values of R^2 are very similar at these two temperatures, it cannot be told which model gave the best fit. At

60°C lowest R^2 values belonged to model I which clearly means that more than one reaction was needed to model the adsorption and desorption of CO_2 at this temperature. At 40°C model III had significant higher values of R^2 for most of the conditions indicating that three parallel reactions represented the kinetic data better than models with two reactions in parallel or two reactions in series. Accounting for all 28 conditions model III provided the best fitting for 71% of the conditions studied. However value of R^2 alone is not an indicator of goodness of fit of a model. Features of the predicted model have to be evaluated as well.

No significant differences were observed in visual examination of the fitted curves, at 60°C and higher temperatures. Therefore to have a better comparison of the models, only results at 40°C where the differences are more pronounced are shown. Figures 1.2-1.6 show the results of all models (I, II, III, IV) for 1.2, 4.8, 14.5, 56.1 and 88.6 vol. % CO_2 in Nitrogen respectively. At this temperature, there are two steps in the adsorption; a fast uptake of CO_2 that occurs at the beginning and a slow uptake that takes place after that. Although less pronounced, these two steps can be seen in desorption, too.

Figure 1.2 shows model predictions for 1.2 vol. %. Model I does not capture the experimental data except for the initial adsorption (t<10 min). Predictions of model II and IV are similar; both fit the data better for 2^{nd} -4^{th} cycles. These models predict higher loading during the slow step of adsorption and as a result in desorption step. Model III fits the data better than others at this pressure.

Figures 1.3 and 1.4 show that for 4.8 and 14.5 vol. % CO_2 in Nitrogen, model I does not capture the features of adsorption and desorption at all. At 4.8 vol. % shown in figure 1.3, models II and IV show similar trends; they fit the adsorption but over predict

the loading in desorption. For 14.5 vol % model II provides a better fit for adsorption compared to model IV, however neither of these models capture the curvature of the desorption curve; indicating that two reactions either in parallel or series cannot represent the adsorption and desorption of CO_2 at these conditions. On the other hand model III fits both fast and slow steps of adsorption as well as predicting the curvature of the desorption curve.

In figures 1.5 and 1.6, similar to figures 1.2 and 1.3 results of model I are far from experimental results. Unlike experiments, models II and IV show three steps of adsorption: a fast uptake followed by two consecutive slow uptakes. The third step becomes flat for model II at 88.6 vol. % (figure 1.6). None of these models fit the desorption curve. Model III under predicts the loading at the end of desorption at 88.6%, however it's the only model that captures all the experimental features. Results at these concentrations confirm the previous conclusion that two reactions either in series or in parallel cannot represent the experiments at this temperature making model III the best mechanism for adsorption and desorption of CO_2.

Figure 1.7 shows the model results for 32.8 and 69.8 vol. % CO_2 in Nitrogen. Trends are similar to other concentrations that are discussed above. Considering all concentrations, model III is the best model of four models studied here that represents the adsorption and desorption of CO_2 on CARiACT G10 solid amine sorbent at 40°C.

At other temperatures, since the results from all models were almost similar, only results of model III are shown here (Figures 1.8-1.11). Except for 1.2 vol. % CO_2 in Nitrogen, there was an excellent agreement between the model and the experiment.

Periodic state working capacity for each condition was calculated by subtracting the loading at the end of desorption from the loading at the end of adsorption in the 4^{th} cycle. It was assumed that 4^{th} cycle represented the periodic state behavior. Model predictions along with experimental working capacities are shown in figure 1.12 for models I-IV. It is clear from figure 1.12-a, that at 40°C model I provides the best fit (R^2=0.9040). However it was shown earlier that this model did not capture the kinetic features at 40°C. Model II (R^2=0.7301) and III (R^2=0.7981) fit the data up to 69.8 vol. %; at higher concentrations they predict higher working capacities. Model IV (R^2=0.5012) over predicts the working capacity at concentrations higher than 32.8 vol. %. At 60°C, models II, III, and IV, fit the data for concentrations lower than 56.1 vol. % and over predict the working capacities at concentrations higher than 56.1 vol. %. R^2 values at this temperature are 0.9286, 0.9673, and 0.9470 for model II, III and IV respectively. On contrary model I over predicts the working capacity at lower concentrations for concentrations lower than 56.1 vol. % and fits the working capacities at concentrations higher than 56.1 vol. % (R^2=0.8827). At 80 and 100°C, displayed in figure c and d, all models could predict the working capacities ($R^2 \geq 0.99$).

All the models were able to predict the equilibrium loadings at 80 and 100°C. Coefficients of determination for each model at these conditions are shown in table 1.6. Since the models overlapped at these conditions, experimental and predicted equilibrium loadings are only shown for model III in figure 13.

At higher temperatures no significant differences were seen between the proposed models. But at lower temperatures model III was able to capture the kinetic features much better than the others. Model III was also able to predict the working capacity as

well as equilibrium loadings at higher temperatures. Since this model is able to fit both kinetic and equilibrium data at a wide range of conditions, it can be used in PSA simulators. However consistency of the model with real reaction/adsorption mechanism and the physical structure of each species need more investigation via material characteristics methods.

1.6 Conclusions

Five semi-empirical, temperature-dependent kinetic models were studied to describe the reversible adsorption of CO_2 in CARiACT® G10 solid amine sorbent over a wide range of conditions: 4 temperatures (40, 60, 80 and 100°C) and 7 concentrations of CO_2 (1.2, 4.8, 14.5, 32.8, 56.1, 69.8, 88.6 vol. %). The experimental data were obtained by measuring the dynamic adsorption-desorption of CO_2 in the solid amine sorbent using a Perkin-Elmer TGA-7 thermogravimetric analyzer. Each run is four cycles of 40 min adsorption in CO_2/CO_2-Nitrogen mixture and 40 min desorption in Nitrogen.

The model constants were determined by fitting the model to first two experimental cycles of 40 minutes adsorption followed by 40 minutes desorption data at 40, 60, 80 and 100°C and different CO_2 concentrations (1.2, 4.8, 14.5, 56.1 and 88.6 vol. %).

Using the parameters obtained by fitting the first two cycles, the model predicted the cycling behavior for different CO_2 concentrations in the adsorption step (1.2, 4.8, 14.5, 56.1 and 88.6 vol. %) at four temperatures (40, 60, 80 and 100^{o}C) successfully. It also predicted the cycling behavior for other CO_2 concentrations (32.8 and 69.8 vol. %) at four temperatures (40, 60, 80 and 100^{o}C) without any further adjustments to the

parameters. Model III was able to predict the working capacities as well as equilibrium loadings.

Goodness of fit of models were evaluated and compared based on predicted features for both adsorption and desorption, values of coefficient of determination, and capability of fitting working capacities at all conditions and equilibrium loading at higher temperatures. Differences between the models were more pronounced at lower temperatures. Model III that is consisted of three parallel reactions provided the best fitting for most of the conditions.

In general, the proposed semi-empirical model was able to predict the cycling adsorption-desorption behavior of CO_2 on CARiACT® G10 solid amine sorbent satisfactorily over a wide range of CO_2 concentrations (1.2-88.6 vol. %) and temperatures (40-100°C). Therefore it can be used in dynamic adsorption process simulator to investigate the performance of PSA.

1.7 Tables

Table 1.1 Adsorption/Reaction sites for models I-V

Model	I	II	III	IV	V
Reactions present in the model	1	1&2	1&2&3	4	1&4

Table 1.2 Model parameters for models I-V

Parameter	I	II	III	IV	V
K_p(min^{-1})	1.06	7.92×10^{-1}	7.94×10^{-1}	8.45×10^{-1}	8.35×10^{-1}
K_q(kg.kPa.K^{-1}.mol^{-1})	2.22×10^{-9}	3.39×10^{-3}	2.59×10^{-3}	3.45×10^{-3}	3.58×10^{-3}
K_{1f0}(kPa^{-1}.min^{-1})	3.24×10^{-3}	1.18×10^{-3}	1.55×10^{-2}	-	7.42×10^{-9}
E_{1f}(kJ.mol^{-1})	-8.32	-1.29×10^{-1}	-3.68×10^{-1}	-	-3.19×10^{1}
K_{1b0}(min^{-1})	1.46×10^{8}	5.92×10^{9}	7.43×10^{2}	-	2.88×10^{8}
E_{1b}(kJ.mol^{-1})	6.13×10^{1}	7.15×10^{1}	2.31×10^{1}	-	6.12×10^{1}
K_{2f0}(kPa^{-1}.min^{-1})	-	1.14×10^{-1}	1.75×10^{-2}	-	-
E_{2f}(kJ.mol^{-1})	-	1.19×10^{1}	8.71	-	-
K_{2b0}(min^{-1})	-	2.48×10^{8}	2.01×10^{11}	-	-
E_{2b}(kJ.mol^{-1})	-	5.92×10^{1}	7.93×10^{1}	-	-
K_{3f0}(kPa^{-1}.min^{-1})	-	-	9.48×10^{-4}	-	-
E_{3f}(kJ.mol^{-1})	-	-	-1.39×10^{1}	-	-
K_{3b0}(min^{-1})	-	-	5.17×10^{10}	-	-
E_{3b}(kJ.mol^{-1})	-	-	7.80×10^{1}	-	-
K_{4f0}(kPa-1.min^{-1})	-	-	-	8.99×10^{-4}	7.76×10^{-4}
E_{4f}(kJ.mol-1)	-	-	-	-1.36×10^{1}	-1.42×10^{1}
K_{4b0}(min-1)	-	-	-	4.04×10^{9}	4.47×10^{9}
E_{4b}(kJ.mol-1)	-	-	-	7.05×10^{1}	7.07×10^{1}
K_{5f0}(kPa-1.min^{-1})	-	-	-	1.53	3.52×10^{-3}
E_{5f}(kJ.mol^{-1})	-	-	-	2.19×10^{1}	3.87
K_{5b0}(min^{-1})	-	-	-	5.09×10^{7}	7.40×10^{-1}
E_{5b}(kJ.mol^{-1})	-	-	-	5.42×10^{1}	3.59×10^{-5}
N_{max}	2.80	3.98	3.79	2.78	3.46
K_α	5.07×10^{-2}	3.26×10^{-2}	3.12×10^{-2}	2.99×10^{-2}	4.40×10^{-2}
T_0	2.88×10^{2}	2.91×10^{2}	2.85×10^{2}	2.87×10^{2}	2.94×10^{2}+
α	1.00	6.97×10^{-1}	1.51×10^{-1}	0.00	2.52×10^{-1}
β	0.00	3.03×10^{-1}	2.05×10^{-1}	0.00	0.00
κ	0.00	0.00	6.44E×10^{-1}	0.00	0.00
$\eta=1-(\alpha+\beta+\gamma)$	0.00	0.00	0.00	1.00	7.48×10^{-1}

Table 1.3 Heat of adsorption/reaction for models I-V

Parameter	I	II	III	IV	V
$\Delta H_{CO_2,1}$ (kJ.mol-1)	-69.67	-84.36	-23.47	-	-93.06
$\Delta H_{CO_2,2}$ (kJ.mol-1)	-	-47.34	-70.63	-	-
$\Delta H_{CO_2,3}$ (kJ.mol-1)	-	-	-91.92	-	-
$\Delta H_{CO_2,4}$ (kJ.mol-1)	-	-	-	-84.09	-84.92
$\Delta H_{CO_2,5}$ (kJ.mol-1)	-	-	-	-32.32	3.87

Table 1.4 R^2 values for models I-IV for four cycles at 40, 60, 80 and 100°C for 1.2, 4.8, 14.5, 56.1 and 88.9 vol. % CO_2 in Nitrogen.

vol.% CO_2 in Nitrogen	I	II	III	IV	Max. R^2	Best Mod.
40°C						
1.2	0.6086	0.9387	0.9659	0.9183	0.9659	III
4.8	0.1369	0.9487	0.9835	0.9538	0.9835	III
14.5	0.8969	0.9493	0.9883	0.8590	0.9883	III
56.1	0.6726	0.9504	0.9622	0.9234	0.9622	III
88.9	0.4519	0.7728	0.8792	0.7442	0.8792	III
60°C						
1.2	0.8551	0.9157	0.8940	0.9131	0.9157	II
4.8	0.9091	0.9781	0.9839	0.9813	0.9839	III
14.5	0.9249	0.9813	0.9883	0.9814	0.9883	III
56.1	0.9130	0.9285	0.9318	0.9257	0.9318	III
88.9	0.9528	0.9611	0.9681	0.9613	0.9681	III
80°C						
1.2	0.9462	0.9876	0.9888	0.9878	0.9888	III
4.8	0.9835	0.9836	0.9887	0.9845	0.9887	III
14.5	0.9943	0.9987	0.9985	0.9990	0.9990	IV
56.1	0.9953	0.9951	0.9952	0.9952	0.9953	I
88.9	0.9959	0.9981	0.9981	0.9983	0.9983	IV
100°C						
1.2	0.4146	0.5078	0.5380	0.4911	0.5380	III
4.8	0.9877	0.9885	0.9892	0.9890	0.9892	III
14.5	0.9991	0.9968	0.9965	0.9969	0.9991	I
56.1	0.9930	0.9942	0.9936	0.9936	0.9942	II
88.9	0.9955	0.9967	0.9972	0.9971	0.9972	III

Table 1.5 R^2 values for models I-IV for four cycles at 40, 60, 80 and 100°C for 32.8 and 69.8 vol. % CO_2 in Nitrogen.

vol.% CO_2 in Nitrogen	I	II	III	IV	Max. R^2	Best Mod
			40°C			
32.8	0.8245	0.9176	0.9671	0.7958	0.9671	III
69.8	0.4527	0.6594	0.8014	0.6064	0.8014	III
			60°C			
32.8	0.9765	0.9914	0.9915	0.9908	0.9915	III
69.8	0.9841	0.9882	0.9915	0.9910	0.9915	III
			80°C			
32.8	0.9976	0.9966	0.9963	0.9956	0.9976	I
69.8	0.9960	0.9964	0.9966	0.9966	0.9966	III, IV
			100°C			
32.8	0.9944	0.9977	0.9970	0.9974	0.9977	II
69.8	0.9972	0.9973	0.9983	0.9979	0.9983	III

Table 1.6 R^2 values for equilibrium loadings predicted by models I-IV at 80 and 100^{o}C.

Model	80°C	100°C
I	0.9905	0.9978
II	0.9964	0.9979
III	0.9984	0.9981
IV	0.9968	0.9980
V	0.9957	0.9977

1.7 Figures

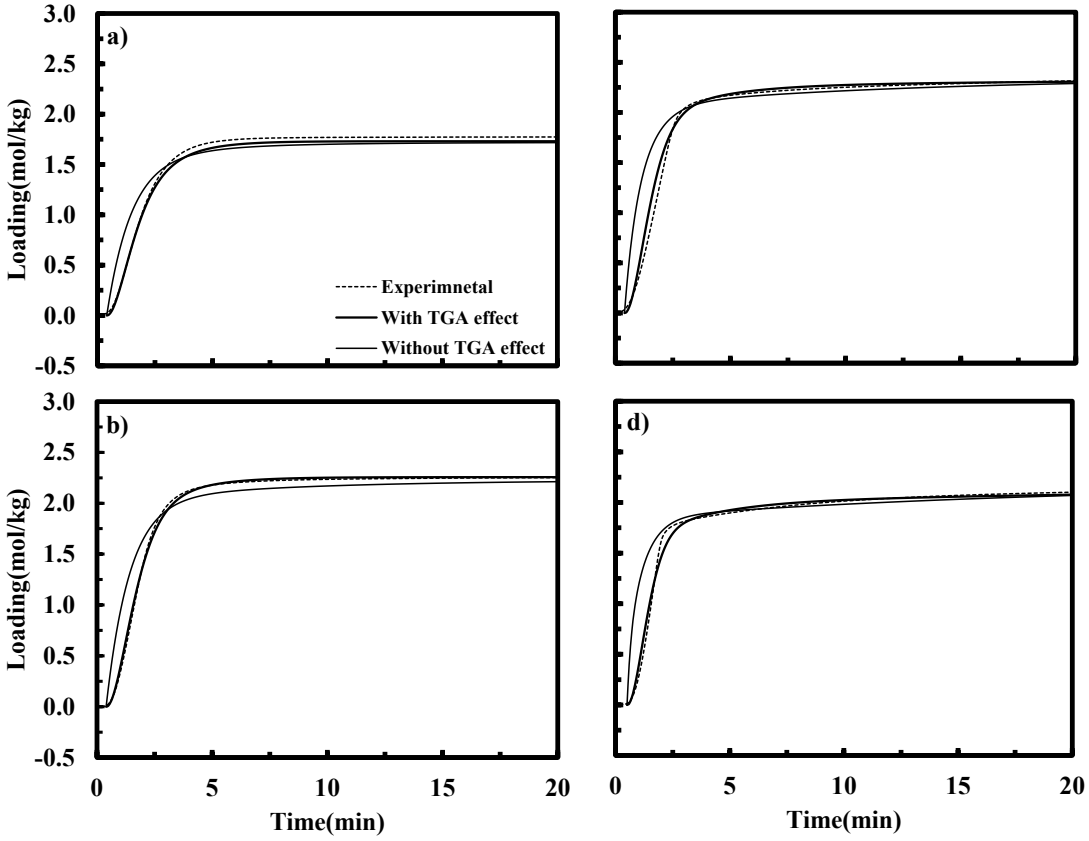

Figure 1.1 Model III predictions (solid line) vs. experimental data (dotted line) with and without TGA effect for 14.5 vol. % CO_2 in Nitrogen at a) 100^{o}C, b) 80^{o}C, c) 60^{o}C, d) 40^{o}C

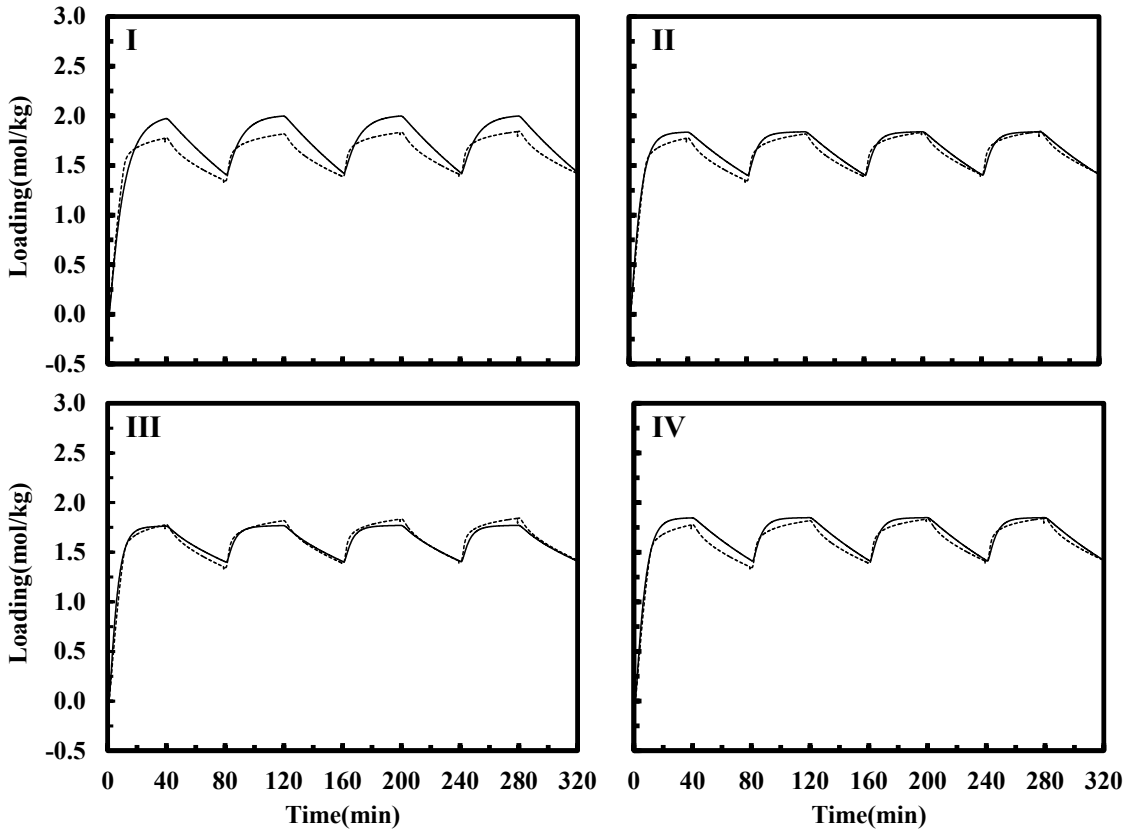

Figure 1.2 Model I-IV predictions (solid line) vs. experimental data (dotted line) at 40^{o}C for 1.2 vol. % CO_2 in Nitrogen

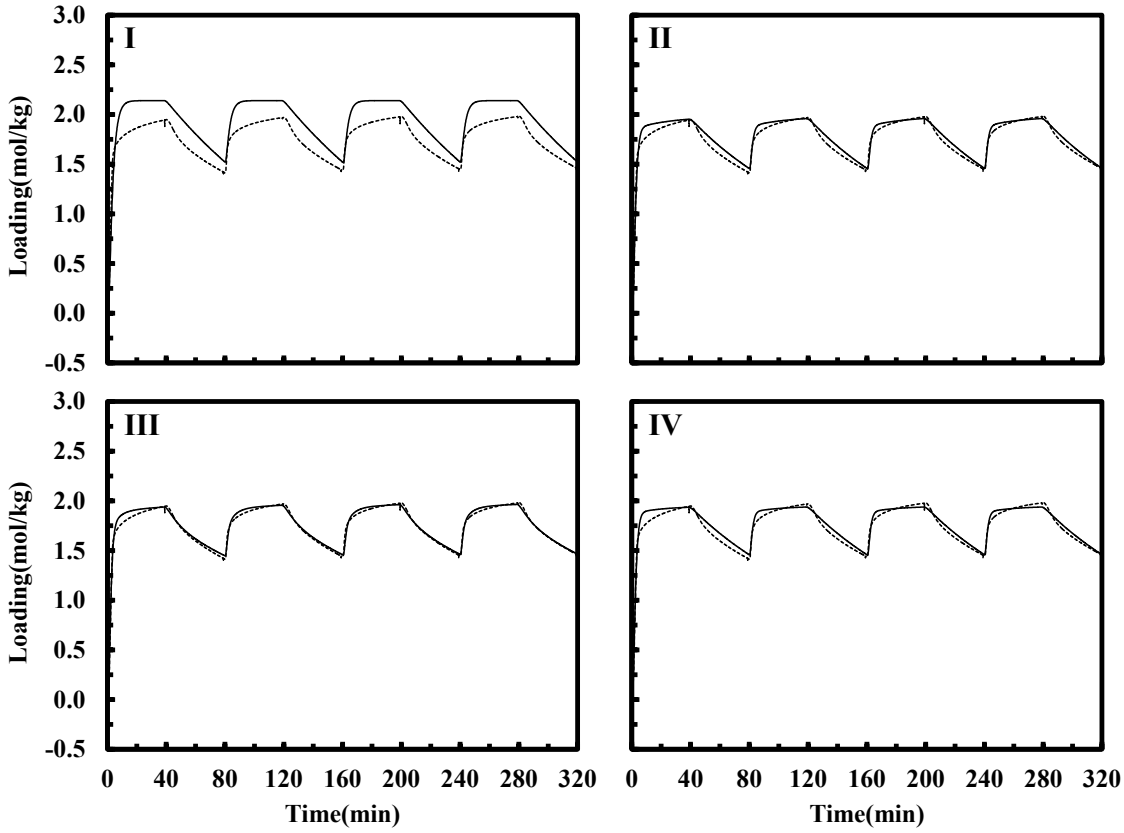

Figure 1.3 Model I-IV predictions (solid line) vs. experimental data (dotted line) at 40^{o}C for 4.8 vol. % CO_2 in Nitrogen

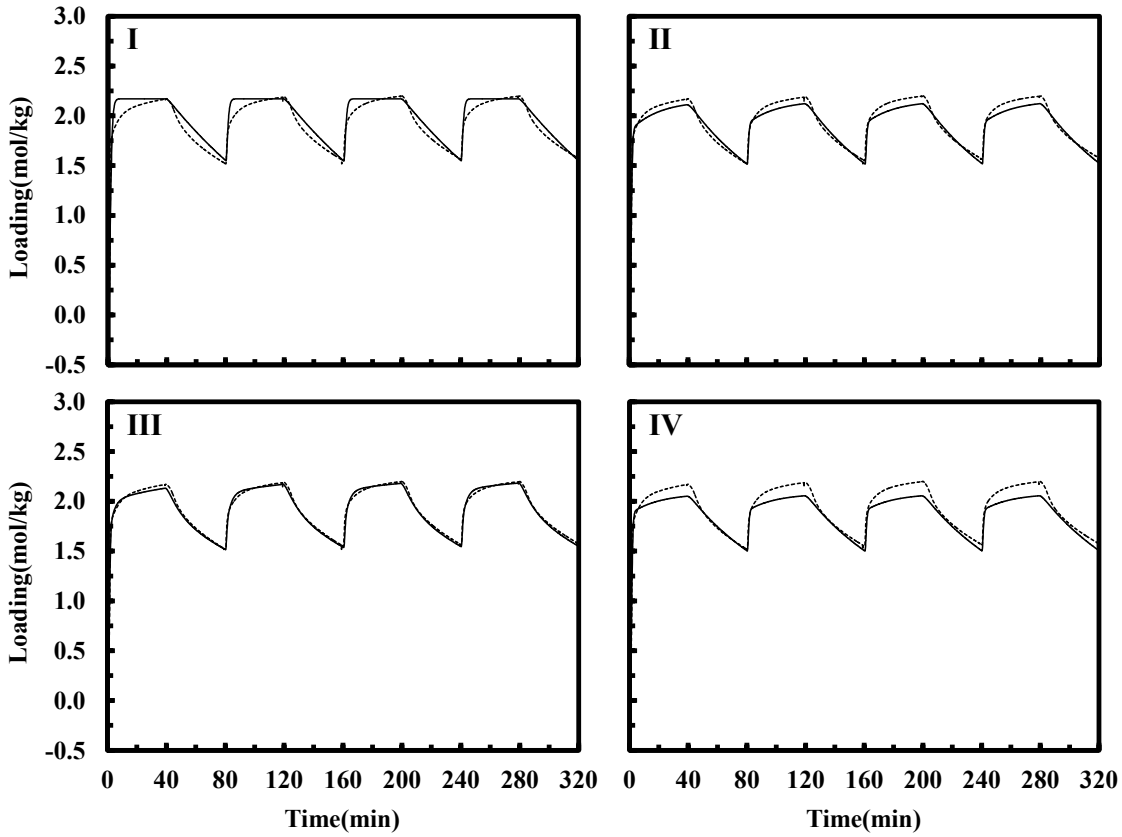

Figure 1.4 Model I-IV predictions (solid line) vs. experimental data (dotted line) at 40^{o}C for 14.5 vol. % CO_2 in N_2

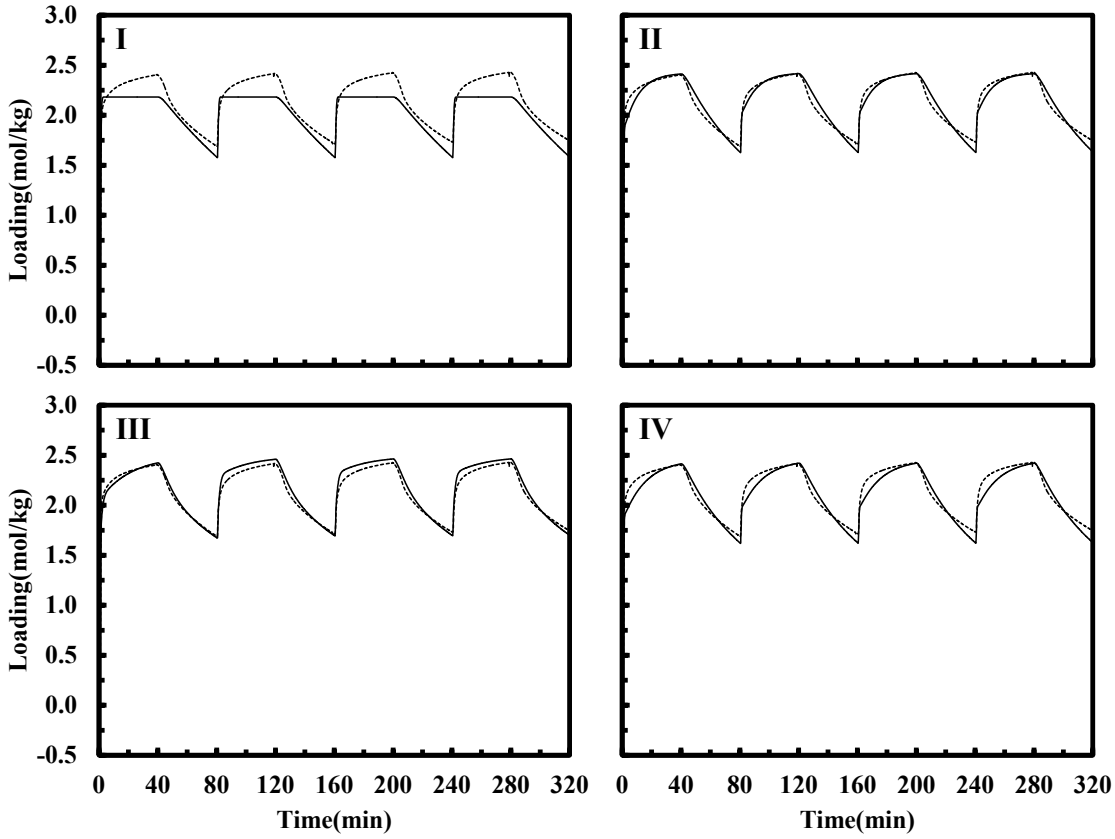

Figure 1.5 Model I-IV predictions (solid line) vs. experimental data (dotted line) at 40^{o}C for 56.1 vol. % CO_2 in Nitrogen

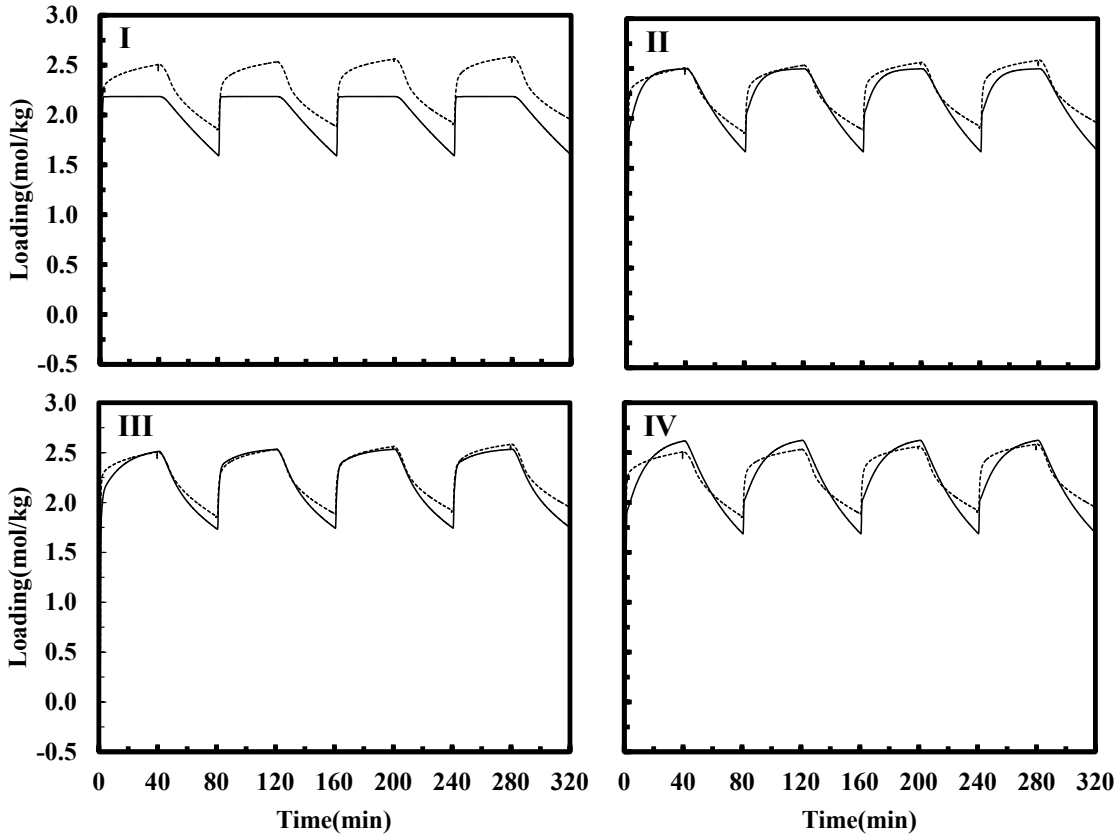

Figure 1.6 Model I-IV predictions (solid line) vs. experimental data (dotted line) at 40^{o}C for 88.6 vol. % CO_2 in Nitrogen

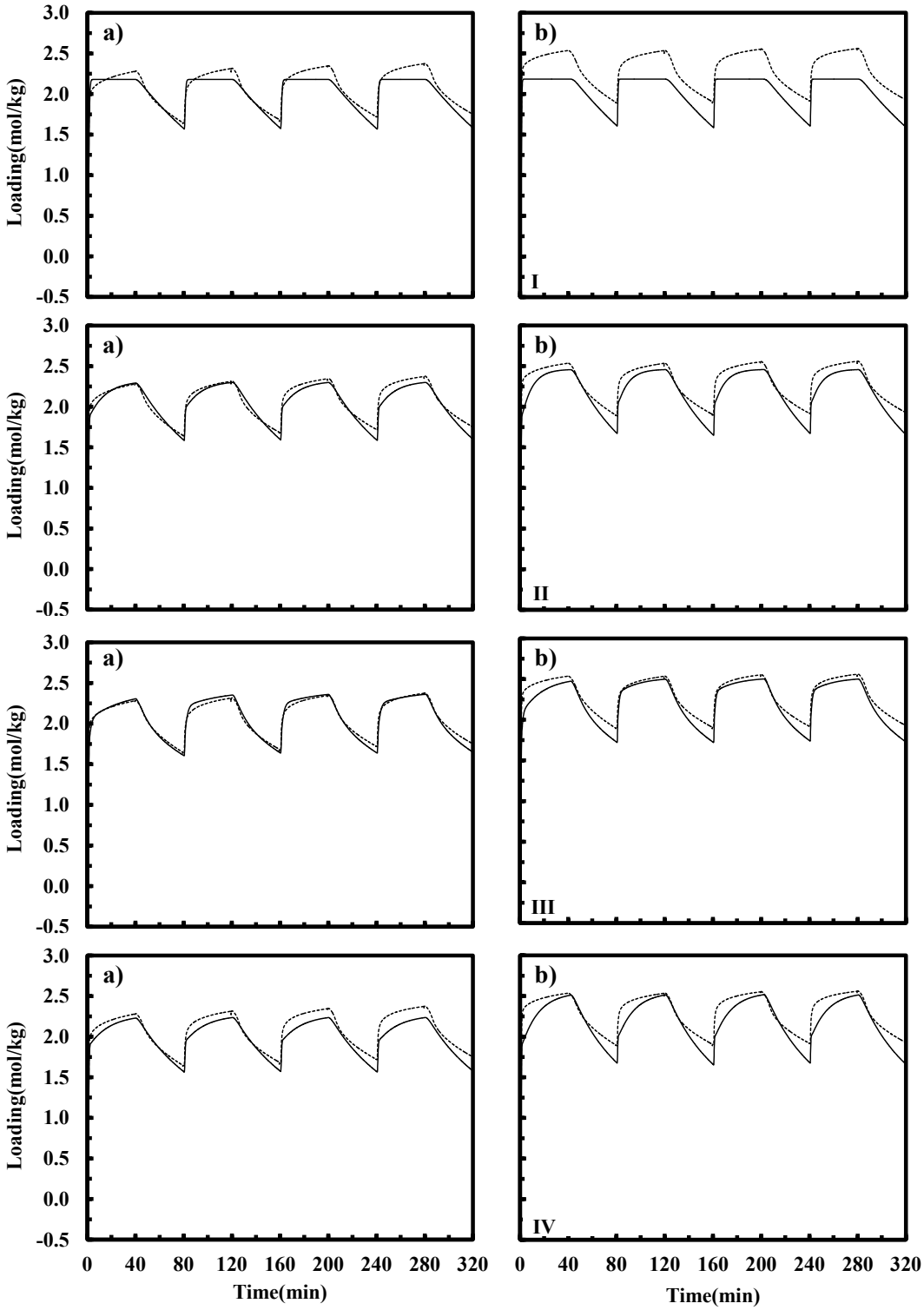

Figure 1.7 Model I-IV predictions (solid line) vs. experimental data (dotted line) at 40^{o}C for a) 32.8 and b) 69.8 vol. % CO_2 in Nitrogen

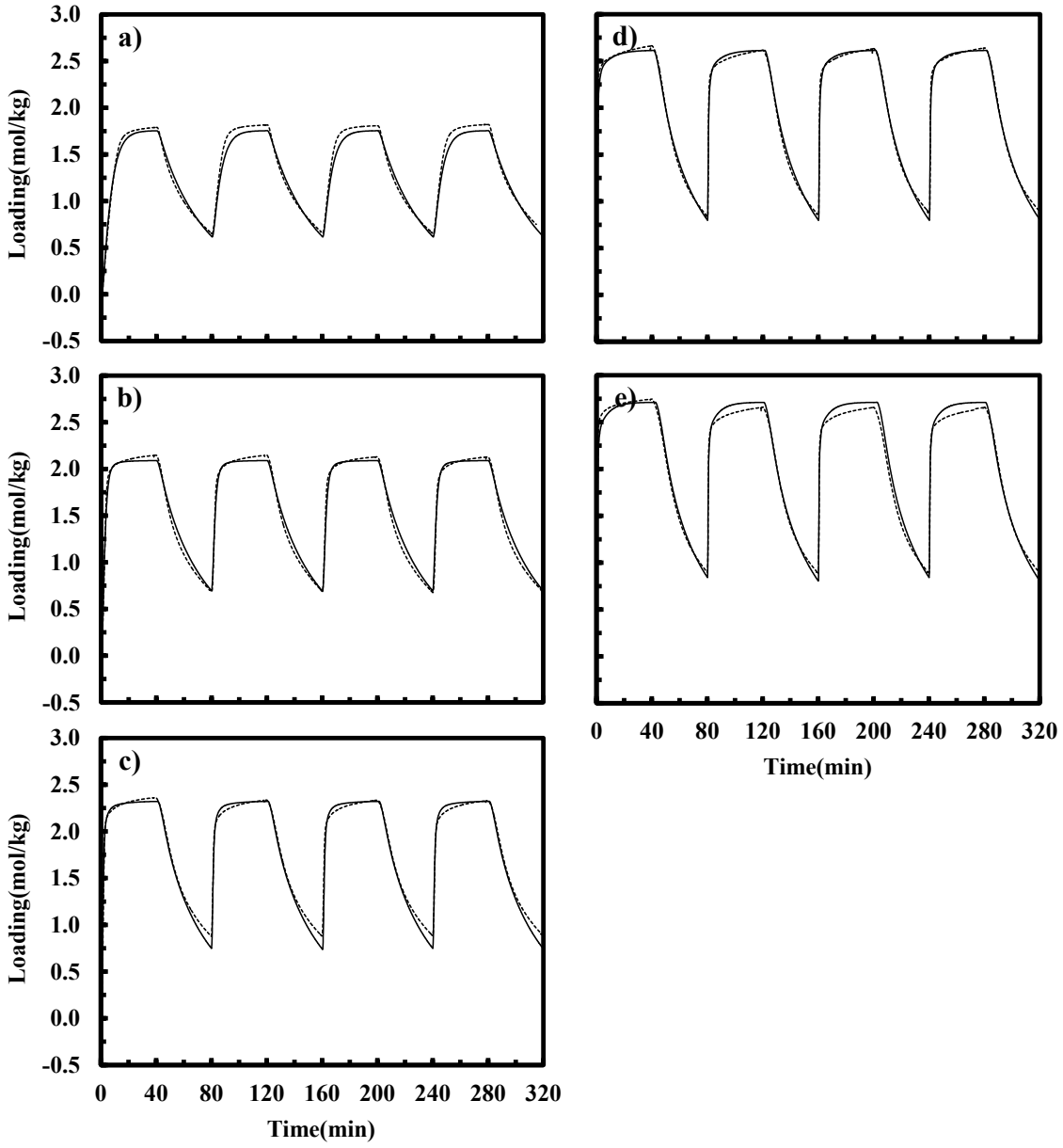

Figure 1.8 Model III predictions (solid line) vs. experimental data (dotted line) at 60^{o}C for a) 1.2, b) 4.8, c) 14.5, d) 56.1 and e) 88.6 vol. % CO_2 in Nitrogen

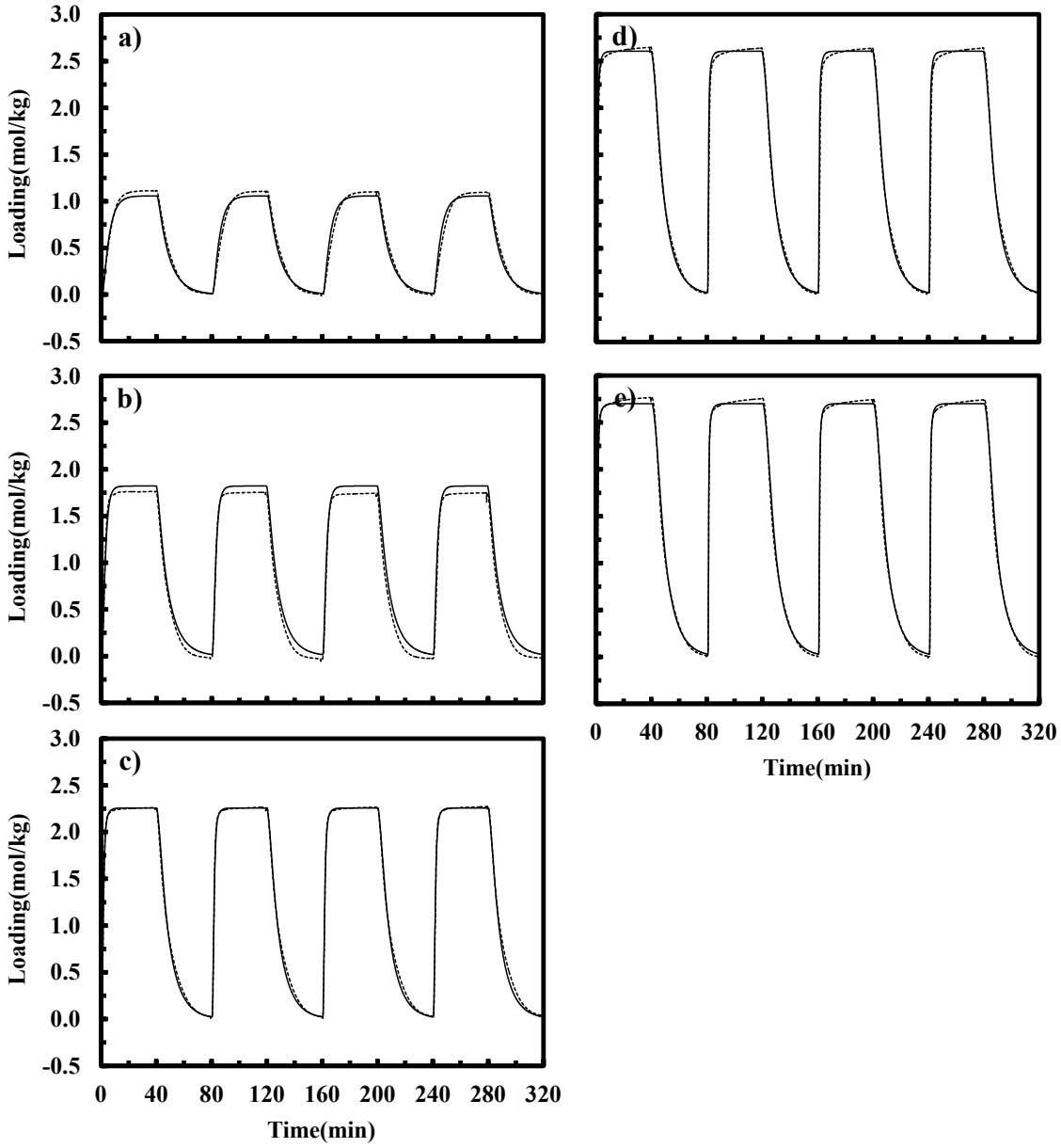

Figure 1.9 Model III predictions (solid line) vs. experimental data (dotted line) at 80^{o}C for a) 1.2, b) 4.8, c) 14.5, d) 56.1 and e) 88.6 vol. % CO_2 in Nitrogen

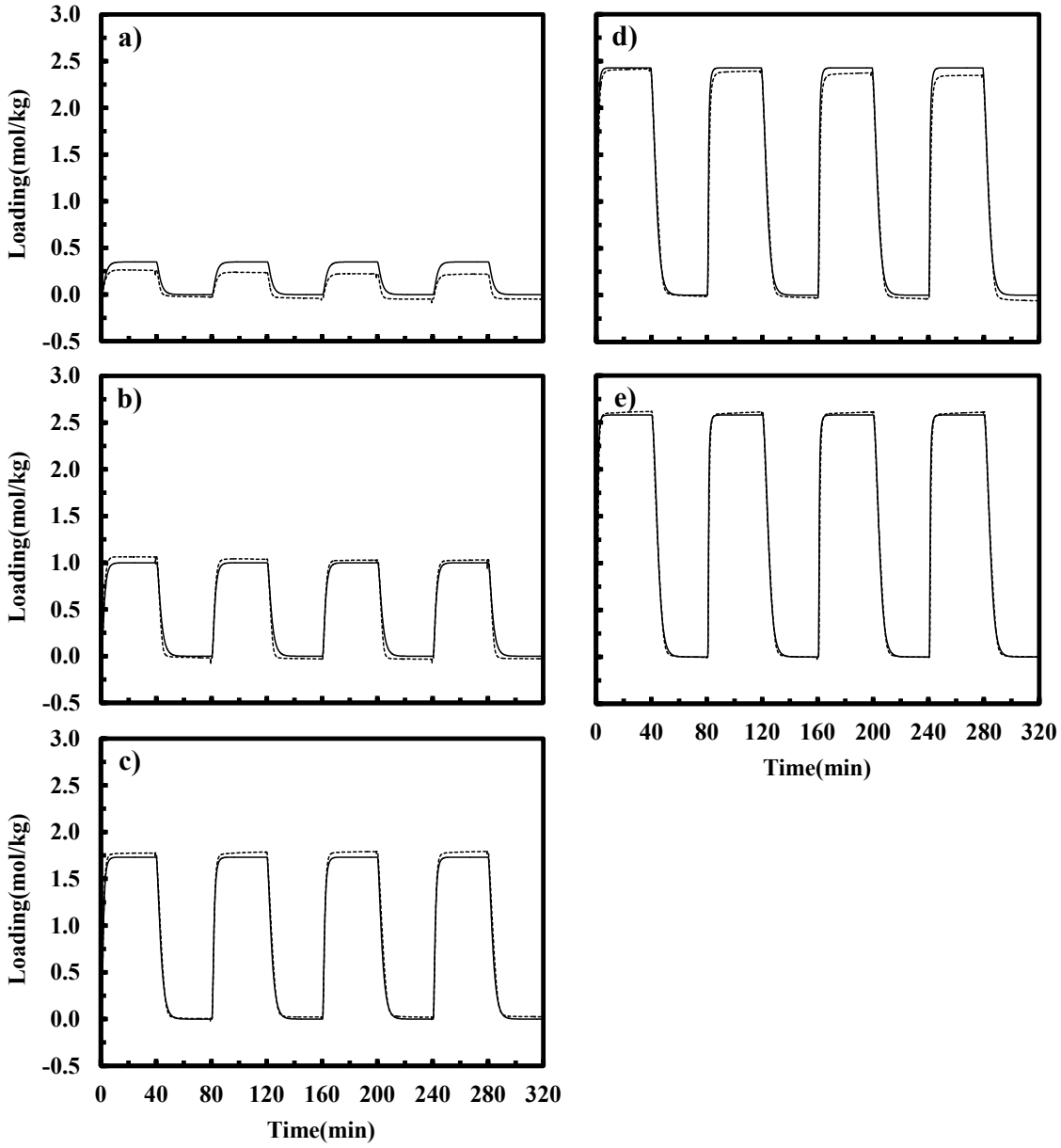

Figure 1.10 Model III predictions (solid line) vs. experimental data (dotted line) at 100^{o}C for a) 1.2, b) 4.8, c) 14.5, d) 56.1, and e) 88.6 vol. % CO_2 in Nitrogen

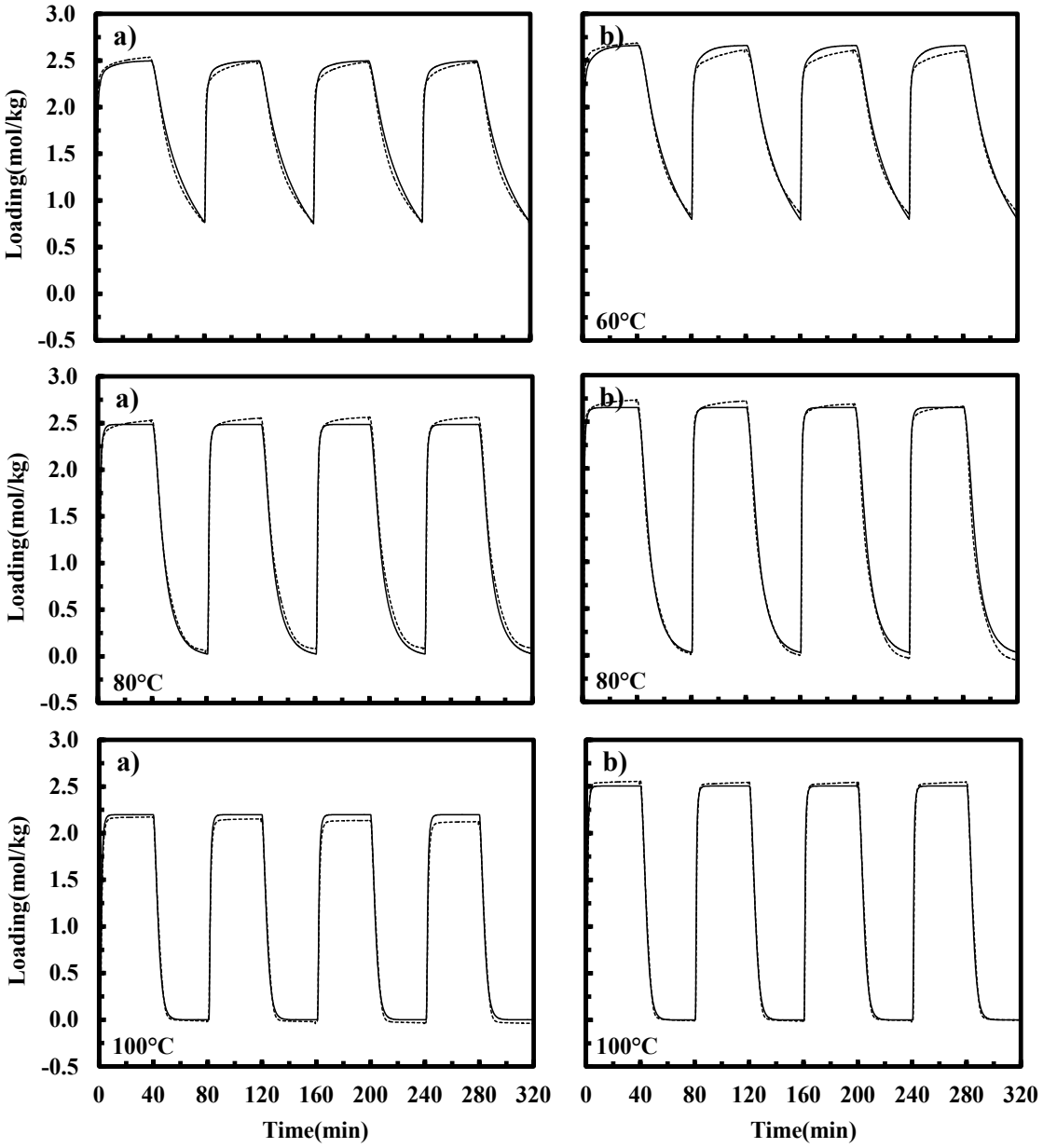

Figure 1.11 Model III predictions (solid line) vs. experimental data (dotted line) at 60, 80, and 100°C for a) 32.8 and 69.8 vol. % CO_2 in Nitrogen

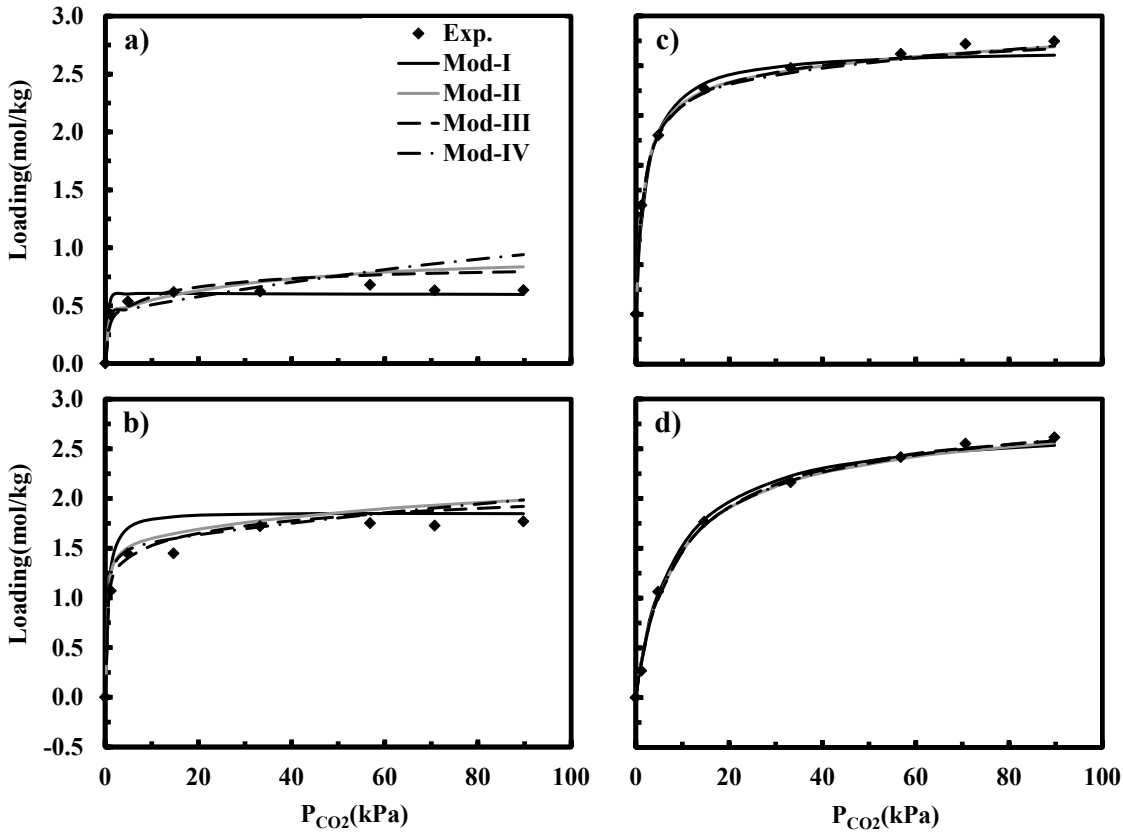

Figure 1.12 Model I-IV predictions (lines) vs. experimental working capacity (symbols) at a) 40°C, b) 60°C, c) 80°C, d) 100°C

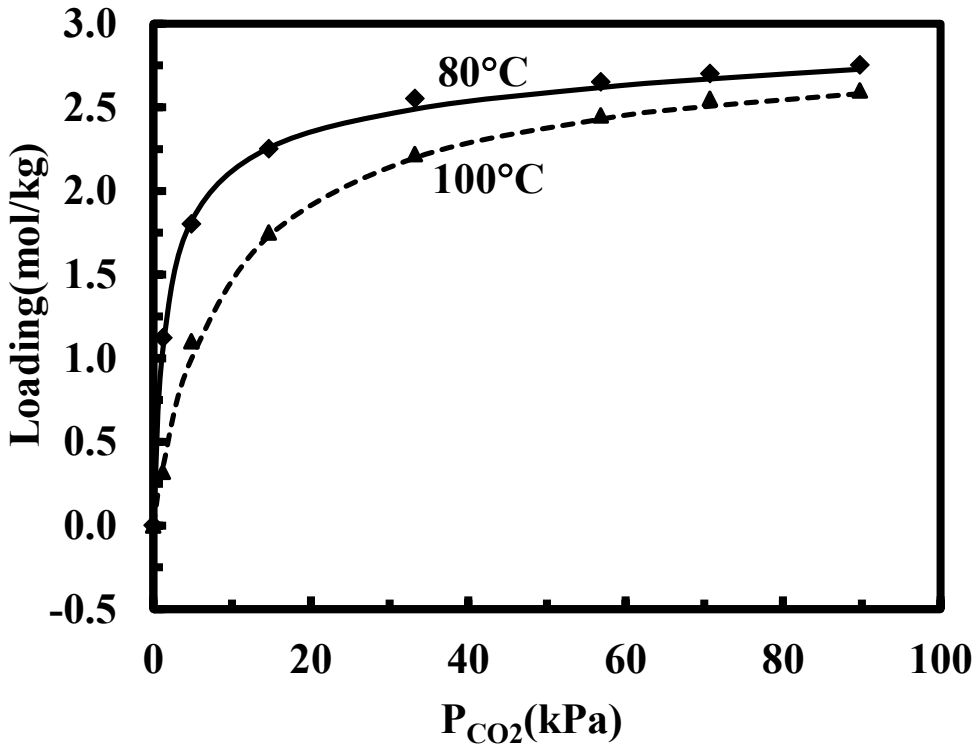

Figure 1.13 Model predictions (lines) vs. experimental equilibrium loadings (symbols) vs. partial pressure of CO_2 at 80 and 100^{o}C

CHAPTER 2

CO_2 CAPTURE FROM FLUE GAS BY PSA USING A SOLID AMINE SORBENT: DRY FEED

2.1 Summary

Two pressure swing adsorption cycles; a 3 bed-8 step and a 4 bed-9 step cycles were designed for the capture of CO_2 from flue gas using a solid amine sorbent. An in-house PSA simulator was utilized to investigate the effect of different parameters on the performance of the PSA process at a fixed pressure ratio (P_H=120 kPa and P_L=5 kPa) and cycle time (300s). For a feed gas comprised of 15.9 % CO_2 in Nitrogen the performance of the proposed cycles in terms of recovery and purity of CO_2 as well as the avoided energy needed for separation and feed throughputs were investigated. Conditions at which the separation goal (>90% recovery and >95% vol. % purity of CO_2) were obtainable, were identified for each cycle. Based on the results of the parametric study, three more simulation runs were carried out for each cycle in order to improve the performance of the process. For the 3 bed-8 step cycle, the separation target was met for throughputs higher than 336.70 (L(STP)/kg/hr) and lower than 448.94 (L(STP)/kg/hr) with avoided energy around 39 (kJ/mol CO_2) and for the 4 bed-9 step cycle, the goal was achieved for throughputs slightly higher than 224.47 (L(STP)/kg/hr) and avoided energy around 28 (kJ/mol CO_2).

2.2 Introduction

CO_2 is one of the greenhouse gases that believed to cause global warming. In USA over 40% of CO_2 is produced by fossil based power plants.[43] In order to prevent adverse climate change and its effects, there will be legislations and/or regulations to reduce CO_2 emissions which will be applied to both existing and new coal-based power plants.[44] Therefore a lot of studies have been carried out on methods to reduce the emission of CO_2 from these plants.

Technologies for CO_2 capture with an emphasis on adsorption and membranes have been thoroughly reviewed by Ebner and Ritter.[2] One technology that has shown potential for this purpose and has been considered by several authors is pressure swing adsorption (PSA). PSA has some advantages like lower capital and operating cost[45], and simplicity of operation.[46] Other prospective separation technologies are membranes, cryogenic distillation and amine scrubbing. Advantages and disadvantages of each of these technologies can be found in details in the review article provided by Aaron and Tsouris.[47]

Efficiency of a PSA process depends on two main factors: adsorbent characteristics and cycle design. For CO_2 capture from flue gas, an appropriate sorbent provides a good working capacity for CO_2 as well as having sufficiently fast kinetics for both adsorption and desorption.[48] Moreover this sorbents is water tolerant because flue gas can contain up to 17% water. Several sorbents have been considered for CO_2 capture from flue gas by using PSA such as activated carbon[49-51], zeolites (5A[52], 13X[45-46, 51, 53-59], CaX type[60]) and HTLc[44, 61-62]. In a critical review on the adsorption of CO_2 on various sorbents at high temperatures carried out by Yong et al., HTLcs and basic alumina were

reported to have a sufficient adsorption capacity for CO_2 at high temperatures.[61] At low temperatures on the other hand, zeolite 13X is the most widely used sorbent for CO_2.[45-46, 51, 53-59] However the main problem with 13X is its sensitivity to water.[3] For example Li et al. explored the capture of CO_2 from a synthesis flue gas with 95% relative humidity at 30°C using 13X.[54] They reported 18.5 % drop in recovery and 22% drop in productivity of CO_2 when water was present. Their study revealed that although it was possible to remove both CO_2 and water with the same 13X, the performance of the PSA process was negatively affected by the presence of water. In solid amines sorbent on the other hand, not only water does not affect the adsorption of CO_2 on amine sites, but also it can improve the adsorption capacity of CO_2.[14, 63] Ebner et al. showed that a particular solid amine sorbent is suitable to be used in a PSA process for CO_2 capture from flue gas.[3] However in their work no results regarding the performance of their material in a PSA process was provided.

Depending on the goal of process, various steps with different number of beds can be combined in a specific way. In capturing CO_2 from flue gas, at least 90% of CO_2 of the feed should be captured and the separated CO_2 should be at least 95 vol. % pure. More over like any other industrial process, in designing a PSA process, cost is an inseparable part that should be taken into account. Both capital and operating cost which are related to feed throughput and power consumption respectively should be considered. In other words for this specific process, an effective PSA process would be a process which provides high CO_2 recovery (>90%) and purity (>95 vol. %), at high feed throughput and low power consumption.

Several PSA/VSA cycles have been explored for CO_2 capture from flue gas. Reported cycle schedules are ranged from simple schedules like a 1bed-4 step cycle (feed pressurization, feed, countercurrent depressurization and light reflux [64-65], or 2 bed-4 step cycle (feed pressurization, feed, co- current depressurization and light reflux),[66]to more complicated cycles like a 4 bed-8 step cycle(feed pressurization, feed, heavy reflux, equalization, counter current depressurization, light reflux, equalization, Idle)[67]. A list of the PSA cycles studied for CO_2 capture from flue gas has been provided by Agarwal et al.[68] and Reynold et al.[62]. These cycles have been designed for sorbents like 13X, HTLc, NaX, and Ac.[62, 68] To our knowledge no PSA processes have been reported for solid amine sorbents for CO_2 capture from flue gas.

In this chapter two PSA cycles are presented for CO_2 capture from flue gas using the solid amine sorbent investigated by Ebner et al.[3] The performance of each PSA cycle in terms of recovery, purity, feed throughput and power consumption at different conditions has been investigated. Also for each cycle a set of conditions under which the goal of 90% CO_2 recovery and 95 vol. % CO_2 purity was achievable, is reported. Effect of different parameters on the performance of each cycle has been investigated. The results reported here provide an overall idea about the behavior of this material in a PSA process. In the current study it has been assumed that there is no water in the feed gas.

2.3 Cycle Description

Cycle schedules shown in figure 2.1 were investigated for CO_2 capture from flue gas using G10 solid amine sorbent. Cycle I is consisted of 3 beds and 8 steps while cycle II is consisted of 4 bed and 9 steps. Steps in these cycles are as follows:

Feed; a feed gas consisting of 15.9% CO_2 in Nitrogen enters the bed at 100°C and 120.0 kPa.

Heavy reflux (HR); a fraction of CO_2-enriched stream leaving the bed during the LR/LR2 step is recycled to the system, through the heavy end

Equalization down (Eq); the bed is depressurized though its light end to an intermediate pressure. The gas that leaves the bed during this step is used to pressurize the bed undergoing the "equalization up" step.

Co-current depressurization (CoD); the bed is depressurized to a pressure lower then equalization pressure and higher than 5 kPa through its light end.

Counter-current depressurization (CnD); the bed is depressurized to the lowest pressure in the process (5kPa) through its heavy end.

Light reflux (LR/LR1/LR2); A fraction of Nitrogen-enriched stream leaving the bed during the feed step is recycled through the light end.

Equalization up (Eq'); the bed is pressurized to an intermediate pressure by provided gas from the bed undergoing Eq step.

Light product pressurization (LPP); A fraction of Nitrogen-enriched stream leaving the bed during the feed step is recycled to re-pressurize the bed.

In cycle I, heavy product is collected at the downstream of the bed undergoing the CnD step, and also a fraction of the gas leaving the bed during the light reflux. In cycle II, CnD step, LR-1 step and a part of the gas exiting the bed during the LR-2 step, provide the heavy product. In both cycles light product is generated during Feed, HR and CoD steps.

2.4 Mathematical Model

An in house dynamic adsorption process simulator (DAPS) developed in FORTRAN was used to simulate the PSA cycles reported in the current work. Finite difference method along with a time adaptive DAE solver (DASPK)[69] were used to solve the equations for mass, energy and momentum balances. For simplification following conditions were applied: the ideal gas law, plug flow, same temperature for gas and solid phase, no heat conduction, and no concentration gradients in both gas and solid phase in pellets. For CO_2 adsorption and desorption, model III that was previously described in chapter 1 was used. It should be noted that the developed model is for a powder, while in this chapter, it has been assumed that sample is in pelletized form with the same characteristics. For adsorption and desorption of Nitrogen, an LDF model was applied; assuming that the adsorption of Nitrogen on this specific sorbent being similar to the adsorption of Nitrogen on silica gel, a two process Langmuir isotherm model with a mass transfer coefficient equal to 0.1 s^{-1} were used.

Equations for overall and component mass balance and energy balance are as follows:

Overall mass balance:

$$(\varepsilon_b + (1-\varepsilon_b)\varepsilon_P)C_T\left(\frac{1}{P}\frac{\partial P}{\partial t} - \frac{1}{T}\frac{\partial T}{\partial t}\right) + \varepsilon_b \frac{\partial v C_T}{\partial z} + \sum_{j=1}^{n} S_j = 0 \quad (1)$$

Component mass balance:

$$(\varepsilon_b + (1-\varepsilon_b)\varepsilon_P)C_T \frac{\partial y_i}{\partial t} + \varepsilon_b C_T v \frac{\partial y_i}{\partial z} - y_i \sum_{j=1}^{n} S_j + S_i = 0 \quad ; i = 1 \text{ to } N\text{-}1 \quad (2)$$

$$y_i + \sum_{j=1, j\neq i}^{n} y_j = 0 \; ; i = 1 \text{ to } N\text{-}1 \quad (3)$$

Where

$$C_T = \frac{P}{RT}; S_i = (1-\varepsilon_b)\rho_P \frac{\partial q_i}{\partial t} \tag{4}$$

In equations 1-4, ρ_p is the pellet density, and ε_p is the pellet porosity, ε_b is the bed porosity, v is the interstitial velocity, C_T is total molar concentration, N is the number of components, y_i is the mole fraction of component i in the gas phase, T is the temperature of both gas and solid phases, P is the total pressure and q_i shows the loading of component i in the solid phase.

Loading changes with time for CO_2:

$$\frac{\partial q_{1,co_2}}{\partial t} = K_{1,f} P y_{CO_2} (N_1 - q_{1,co_2}) - k_{1,b} q_{1,co_2} \tag{5}$$

$$\frac{\partial q_{2,co_2}}{\partial t} = K_{2,f} P y_{CO_2} (N_2 - q_{2,co_2}) - k_{2,b} q_{2,co_2} \tag{6}$$

$$\frac{\partial q_{3,co_2}}{\partial t} = K_{3,f} P y_{CO_2} (N_3 - q_{3,co_2}) - k_{3,b} q_{3,co_2} \tag{7}$$

$$q_{1,co_2} + q_{2,co_2} + q_{3,co_2} = q_{t,co_2} \tag{8}$$

$$N_1 = \alpha N_t \tag{9}$$

$$N_2 = \beta N_t \tag{10}$$

$$N_3 = (1-\alpha-\beta) N_t \tag{11}$$

$$N_t = \frac{N_{\max}}{1+\exp(-k_\alpha (T - T_{FD}))} \tag{12}$$

$$\Delta H_k = E_{k,f} - E_{k,b} \tag{13}$$

Temperature dependency of reaction constants was expressed by Arrhenius equation:

$$K_{k,f} = K_{k,f,0} \exp\left(\frac{-E_{k,f}}{RT}\right); k = 1, 2, 3 \quad (14)$$

$$k_{k,b} = k_{k,b,0} \exp\left(\frac{-E_{k,b}}{RT}\right); k = 1, 2, 3 \quad (15)$$

In the above equations, all the constantans are the same as the constants defined in chapter 1.

Loading changes for Nitrogen:

$$\frac{\partial q_{N_2}}{\partial t} = k_{N_2}\left(q^*_{N_2} - q_{N_2}\right) \quad (16)$$

$$q^*_{N_2} = q^s_{1,N_2}\frac{b_{1,N_2} Py_{N_2}}{1 + b_{1,N_2} Py_{N_2}} + q^s_{2,N_2}\frac{b_{2,N_2} Py_{N_2}}{1 + b_{2,N_2} Py_{N_2}} \quad (17)$$

$$b_{1,N_2} = b^0_{1,N_2} exp\left(\frac{B_{1,N_2}}{T}\right) \quad (18)$$

$$b_{2,N_2} = b^0_{2,N_2} exp\left(\frac{B_{2,N_2}}{T}\right) \quad (19)$$

In equations 17-20, k_{N_2} is the mass transfer coefficient of Nitrogen, $q^*_{N_2}$ is the equilibrium loading of Nitrogen, q_{N_2} is the loading of Nitrogen at time t. q^s_{1,N_2}, q^s_{2,N_2}, b_{1,N_2}, and b_{2,N_2} are the parameters for Dual Process Langmuir isotherm for Nitrogen. b^0_{1,N_2}, b^0_{2,N_2}, B_{1,N_2} and B_{2,N_2} are pre-exponential and energy constants in the Arrhenius equations describing temperature dependency of b_{1,N_2} and b_{2,N_2}.

Energy balance:

$$(\varepsilon_b + (1-\varepsilon_b)\varepsilon_P)\left(Cp_g C_T \frac{\partial T}{\partial t} - \frac{\partial P}{\partial t}\right) + \left((1-\varepsilon_b)\rho_P Cp_p\right)\frac{\partial T}{\partial t} + \varepsilon_b Cp_g C_T v \frac{\partial T}{\partial z} +$$
$$(1-\varepsilon_b)\rho_P \sum_{j=1}^{n}\left(Cp_{a,j} q_j \frac{\partial T}{\partial t} + \Delta H_i \frac{\partial q_i}{\partial t}\right) + \frac{2}{r_{b,i}} h_w (T - T_o) = 0 \quad (20)$$

Where:

$$Cp_g = \sum_{j=1}^{n}\left(y_j Cp_{g,j}\right) \quad (21)$$

In the above equations, $Cp_{g,i}$ is the molar heat capacity of component i in the gas phase, $Cp_{a,j}$ is the molar heat capacities of component *i* in the solid phase which were assumed to be equal, Cp_p is the heat capacity of the pellet, ΔH_i is the heat of adsorption of component i, h_w is the heat transfer coefficient at the wall and r_i is the internal radius of the bed.

Ergun's equation was applied for the pressure drop along the bed (eq 23), in which ρ_p is the viscosity and M_g is the average molecular weight of the gas phase and r_p shows effective radius of the pellet.

$$\frac{\partial P}{\partial z} + 1.5 \times 10^{-1} \mu_g \left(\frac{1-\varepsilon_p}{2 r_p \varepsilon_p}\right)^2 v + 1.75 \times 10^{-3} C_T M_g \frac{1-\varepsilon_p}{2 r_p \varepsilon_p} v|v| = 0 \quad (22)$$

Bed characteristics, adsorbent properties, components' kinetic and equilibrium data, and process conditions are shown in table 2.1. Initial and boundary conditions for each step are listed in tables 2.2 and 2.3 for cycles I and II respectively. At given boundaries the molar flow rate (F) through the valve is defined according to the valve equation, which is defined according to

$$F = c_v v_{sign} \frac{1}{\sqrt{S_g T}} \min\left(49.08\left|P^2 - P_o^2\right|^{0.5}, 41.63 P_o\right) \quad (23)$$

In equation 23, c_v is the valve coefficient, S_g is the specific gravity of the gas relative to air at 1 atm and 21.45°C; P_o is the pressure outside the valve. Two parts in the parentheses in the equations were considered in order to distinguish choking from non-choking conditions. At each boundary whenever a condition for temperatures, concentrations, flows and valve equations is not specified or required, mass and energy balances along with the Ergun's equation were utilized to retain consistency. In both cycles equalization pressure was step, final pressure was found by trial and error, in such way that the two beds undergoing equalization step reached the same pressure at the end step time. For each run that was carried out, the run was continued until the periodic state behavior was achieved where flows, recovery and purity of each component did not change with time, and mass balance over the whole cycle for each component was closed. Recovery, purity and feed throughputs were obtained using equations 24-25 respectively.

$$\mathrm{CO_2\ Recovery\ (\%)} = \frac{\mathrm{CO_2(moles)}\big|_{\mathrm{Heavy\ Product}}}{\mathrm{CO_2(moles)}\big|_{\mathrm{Feed}}} \times 100 \tag{24}$$

$$\mathrm{CO_2\ Purity\ (\%)} = \frac{\mathrm{CO_2(moles)}\big|_{\mathrm{Heavy\ Product}}}{\mathrm{CO_2(moles)}\big|_{\mathrm{Heavy\ Product}} + \mathrm{N_2(moles)}\big|_{\mathrm{Heavy\ Product}}} \times 100 \tag{25}$$

$$\mathrm{Throughput} = \frac{\mathrm{Feed\ flow} \times \mathrm{time}\big|_{\mathrm{feed\ step}}}{\mathrm{Amount\ of\ adsorbent\ in\ the\ bed} \times \mathrm{cycle\ time}} \tag{26}$$

In addition to recovery and purity, avoided energy which is an indicator of the operation cost of the process for each condition was calculated by following equation:

$$\mathrm{Avoided\ Energy} = \frac{\sum_{i=1}^{i=s} \int_{t=0}^{t_{step}} \left(\frac{\gamma}{\gamma-1}\right) RT \left[\left(\frac{P_H}{P(t)}\right)^{\frac{\gamma-1}{\gamma}} - 1\right] \frac{1}{\delta} m(t)\,dt}{\mathrm{CO_2(moles)}\big|_{\mathrm{Heavy\ Product}} - \mathrm{CO_2(moles)}\big|_{\mathrm{Produced\ because\ of\ separation\ process}}} \tag{27}$$

In the above equation, s is the number of energy consuming steps. t_{step} is the total time of a specific step which the energy is calculated for. Recovered CO_2 moles are the CO_2 moles that are in the heavy product. Produced CO_2 moles because of CO_2 separation process are the moles of CO_2 produced in order to provide the electricity needed for the PSA for separating and concentrating CO_2 which is assumed to be 0.0052 (moles/kJ) which is equivalent to 0.83 (kg/kWh)[4]. γ is the ratio of heat capacities and has been considered to be 1.4 in all energy calculations in this work. $m(t)$ is the molar flow leaving the bed at time t. δ is the efficiency and has been assumed to be 85%. In the cycles studied in this work, energy consuming steps are CoD, CnD, LR1 and LR2. P_H for CoD step is 101.325 kPa, while P_H for the other three steps, were determined based on the cycle schedule; if the gas leaving the bed during of each of these steps was collected as heavy product, then P_H was equal to 137.86 kPa but if it was recycled back to the bed undergoing HR step, then the P_H was equal to the feed pressure (120.0kPa). $P(t)$ is the pressure at the downstream of the bed at time t.

2.5 Results and Discussion

Seven runs were carried out to investigate the effect of three parameters on the performance of each cycle; light reflux ratio (ω), heavy reflux ratio (λ) and vacuum pressure applied at the downstream of the bed during the cocurrent depressurization step (P_{CoD}). Conditions for runs 1-7 are summarized in table 2.3.

Results for runs 1-3 (effect of light reflux ration (ω)) are shown in figure 2.2 for cycles I and II. In both cycles higher ω resulted in higher recovery, indicating the effect of quantity of the purge gas. However the effect on the purity was not the same in the

cycles studied in this work; at higher ω, purity was higher in cycle I while it was lower in cycle II. This difference is due to the different steps that the heavy product is taken from in each cycle. In order to obtain a better understanding, bed profiles for CO_2 were plotted for throughput equal to 224.47 (L(STP)/kg/hr) and are shown in figure 2.3. Since the differences were not significant during the feed and LPP steps, these steps are not shown. Moles leaving the bed in CoD, CnD, and LR steps in table 2.4. In both cycles, at larger ω, more nitrogen-enriched gas is provided during the LR steps, thus CO_2 front gets closer to the heavy end (figure 2.3), and as result more CO_2 leaves the bed during the LR step(table 2.4). In cycle I, this stream is totally recycled to the bed undergoing the HR step. Therefore when more purge gas is provided, more CO_2-enriched gas enters the bed during the HR step, and pushes the CO_2 front towards the light end. This front will be furthered pushed towards the light end during the Eq and CoD step, and thus the bed is left with more CO_2 at the beginning of the CnD step. Consequently at higher LR ratios, during the CnD step more CO_2 leaves the bed with less amount of Nitrogen (table 2.4), in other words, the performance is improved in terms of both recovery and purity of CO_2. In cycle II the amount of recycled moles is less than cycle I for two reasons; most of the CO_2 has already desorbed and left the bed (during the LR1 and CnD) and the time of this step is shorter (25s) than LR step in cycle I (50s). Therefore even at higher ω the front of CO_2 remains close to the heavy end of the end. In this cycle, applying more light gas during the LR steps leads to lower recovery of CO_2 with lower purity during the CnD step (table 2.4). However since the stream exiting the bed during the LR1 step is also collected as the heavy product, the more the purge gas, the more CO_2 with more Nitrogen in the heavy product is produced during the LR1 step (table 2.4), causing the recovery to

increase and the purity to drop. As it can be seen in table 2.4, more light reflux, needs more energy, because the higher the amount of purge, the more gas should be compressed either to be recycled to the HR step or to be collected as the heavy product.

In both cycles at higher throughputs, the recovery of CO_2 is lower while the purity is higher. The reason for this is that at higher throughputs, a bigger amount of CO_2 enters the bed during the feed step with a fixed step time, so a larger fraction of the CO_2 that enters the bed does not adsorb and leave the bed through the light end. Overall at higher throughputs the CO_2 front is closer to the light end, causing more breakthrough of the CO_2 through the light end. On the other hand, at higher throughputs less amount of Nitrogen is remained in the bed as CO_2 gets closer to the light end, and therefore the purity is enhanced.

Results for runs 1, 4 and 5 and their corresponding bed profiles are shown figures 2.4 and 2.5 respectively. In both cycles, less amount of HR reflux resulted in lower purity. At higher λ values, since more CO_2 rich gas is recycled to the HR step, similar to the runs at a higher LR ratio, the CO_2 front is closer to the light end (HR step, figure 2.5), and therefore the purity of CO_2 is increased. Moreover since more CO_2 is taken as the heavy product at lower HR ratio, recovery of CO_2 is slightly higher at lower HR ratio. In terms of energy, more heavy reflux, needs more energy for compression during the CnD, and LR/LR1 steps in cycles I/II (table 2.4), and that causes the energy to increase.

Results for runs 1, 6-7 are shown in figure 2.6 and 2.7. The bed profiles for these runs are shown in figure 2.5. In cycle II, run 7, for the lowest throughput the goal of 90% recovery and 95 vol. % purity was achieved. In both cycles, lowering the CoD pressure, improves the purity while decreasing recovery. By lowering the P_{CoD}, more Nitrogen is

taken from the bed during the CoD step, in other words at lower CoD pressure, CO_2 front gets closer to light end and, more pure CO_2 is produced. However at the same time as the CO_2 reaches the light end and some CO_2 leaves the bed through the light end (CoD step in figure 2.7), and therefore the CO_2 recovery drops. In terms of energy, at lower CoD pressure, more energy is needed for the CoD step, but on the other hand during the CnD step, since fewer moles leave the bed (table 2.5) because the change in the pressure is lower, less energy is need. However when the partial pressure of the CO_2 is reduced by the presence of the purge gas in the LR steps, more CO_2 moles leaves (table 2.5) the bed and thus the energy of this step increases. Total energy is sum of the energies of the above steps, and the results of this part showed that the total energy increased with lowering the P_{CoD}, revealing that by lowering the CoD pressure, the amount of the additional energy needed during the CoD and LR steps is higher than the reduction in energy in the CnD step.

Based on the results of the parametric study, 3 more runs were carried out for each cycle. The conditions for each run are shown in table 2.6. In figure 2.2 it was shown that for cycle I run 3 met the goal of recovery and purity while runs with lower HR ratio (4, 5) had lower avoided energy (figure 2.4). Thus in runs 8-10, the goal was to improve runs 4 and 5 in terms of recovery and purity. To reach this goal, the effect of HR and LR ratios were both taken into account: lower HR ratio for lower energy, and higher LR ratio for reaching the desired recovery and purity of CO_2. The results are shown in figure 2.8. Runs 9 and 10 met the recovery and purity, and the energy for these two runs is lower compared to run 3. On the other hand, parametric studied showed that for cycle II, run 7 gave the needed recovery and purity but for low throughputs (figure 2.6) and also for the

higher throughputs the performance of run 6 was very close to the desired region of recovery and purity. Thus runs 8-10 were carried out in order to investigate the possibility of improving the throughputs and thus reducing the capital cost for this specific cycle; in run 8, the effect of lowering the LR ratio on the performance of run 6 (in order to improve the purity) and in runs 9 and 10, the effect of increasing the LR ratio on the performance of run 7 were investigated. Results are shown in figure 2.8. Only run 10, met the criteria for recovery and purity with throughputs slightly higher than throughputs in run 7. The energy is also slightly higher.

Parametric study showed that cycle I provided better performance in terms of purity whereas cycle II provided a better performance in terms of recovery. For the conditions that the cycles met the goal of 90% recovery and 95 vol. % purity, cycle I needed more energy (run 3) compared to cycle II (run 7). But it should also be noted that cycle I is a three bed system, and also it showed more throughput compared to cycle II which is a 4 bed cycle with lower throughputs. Overall the current study showed that the goal of 90% CO_2 recovery with a purity of 95 vol. % is obtainable with both these cycles; cycle I with higher operating cost and lower capital cost and cycle II with lower operating cost and higher capital cost.

2.6 Conclusions

Comparing the performance of two cycles studied here, showed that recoveries were higher in cycle II with more LR steps, and purities were higher in cycle I where heavy product was taken from CnD step (except for runs 4, and 5). The results obtained here indicates that applying more purge gas, and for a longer time, facilitates the

desorption of CO_2 but at the same time, more purge gas leads to lower purity. In both cycles recycling more either to the HR step, or LR step resulted in higher energy needed. It was seen that the amount of the CO_2 in the gas phase, in other words, the location and shape of the CO_2 front at the beginning of the counter current depressurization, plays an important role in the purity of the gas stream leaving the bed during this step. Also it should be taken into account if the CO_2 front gets too close to the light end, some CO_2 leave the bed through the light end, and thus the recovery drops. Overall this study showed that for the solid amine sorbent studied here, 90% recovery of the CO_2 with the 95 vol. % purity can be obtained using specific conditions for each of the cycles shown in this work. In terms of cost, cycle I showed lower capital cost and higher operating cost while cycle II showed capital cost and lower operating cost.

2.7 Tables

Table 2.1 Bed and adsorbent characteristics, gas properties and process condition

Bed and adsorbent characteristics	
Bed radius (m)	0.049
Bed length (m)	0.12
Bed porosity	0.36
Heat transfer coefficient (kW/m^2/K)	0.0
Pellet radius (m)	0.0014
Pellet density (kg/m^3)	1093.0
Pellet porosity	0.54
Pellet heat capacity (kJ/kg/K)	0.921
Species properties- nitrogen	
B_{1,N_2} (K)	2029.24
B_{2,N_2} (K)	0.09084
b^0_{1,N_2} (kPa^{-1})	5.7564×10^{-7}
b^0_{2,N_2} (kPa^{-1})	7.6048×10^{-6}
q^s_{1,N_2} (mol/kg)	0.8952
q^s_{2,N_2} (mol/kg)	7.2146
ΔH (kJ/mol)	14.84
k_{N_2} (s^{-1})	0.1
Species information-CO_2	
K_{1f0}(kPa^{-1}.min^{-1})	1.55×10^{-2}
E_{1f}(kJ.mol^{-1})	-3.68×10^{-1}
k_{1b0}(min^{-1})	7.43×10^{2}
E_{1b}(kJ.mol^{-1})	2.31×10^{1}
K_{2f0}(kPa^{-1}.min^{-1})	1.75×10^{-2}
E_{2f}(kJ.mol^{-1})	8.71
k_{2b0}(min^{-1})	2.01×10^{11}
E_{2b}(kJ.mol^{-1})	7.93×10^{1}
K_{3f0}(kPa^{-1}.min^{-1})	9.48×10^{-4}
E_{3f}(kJ.mol^{-1})	-1.39×10^{1}
k_{3b0}(min^{-1})	5.17×10^{10}
E_{3b}(kJ.mol^{-1})	7.80×10^{1}
N_{max}	3.79
K_α	3.12×10^{-2}
T_{FD}	2.85×10^{2}
α	1.51×10^{-1}
β	2.05×10^{-1}
Process Conditions	
CO_2 feed mole fraction	0.159
Feed temperature (K)	373.15
Wall temperature (K)	373.15
High pressure (kPa)	120.0
Low pressure (kPa)	5.0
Cycle time (s)	300.0

Table 2.2 Initial and boundary conditions for cycle I. f: final; C.M.B.: component mass balance; O.M.B.: overall mass balance; K.M.: kinetic model for CO_2; LDF.E: LDF equation, E.B.: energy balance; M.B.: momentum balance, V.E.: valve equation, 1: CO_2, 2: Nitrogen, Fv: Flow calculated with valve equation.

Feed	t = 0	$y_i=y_{i,LPP,f}$, $v_i=v_{i,LPP,f}$, $q_i=q_{i,LPP,f}$, $T=T_{LPP,f}$, $P=P_{LPP,f}$
	z/L = 0	$y_i=y_{i,Feed}$, $F=F_{Feed}$, 1=K.M., 2=LDF.E., $T=T_{Feed}$, M.B.
	z/L = 1	C.M.B., O.M.B., 1=K.M., 2=LDF.E., E.B., V.E. ($P_o=P_H$)
HR	t = 0	$y_i=y_{i,F,f}$, $vi=v_{i,F,f}$, $q_i=q_{i,Feed,f}$, $T=T_{Feed,f}$, $P=P_{Feed,f}$
	z/L = 0	$y_i=y_{LR} \mid z/L=1$, $F=-\lambda F_{LR} \mid z/L=0$, 1=K.M., 2=LDFE,
	z/L = 1	C.M.B., O.M.B., 1=K.M., 2=LDF.E., E.B., V.E. ($P_o=P_H$)
Eq	t = 0	$y_i=y_{i,HR,f}$, $v_i=v_{i,HR,f}$, $q_i=q_{i,HR,f}$, $T=T_{HR,f}$, $P=P_{HR,f}$
	z/L = 0	C.M.B., V.E. (Cv=0),1=K.M., 2=LDF.E., E.B., M.B.
	z/L = 1	C.M.B., O.M.B., 1=K.M., 2=LDF.E., E.B., V.E. ($P_o=P_{Eq}$)
CoD	t = 0	$y_i=y_{i,Eq,f}$, $v_i=v_{i,Eq,f}$, $q_i=q_{i,Eq,f}$, $T=T_{Eq,f}$, $P=P_{Eq,f}$
	z/L = 0	C.M.B., V.E. (Cv=0), 1 = K.M., 2 = LDF.E., E.B., M.B.
	z/L = 1	C.M.B., O.M.B., 1 = K.M., 2 = LDF.E, E.B., V.E.
CnD	t = 0	$y_i=y_{i,CoD,f}$, $v_i=v_{i,CoD,f}$, $q_i=q_{i,CoD,f}$, $T=T_{CoD,f}$, $P=P_{CoD,f}$
	z/L = 0	C.M.B., O.M.B., 1=K.M., 2=LDF.E., E.B., V.E. ($P_o=P_L$)
	z/L = 1	C.M.B., V.E. (Cv=0), 1=K.M., 2=LDF.E., $T=T_F$
LR	t = 0	$y_i=y_{i,CnD,f}$, $v_i=v_{i,CnD,f}$, $q_i=q_{i,CnD,f}$, $T=T_{CnD,f}$, $P=P_{CnD,f}$
	z/L = 0	$y_i=y_F \mid z/L=1$, O.M.B., 1=K.M., 2=LDF.E., E.B., V.E.
	z/L = 1	C.M.B., $F=-\omega F_{Feed} \mid z/L=1$, 1=K.M., 2=LDF.E, $T=T_F$, M.B.
Eq'	t = 0	$y_i=y_{i,LR,f}$, $v_i=v_{i,LR,f}$, $q_i=q_{i,LR,f}$, $T=T_{LR,f}$, $P=P_{LR,f}$
	z/L = 0	$y_i=y_{Eq} \mid z/L=1$,V.E. (Cv=0), 1=K.M., 2=LDF.E, E.B., M.B.
	z/L = 1	C.M.B., $F=-F_{Eq} \mid z/L=1$, 1=K.M., 2=LDF.E., $T=T_F$, M.B.
LPP	t = 0	$y_i=y_{i,Eq',f}$, $v_i=v_{i,Eq',f}$, $q_i=q_{i,Eq',f}$, $T=T_{Eq',f}$, $P=P_{Eq',f}$
	z/L = 0	$y_i=y_F \mid z/L=1$, V.E. (Cv=0), 1=K.M., 2=LDF.E, E.B., M.B.
	z/L = 1	C.M.B., $F=F_V$, 1=K.M., 2=LDF.E., $T=T_F$, V.E. ($P_o=P_H$)

Table 2.3 Initial and boundary conditions for cycle II. f: final; C.M.B.: component mass balance; O.M.B.: overall mass balance; K.M.: kinetic model for CO_2; L.D.F.E: LDF equation, E.B.: energy balance; M.B.: momentum balance, V.E.: valve equation, 1: CO_2, 2: Nitrogen, Fv: Flow calculated with valve equation.

Feed	t = 0	$y_i=y_{i,LPP,f}$, $v_i=v_{i,LPP,f}$, $q_i=q_{i,LPP,f}$, $T=T_{LPP,f}$, P=PLPP,f
	z/L = 0	$y_i=y_{i,F}$, $F=F_{Feed}$, 1=K.M., 2=LDF.E., $T=T_{Feed}$, M.B.
	z/L = 1	C.M.B., O.M.B., 1=K.M., 2=LDF.E., E.B., V.E. ($P_o=P_H$)
HR	t = 0	$y_i=y_{i,F,f}$, $vi=v_{i,F,f}$, $q_i=q_{i,Feed,f}$, $T=T_{Feed,f}$, $P=P_{Feed,f}$
	z/L = 0	$y_i=y_{LR} \mid z/L=1$, $F=-\lambda F_{LR} \mid z/L=0$, 1=K.M., 2=LDFE, $T=T_{Feed}$,
	z/L = 1	C.M.B., O.M.B., 1=K.M., 2=LDF.E., E.B., V.E. ($P_o=P_H$)
Eq	t = 0	$y_i=y_{i,HR,f}$, $v_i=v_{i,HR,f}$, $q_i=q_{i,HR,f}$, $T=T_{HR,f}$, $P=P_{HR,f}$
	z/L = 0	C.M.B., V.E. (Cv=0),1=K.M., 2=LDF.E., E.B., M.B.
	z/L = 1	C.M.B., O.M.B., 1=K.M., 2=LDF.E., E.B., V.E. ($P_o=P_{Eq}$)
CoD	t = 0	$y_i=y_{i,Eq,f}$, $v_i=v_{i,Eq,f}$, $q_i=q_{i,Eq,f}$, $T=T_{Eq,f}$, $P=P_{Eq,f}$
	z/L = 0	C.M.B., V.E. (Cv=0), 1 = K.M., 2 = LDF.E., E.B., M.B.
	z/L = 1	C.M.B., O.M.B., 1 = K.M., 2 = LDF.E, E.B., V.E. ($P_o=P_{CoD}$)
CnD	t = 0	$y_i=y_{i,CoD,f}$, $v_i=v_{i,CoD,f}$, $q_i=q_{i,CoD,f}$, $T=T_{CoD,f}$, $P=P_{CoD,f}$
	z/L = 0	C.M.B., O.M.B., 1=K.M., 2=LDF.E., E.B., V.E. ($P_o=P_L$)
	z/L = 1	C.M.B., V.E. (Cv=0), 1=K.M., 2=LDF.E., $T=T_F$
LR1	t = 0	$y_i=y_{i,CnD,f}$, $v_i=v_{i,CnD,f}$, $q_i=q_{i,CnD,f}$, $T=T_{CnD,f}$, $P=P_{CnD,f}$
	z/L = 0	$y_i=y_F \mid z/L=1$, O.M.B., 1=K.M., 2=LDF.E., E.B., V.E.
	z/L = 1	C.M.B., $F=-\omega F_{Feed} \mid z/L=1$, 1=K.M., 2=LDF.E, $T=T_F$, M.B.
LR2	t = 0	$y_i=y_{i,LR1,f}$, $v_i=v_{i,LR1,f}$, $q_i=q_{i,LR1,f}$, $T=T_{LR1,f}$, $P=P_{LR1,f}$
	z/L = 0	$y_i=y_F \mid z/L=1$, O.M.B., 1=K.M., 2=LDF.E., E.B., V.E.
	z/L = 1	C.M.B., $F=-\omega F_{Feed} \mid z/L=1$, 1=K.M., 2=LDF.E, $T=T_F$, M.B.
Eq'	t = 0	$y_i=y_{i,LR,f}$, $v_i=v_{i,LR,f}$, $q_i=q_{i,LR,f}$, $T=T_{LR,f}$, $P=P_{LR,f}$
	z/L = 0	$y_i=y_{Eq} \mid z/L=1$,V.E. (Cv=0), 1=K.M., 2=LDF.E, E.B., M.B.
	z/L = 1	C.M.B., $F=-F_{Eq} \mid z/L=1$, 1=K.M.,2=LDF.E., $T=T_F$, M.B.
LPP	t = 0	$y_i=y_{i,Eq',f}$, $v_i=v_{i,Eq',f}$, $q_i=q_{i,Eq',f}$, $T=T_{Eq',f}$, $P=P_{Eq',f}$
	z/L = 0	$y_i=y_F \mid z/L=1$, V.E. (Cv=0), 1=K.M. 2=LDF.E, E.B., M.B.
	z/L = 1	C.M.B., $F=F_V$, 1=K.M., 2=LDF.E., $T=T_F$ V.E. ($P_o=P_H$)

Table 2.4 Conditions for parametric study (runs 1-7) for cycles I and II.

Run	Throughput(L(STP)/kg/hr)	LR-Ratio(ω)	HR-Ratio($\underline{\lambda}$)	P_{CoD}(kPa)
1	224.47, 336.71, 448.95	0.0090	1.00	30.0
2	224.47, 336.71, 448.95	0.0045	1.00	30.0
3	224.47, 336.71, 448.95	0.0180	1.00	30.0
4	224.47, 336.71, 448.95	0.0090	0.75	30.0
5	224.47, 336.71, 448.95	0.0090	0.50	30.0
6	224.47, 336.71, 448.95	0.0090	1.00	20.0
7	224.47, 336.71, 448.95	0.0090	1.00	10.0

Table 2.5 Moles of CO_2 and Nitrogen leaving the bed and the corresponding energy needed during CoD, CnD and LR/LR1-LR2 steps in cycles I and II for throughput=224.47(L(STP)/kg/hr) in runs 1-7.

Run	CO_2 (moles)	Nitrogen	CO_2 (moles)	Nitrogen
	Cycle I		Cycle II	
		CoD		
1	0.0004	0.0103	0.0004	0.0103
2	0.0006	0.0102	0.0006	0.0102
3	0.0002	0.0103	0.0002	0.0103
4	0.0004	0.0103	0.0004	0.0103
5	0.0004	0.0103	0.0004	0.0103
6	0.0007	0.0133	0.0007	0.0133
7	0.0018	0.0160	0.0018	0.0160
		CnD		
1	0.0803	0.0050	0.0526	0.0069
2	0.0783	0.0051	0.0538	0.0068
3	0.0829	0.0048	0.0510	0.0069
4	0.0679	0.0057	0.0511	0.0070
5	0.0580	0.0063	0.0496	0.0070
6	0.0791	0.0027	0.0511	0.0039
7	0.0696	0.0011	0.0459	0.0012
	LR		LR1	
1	0.0569	0.0025	0.0307	0.0029
2	0.0520	0.0015	0.0267	0.0015
3	0.0636	0.0045	0.0355	0.0057
4	0.0506	0.0025	0.0302	0.0029
5	0.0454	0.0026	0.0297	0.0029
6	0.0600	0.0023	0.0315	0.0028
7	0.0634	0.0022	0.0345	0.0027
	-		LR2	
1	-	-	0.0081	0.0014
2	-	-	0.0066	0.0007
3	-	-	0.0098	0.0028
4	-	-	0.0080	0.0014
5	-	-	0.0079	0.0014
6	-	-	0.0083	0.0014
7	-	-	0.0094	0.0014

Table 2.6 Conditions for runs 8-10 for cycles I and II.

Run	Throughput(L(STP)/kg/hr)	LR -Ratio(ω)	HR -Ratio(λ)	P_{CoD}(kPa)
Cycle I				
8	224.47, 336.71, 448.95	0.0180	0.50	30.0
9	224.47, 336.71, 448.95	0.0180	0.75	30.0
10	224.47, 336.71, 448.95	0.0360	0.75	30.0
Cycle II				
8	224.47, 336.71, 448.95	0.0045	1.00	20.0
9	224.47, 336.71, 448.95	0.0180	1.00	10.0
10	224.47, 336.71, 448.95	0.0100	1.00	10.0

2.8 Figures

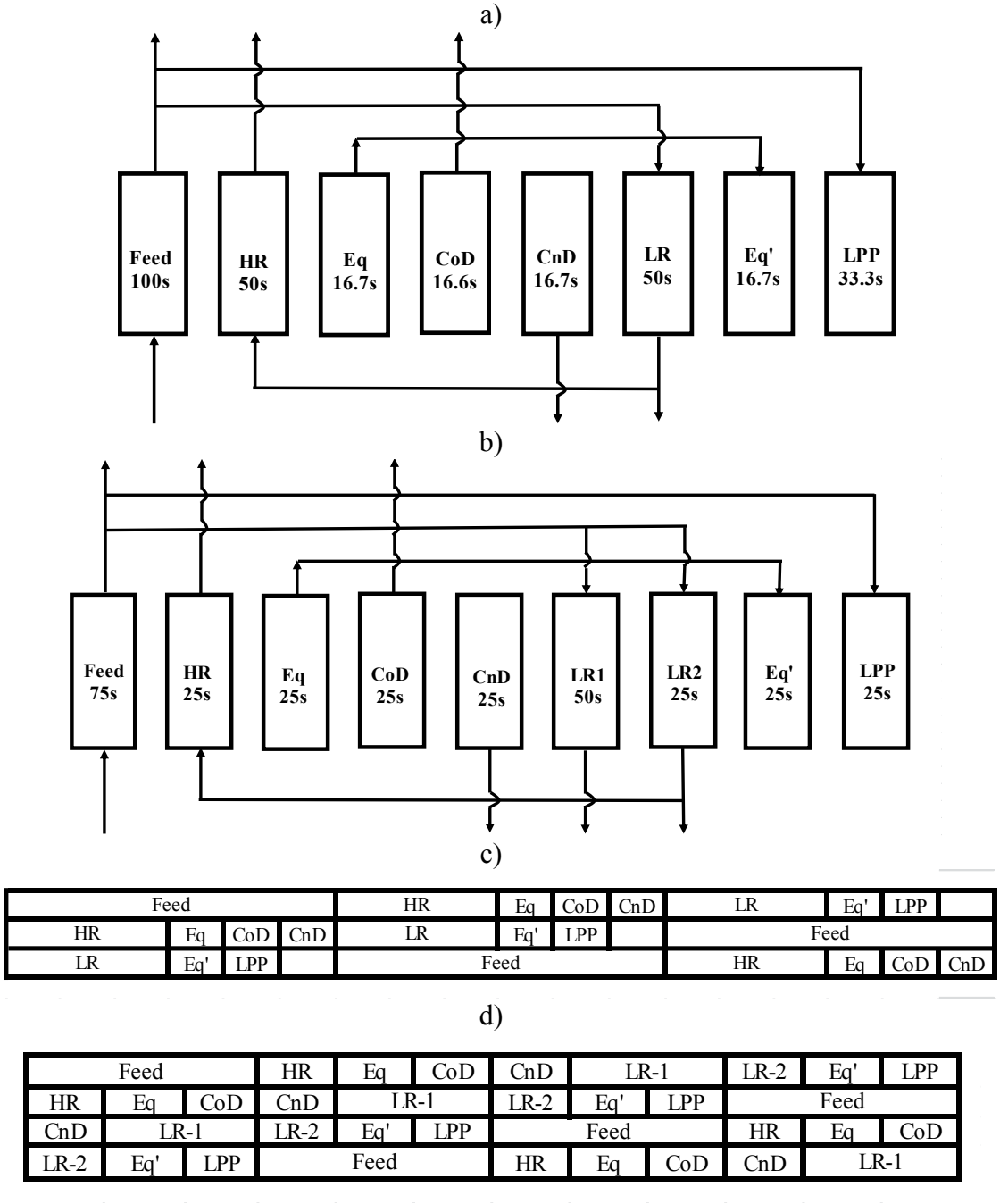

Figure 2.1 Cycle steps for a) cycle I and b) cycle II, and cycle schedule for c) cycle I and d) cycle II

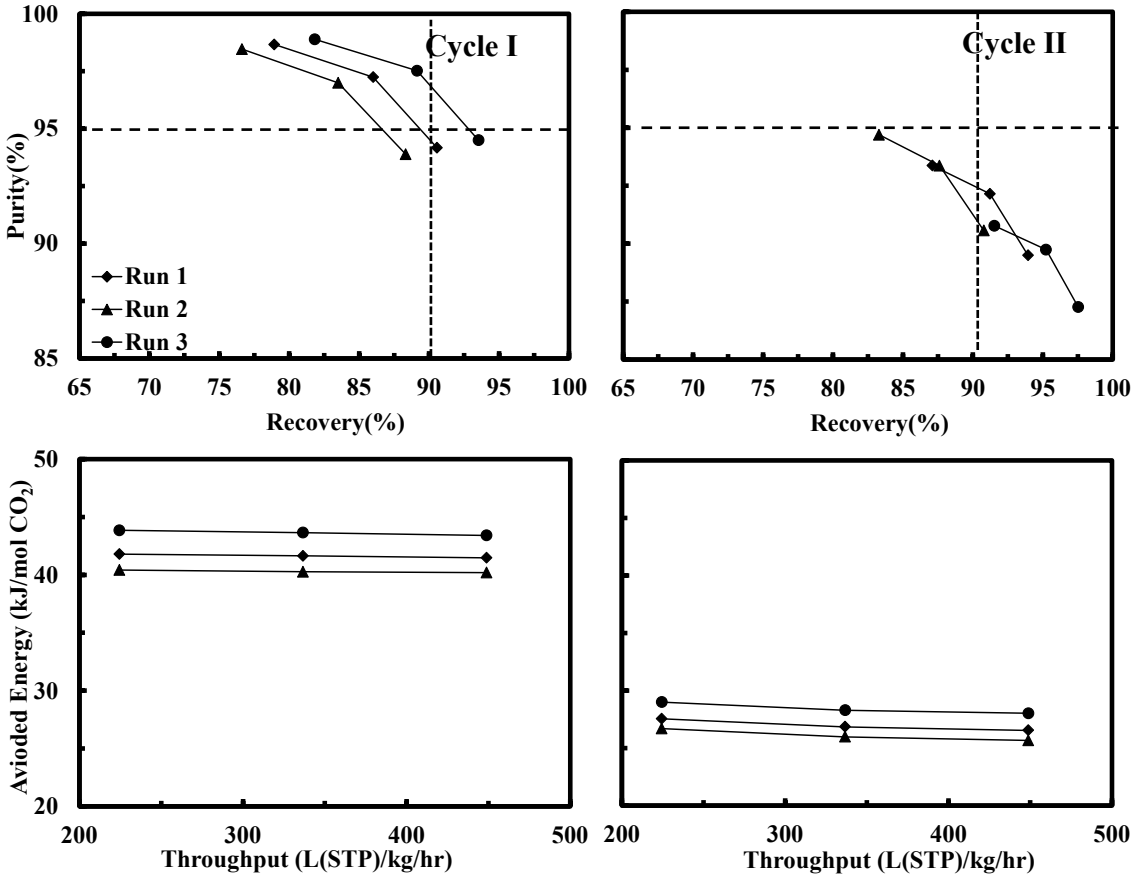

Figure 2.2 Results of runs 1-3 (effect of LR ratio (ω)) for cycles I and II.

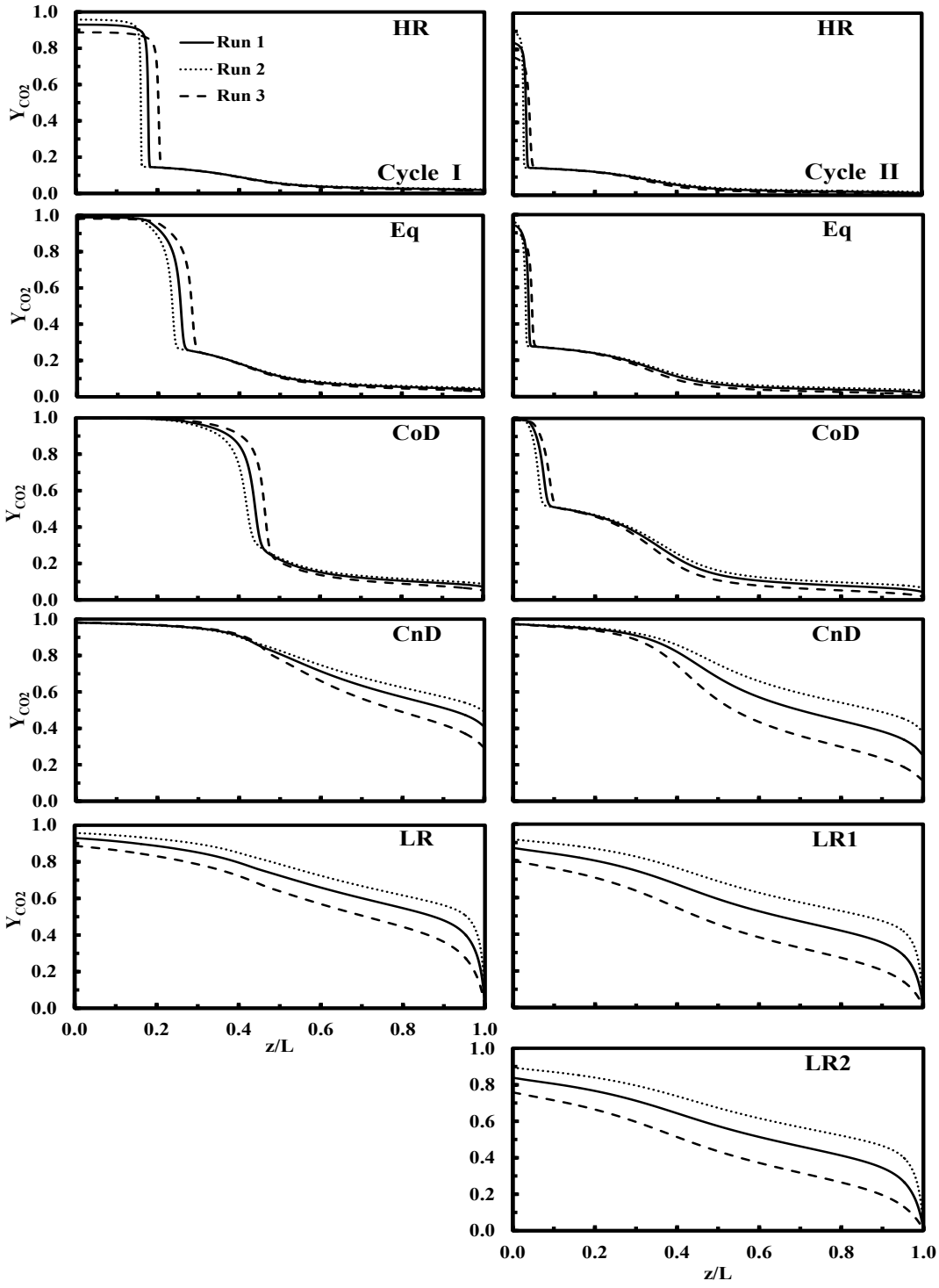

Figure 2.3 Bed profiles for throughput=224.47 (L(STP)/kg/hr) for runs 1-3, for cycles I and II.

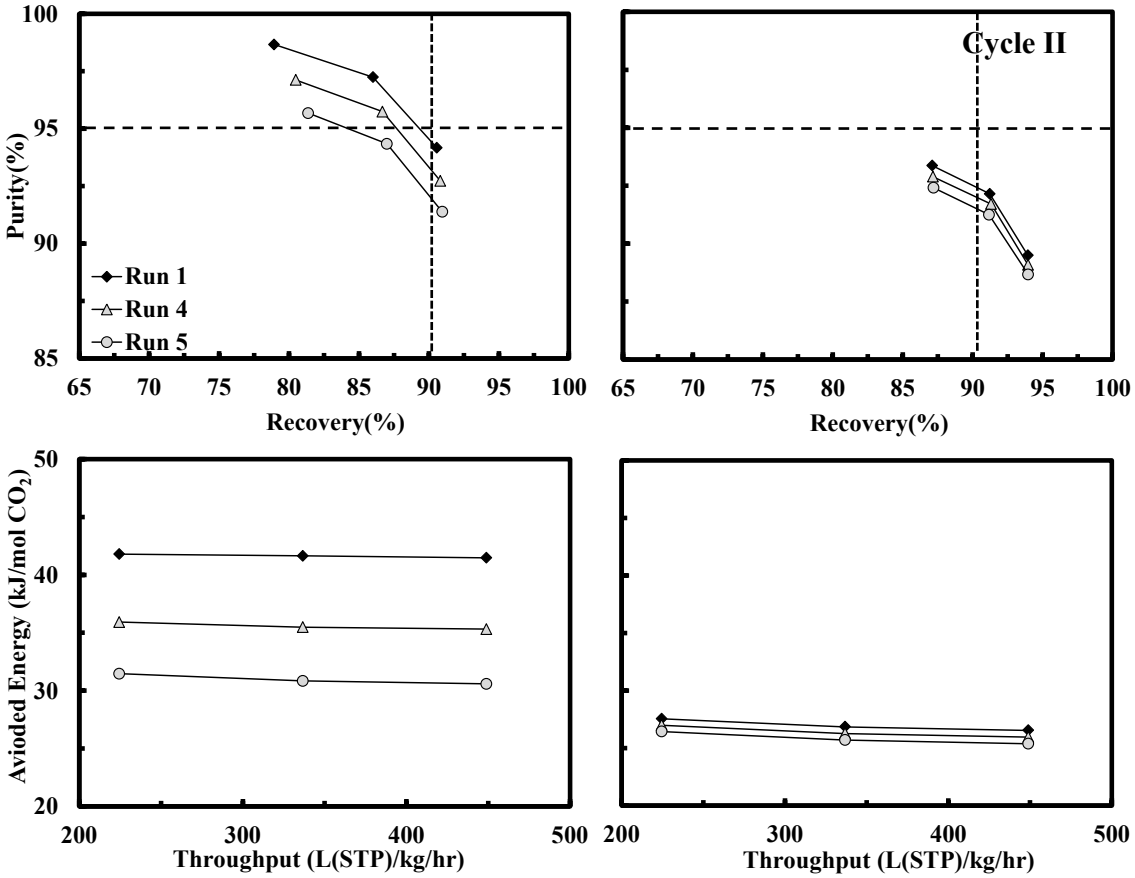

Figure 2.4 Results for runs 1, 4-5 (effect of HR ratio (λ)) for cycles I and II.

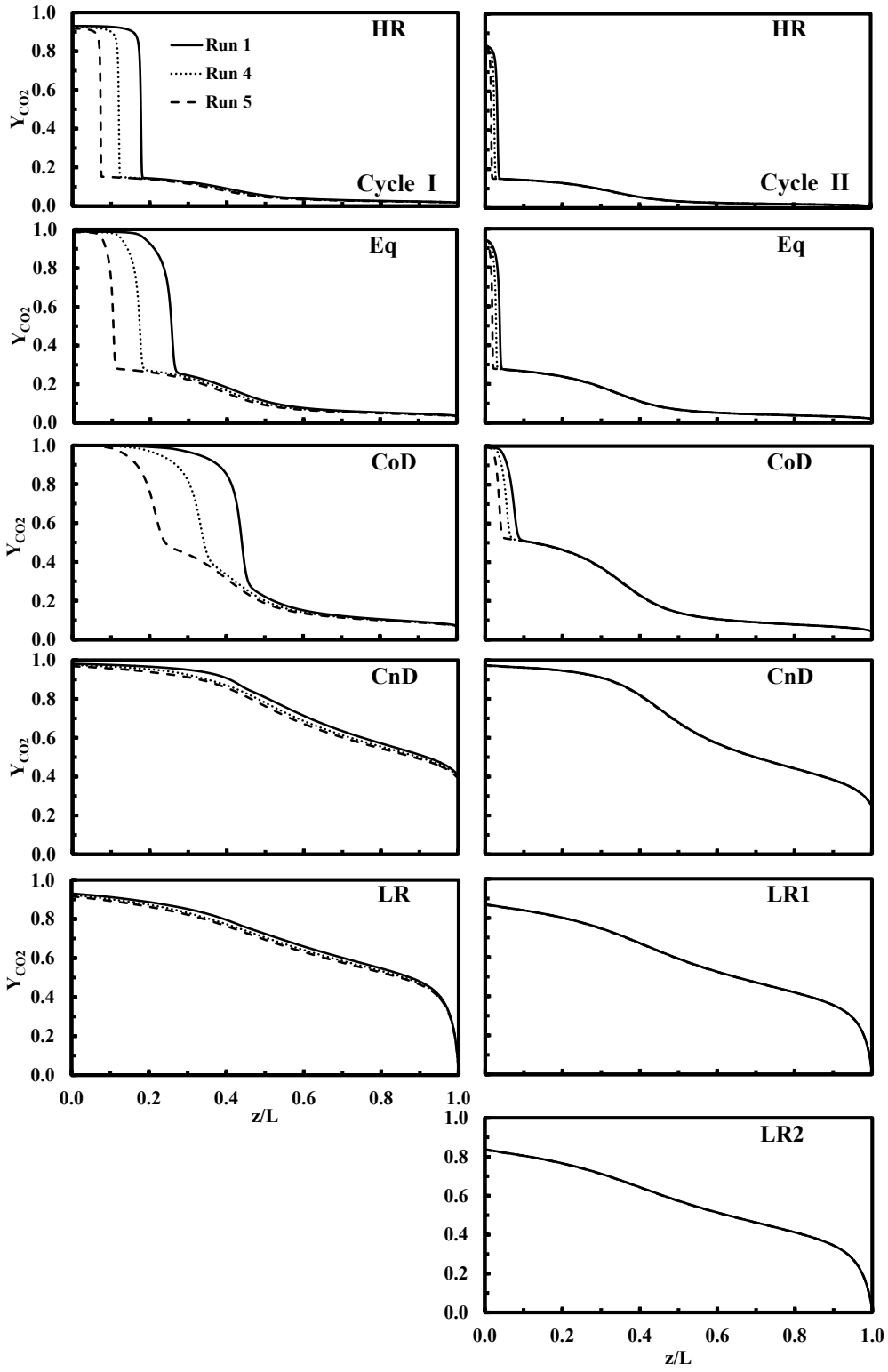

Figure 2.5 Bed profiles for θ=224.47 (L(STP)/kg/hr) for runs 1, 4-5, for cycles I and II.

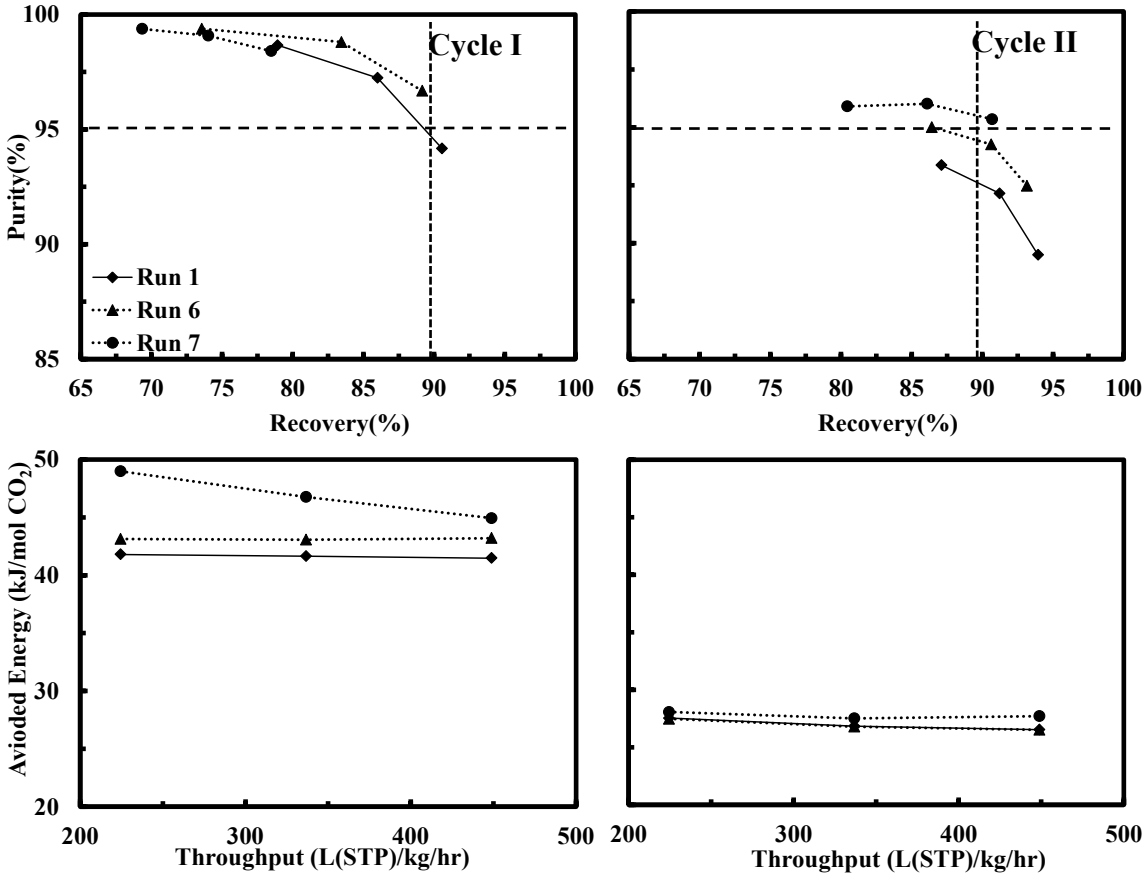

Figure 2.6 Results for runs 1, 6-7 (effect of P_{CoD}) for cycles I and II.

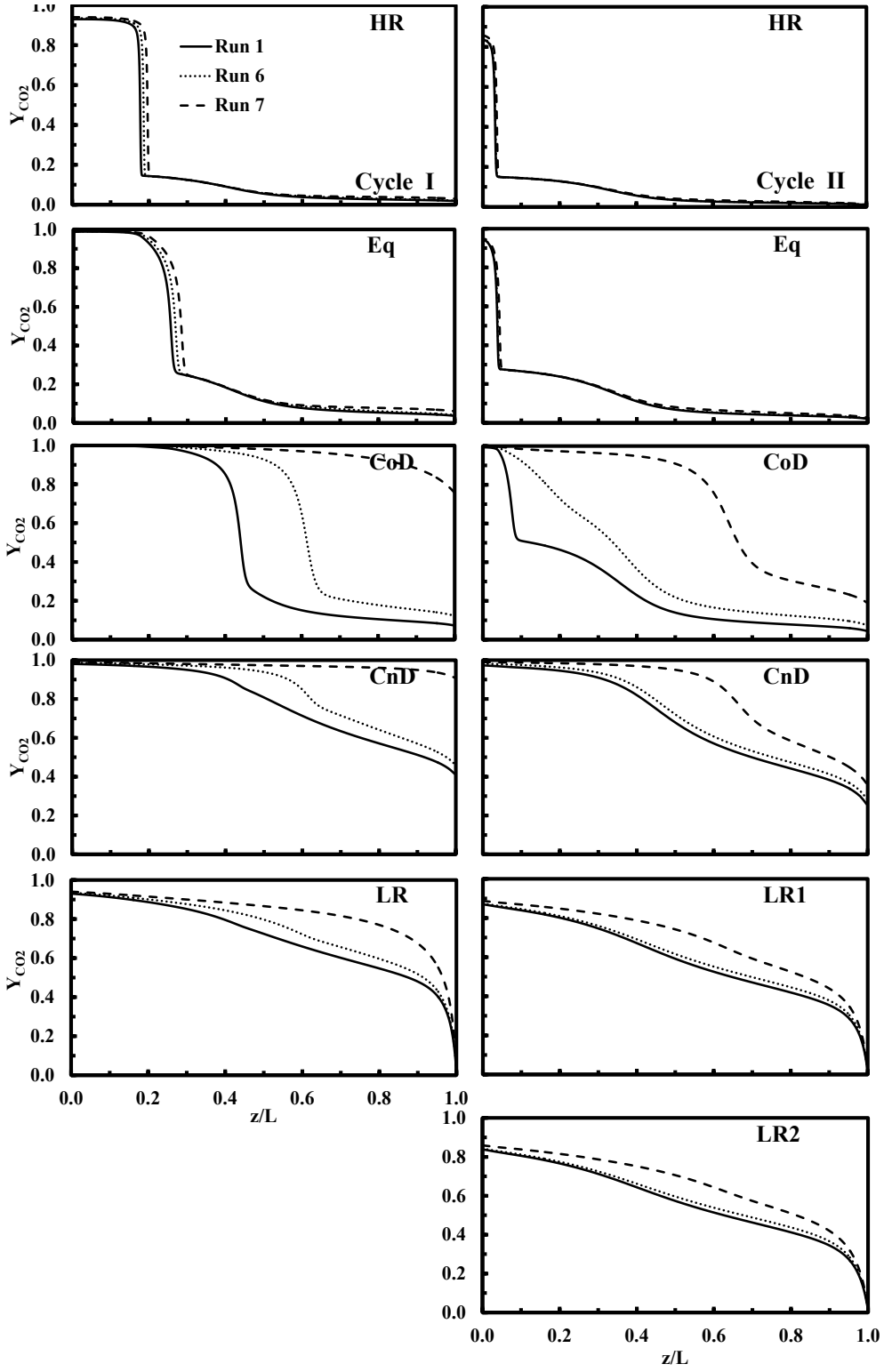

Figure 2.7 Bed profiles for θ=224.47 (L(STP)/kg/hr) for runs 1, 6-7, for cycles I and II.

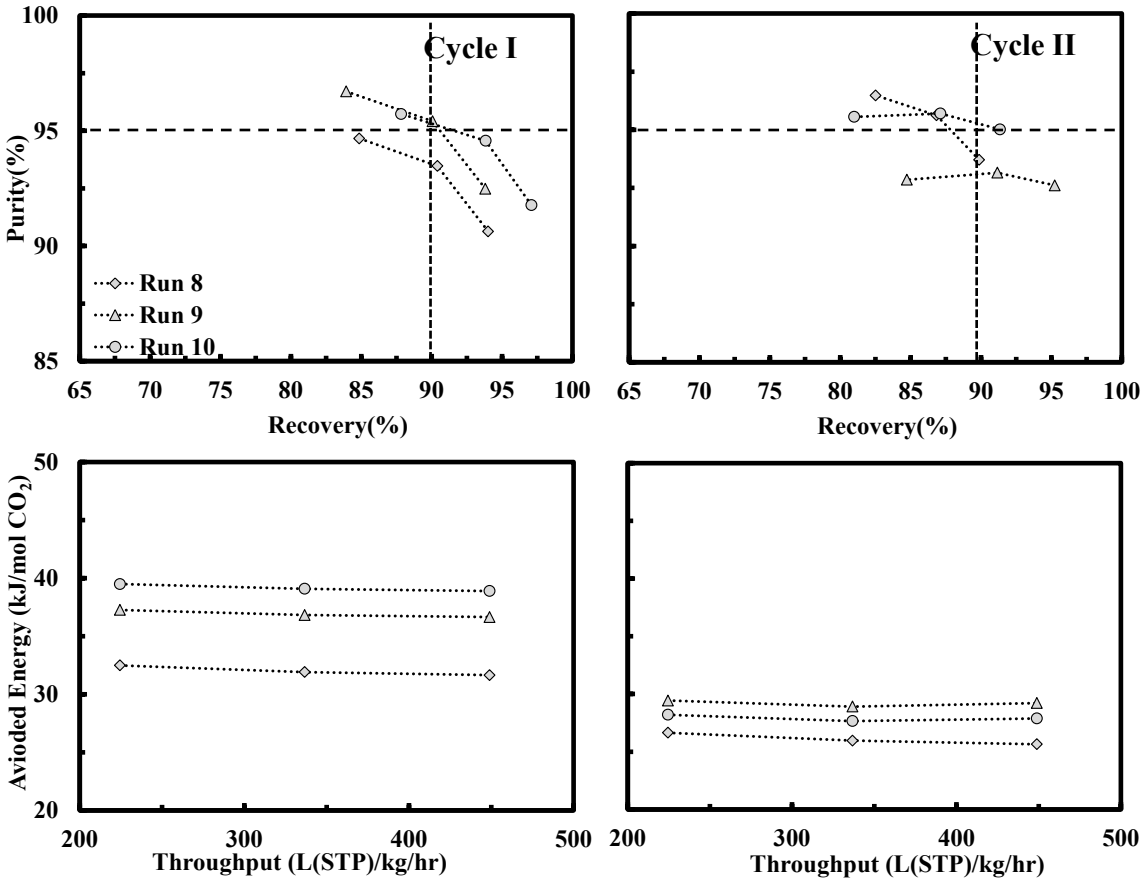

Figure 2.8 Results for runs 8-10 for cycles I and II.

CHAPTER 3

EFFECT OF WATER ON ADSORPTION AND DESORPTION OF CO_2 IN A SOLID AMINE SORBENT

3.1 Summary

Effect of water on the adsorption and desorption of CO_2 on a solid amine sorbent and vice versa was studied using thermo gravimetric method (TGA). The solid amine studied here was prepared by physically immobilizing PEI in a porous silica support. Studies were carried out at two concentrations of CO_2 (2 and 100 vol. %) in Nitrogen, one concentration of water (2 vol. %) and four temperatures: 40, 60, 80 and 100°C. More over a set of experiments were carried out to study the equilibrium at 40°C where the kinetics of the adsorption of CO_2 is very slow. Results obtained in this work showed that adsorption and desorption of water and CO_2 are independent at 100 and 80°C for both concentrations that studied. At lower temperatures however the presence of CO_2 affected the adsorption of water in two ways; enhancing the adsorption capacity of water and slowing down the kinetics of adsorption in the run where the sample was exposed to pure CO_2 prior to being exposed to water. The effect of water on the adsorption and desorption of CO_2 was only seen in the kinetics of desorption of CO_2 at 40°C. Overall the effect of water and CO_2 on each other's adsorption and desorption, if existed, were not significant.

3.2 Introduction

Solid amine sorbents have specific characteristics that have made them more attractive over other common adsorbents and thus several studies have been done on CO_2 adsorption on them. [3-8, 11-13, 15, 19-20, 22, 24-25, 27-32, 35-37, 70-83] Unlike liquid amines which are widely used for CO_2 capture, solid amine sorbents do not cause corrosion, and also they need less energy for regeneration.[25, 35] Moreover unlike zeolites which have a high working capacity for CO_2, but can be easily affected by the presence of water in the feed ,[2-3] solid amine sorbents can adsorb substantial amount of CO_2 in the presence of water. [3, 14, 16-17, 22, 63, 84, 85]

Based on the studies on the reaction between CO_2 and liquid alkanolamines; theoretically in the absence of water, CO_2 reacts with amine groups and forms carbamates. In this reaction, one mole of CO_2 needs two moles of amine to form one mole of carbamate. In the presence of water CO_2 reacts with water and amine groups and forms bicarbonate. Each mole of bicarbonate needs one mole of CO_2, one mole of water and one mole of amine. So, if the reaction between CO_2 and solid amines is similar to the reaction of CO_2 and liquid amines, in the presence of water, CO_2 adsorption capacity should be doubled.[38]

Water effects on the CO_2 adsorption on solid amines have been reported by several authors. Different amine types (PEI,[70-71, 12-13] TEPA/DEA,[32, 72-73] Triamine, [16-17, 19, 74, 84] APS & AEPAPS,[75] APTES,[76] 3-aminopropyltuethoxy-silane,[77, 63] N-[3-(trimethoxysilyl)propyl] diethylenetiramine,[78] APTS, [85] and different support types which are mostly Silica; MCM-41,[70-71, 21, 84] SBA-15, [12, 72, 75, 79-80, 82, 85] Silica gel,[13, 81] KIT-6,[73] HMS,[77-78] and PE-MCM-41 [16-17, 19, 32, 74, 84] at different temperatures (20-75°C) and

different concentrations of CO_2 (0.04-100%) have been studied. [7-8, 11-17, 19-22, 24, 27-32, 36-37, 63, 70-85] The methods used in these studies are not the same. Some authors have used thermograveimetric methods (TGA, TG-MS), [13, 19, 21, 32, 72, 78, 84] and some have used fixed beds and breakthrough curves.[13, 16, 19, 73, 79, 82,] As mentioned before according to reactions between CO_2 and liquid amines, water should increase CO_2 adsorption. However in the reported studies, some have reported a significant enhancement in CO_2 adsorption in the presence of water,[14, 63] while others reported a slight increase [12, 71, 74,, 21, 84] or even hindrance in CO_2 adsorption when water was present,[78] For example Xiaochun Xu et al. reported 50% more CO_2 adsorption on "molecular basket" adsorbent (MCM-41-PEI-50) in the presence of water at 75°C. Their feed composition was 14.9% CO_2, 4.25% O_2 and 80.85% N_2 for "dry" feed and was 12.61% CO_2, 3.56% O_2, 68.25% Nitrogen and 15.59% H_2O for "moist" feed.[71] In another work Norihito Hiyoshi et al. studied adsorption of CO_2 on different solid amines in the presence and absence of water. They grafted different amino silanes to SBA-15 at different amine surface densities. CO_2 adsorption capacity increased 0-30% at 60°C when water was present.[79] Gregory P. Knowles et al. showed when water was present; CO_2 adsorption was slightly less than the case when water was not present at 20°C.[78] Rodrigo Serna-Guerrero et al. showed that CO_2 capacity was higher in the presence of water for adsorption of 5% CO_2 in Nitrogen on aminopropyl-grafted pore expanded MCM-41 silica.[21] They also reported that CO_2 adsorbed more when relative humidity of the feed was higher. In another work, Youssef Belmabkhout et al. showed that at a higher relative humidity, CO_2 was adsorbed more compared to a lower relative humidity.[16] They studied adsorption of 0.04% CO_2 in Nitrogen on triamine-grafted pore expanded mesoporous silica at 25°C.

Since different authors have used different amines, supports, experimental methods both in material preparation and adsorption-desorption analysis, and various experimental conditions (feed concentration and temperature), it is not possible to predict what is the water effect on a specific solid amine sorbent unless by doing experiments on that sorbent at the desired conditions. In previous studies, Ebner et al.[3] showed that a solid amine sorbent made of polyethylenimine (PEI) impregnated on CARiACT® G10 is suitable for CO_2 capture from flue gas by using PSA. In this study effect of water on adsorption and desorption of CO_2 and vice versa on CARiACT® G10 solid amine sorbent was studied for two concentrations of CO_2: 100 and 2.0 vol. % and at four temperatures: 100, 80, 60, and 40°C using TGA. Since at 40°C, it takes a long time for CO_2 adsorption to reach equilibrium, additional experiments have been done at 40°C for studying the equilibrium. Water concentration whenever present was set to be 2.0 vol. %. Results obtained here reveal the role of water in CO_2 on the solid amine sorbent that is being considered for CO_2 capture from flue gas.

3.3 Experimental

The amine sorbent was prepared by immobilizing 40 wt% polyethylenimine on silica like solid support CARiACT® G10. Details of the method are given elsewhere.[3, 8] Effect of water on adsorption and desorption of CO_2 on the amine sorbent and vice versa were studied using a thermogravimetric analyzer (Perkin Elmer TGA-7). Figure 3.1 shows a schematic of the experimental set up which is similar to the setup used by Ebner et al.[3] Gas flow rates were set at 40 CC/min at 1 atm. Water was provided to the feed gas at 2.0 vol. % by using a Cole Parmer 74900 series syringe pump. In order to evaporate

the water exiting the needle, the port connecting the needle to the feed gas was kept at a temperature around 230°C using a heating band.

To investigate the interplay of CO_2 and water in adsorption on solid amine sorbent, two sets of experiments were carried out: "CO_2 Before/After" and "H_2O Before/After". The former was performed to study the adsorption and desorption of water in the presence of CO_2 and the adsorption and desorption of CO_2 in the absence of water. The later was done to analyze the adsorption and desorption of CO_2 in the presence of water and adsorption and desorption of water in the absence of CO_2. Each set was done at 2 concentrations: 100 and 2.0 vol. % and 4 temperatures: 40, 60, 80 and 100°C. Prior to every run, sample was regenerated at 100°C over-night in Nitrogen (UHP Grade, Airgas). Then temperature was adjusted to a desired temperature using a 5°C/min ramp. The sample was then kept in Nitrogen flow for 50 minutes for the weight to be stabilized. After that the experiment was started. Steps in each run are described below.

In "CO_2 Before/After", sample was exposed to CO_2 (UHP Grade, Airgas) for 40 minutes. Then water was injected into the CO_2 flow. At this point sample started to adsorb water in the presence of CO_2. After 40 minutes water flow was stopped while CO_2 flow was continued for another 40 minutes. This step was considered to investigate the desorption of water in the presence of CO_2. The feed was then switched back to Nitrogen and kept for 50 minutes in order to let the CO_2 to desorb while there was no water in the feed.

In "H_2O First/After" sorbent was first exposed to a flow of 2.0 vol. % in the Nitrogen for 40 minutes. Then Nitorgen flow was switched to CO_2 while keeping the water flow constant. CO_2 flow was continued for 40 minutes and then, it was switched

back to Nitrogen while water flow was kept the same for another 40 minutes. During this time CO_2 adsorbed and desorbed in the presence of water. The pump was then turned off and N_2 flow was kept for about 50 minutes. During this time water desorbed in the absence of CO_2.

At 40°C, the kinetic of adsorption is slower compared to higher temperatures[3]. Therefore another set of experiments was performed to analyze the effect of water on adsorption of CO_2 at equilibrium. This study was consisted of four runs, all with the same sample, in four consecutive days:

Day 1: "CO_2 Before-1"

Day 2: "H_2O Before"

Day 3:"CO_2 Before-2"

Day 4:"CO_2-Dry".

Before every run, sample was regenerated and activated similar to the runs described earlier. All the experiments were carried out for both 100 and 2.0 vol. % CO_2. Runs are explained below.

In "CO_2 Before-1", which was carried out in the first day, sample was exposed to CO_2 for 40 minutes, and then water was injected to the feed. Water and CO_2 flow was kept for about 3 hours. In "H_2O Before", water was injected to N_2 for 40 minutes and after that N_2 was switched to CO_2. Again water and CO_2 flow was continued for 3 hours. "CO_2 Before-2", which was done in day 3, is the same as "CO_2 Before-1". In "CO_2-Dry" no water was added to the system. The sample was exposed to CO_2 for more than 3 hours.

3.4 Results and discussion

TGA Results of "CO_2 Before/After" and "H_2O Before/After" are shown in figures 3.2 and 3.3 for 100 and 2.0 vol. % CO2, respectively. Results are displayed in terms of the total loading (weight % based on the adsorbent weight at t=0), whether it is due to CO_2, water or both, versus time. Each graph is divided into 5 sections which are corresponded to different gases that interacted with the sorbent during the experiment:

0-A: 50 min; Same for both runs: pure Nitrogen for both runs

A-B: 40 min; Pure CO_2 (figure 3.2)/2.0 vol. % CO_2 in N_2 (figure 3.3) in "CO_2 Before-After"; 2.0 vol. % H_2O in Nitroegn in "H_2O Before-After"

B-C: 40 min; Same for both runs: 2.0 vol. % H_2O in pure CO_2 (figure 3.2)/2.0 vol. % CO_2 in Nitrogen (figure 3)

C-D: 40 min; Pure CO_2 (figure 2)/2.0 vol. % CO_2 in Nitrogen (figure 3.3) in "CO_2 Before-After"; 2.0 vol. % H_2O in N_2 in "H_2O Before-After"

D-E: 40 min; Same for both runs: Pure Nitrogen

Figures 3.2-a, and 3.2-b show a same amount of loading at point C in both curves indicating that at 100 vol. % CO_2 and temperatures of 80 and 100°C the total loading is independent of the type of the gas (CO_2/water) interacting with the sample first, as expected merely from the thermodynamics point of view. However, the differences observed at the same point C and temperatures of 40 and 60°C (Figures 3.2-c, d) are most likely due to the much slower kinetics of water and the influence that the partial pressure CO_2 has on water adsorption as it is discussed later. Also, in all temperatures and runs, the loading at point E is bigger than the loading at point A. From still perceivable values at 100^{o}C (3.2-a), the difference between the two points becomes more pronounced as the

temperature decrease with expectedly lower desorption kinetics. It is particularly interesting that at 100 and 80°C both curves merged into one curve forming a plateau right before point E. This plateau indicates the existence of a species remaining in the sorbent desorbing at a very slow kinetic. At 80°C the difference between point E and A is identified as δ_2 (Figure 3.2-b). By inspecting the "H_2O Before-After" in the same figure, it is apparent that the loadings at points D and B are identical at both 100 and 80°C indicating that the adsorption of CO_2 occurring in B-C has been fully and reversibly desorbed by point D and that whatever is left remaining in the sample is just very slowly desorbing water. Unless there is any non-apparent evidence to the contrary, it can be concluded that at these higher temperatures no CO_2 remains in the sample at point E in any of the two runs. In other words that the difference identified by δ_2 (Figure 3.2-b) is solely due to undesorbed water. In fact, it is noteworthy that the difference between loadings at points D and B in the "CO_2 Before/After" run (identified as δ_1 in figure 3.2-b) at both 80 and 100°C matches exactly in magnitude with δ_2, also indicating that the observed difference δ_1 is also solely associated with undesorbed water. The differences observed between both curves at by point E at temperatures of 40 and 60°C, also analyzed and discussed in more detail later, are ascribed to the influences on CO_2 on the loadings and kinetics adsorption/desorption of water mostly and some small influence of water on CO_2 kinetics at 40°C.

Identical conclusions can be reached from the results obtained with 2.0 vol. % CO_2 (Figure 3.3), except for the obvious fact that in this case the observed loadings of CO_2 were lower. The unique difference between the results of Figure 3.3 with those in Figure 3.2 is that both curves in Figure 3.3 at all temperatures tend to match at point C,

even at 40°C. This result suggests the existence of faster adsorption kinetics when in the presence of a lower gas concentration of CO_2, i.e., 2.0 vol. % versus 100%. Is indicated earlier, the observed kinetics leading to point C will be later associated with the kinetics of water alone.

In order to obtain a better understanding of the nuances behind the differences between the two curves in figures 3.2 and 3.3, the results shown will be re-plotted differently to capture and compare in both runs the dynamics of adsorption of the sample right after is exposed with CO_2 in the feed and the dynamics of desorption of the sample right after is no longer exposed with CO_2 in the feed. To achieve this, two sections of the curves in figures 3.2 and 3.3 are to be compared: 1) the dynamics of adsorption between points B and C for the "H_2O Before/After" curve against the dynamics of adsorption between points A and B for the "CO_2 Before/After" curve and 2) the dynamics of desorption between points C and D for the "H_2O Before/After" curve against the dynamics of desorption between points D and E for the "CO_2 Before/After" curve. This was done in figures 3.4 through 3.7, which respectively represent the results at 100, 80, 60 and 40°C, according to the following procedure:

For adsorption and for the "CO_2 Before/After" curve: loadings between points A and B minus the loading at point A in figures 3.2 and 3.3. For adsorption and for the "H_2O Before/After" curve: loadings between points B and C minus the loading at point B in figures 3.2 and 3.3. These results are shown in figures "3.4a, 3.5a, 3.6a and 3.7a" for the results in Figures 3.2 and figures "3.4c, 3.5c, 6c and 3.7c" for the results in Figures 3.3

For desorption and for the "CO_2 Before/After" curve: loadings between points D and E minus the loading at point E in figures 3.2 and 3.3; for desorption and for the "H_2O Before/After" curve: loadings between points C and D minus the loading at point D in figures 3.2 and 3.3. These results are shown in figures "3.4b, 3.5b, 3.6b and 3.7b" for the results shown in Figures 3.2 and figures "3.4d, 3.5d, 3.6d and 3.7d" for the results shown in Figures 3.3

The resulting results represent for most part adsorption and desorption of CO_2 in the absence and presence of H_2O in the gas phase. For this reason, the results corresponding to "CO_2 Before/After" are labeled as "in the absence of water", while the results corresponding to "H_2O Before/After" are labeled as "in the presence of water". It must be noted however, that water may still be present and undergoing desorption in the sample during the desorption plots of the "in the absence of water" curves. Also, for a better comparison, both curves in each graph were shifted in time in such a way that they both started from the same point.

Figure 3.4 shows an excellent overlap at 100^oC between the two curves in both adsorption and desorption at both 100 and 2.0 vol. % CO_2. This shows that the changes observed in figure 3.4 are very likely due that solely due to CO_2. In other words, that at this temperature water plays no role on both the thermodynamics and the kinetics of adsorption of CO_2. Because it was shown earlier that the total loading at point C and total desorption at point E in figures 3.2-a and 3.3-a were the same regardless of the type of gas (CO_2/H_2O) fed to the TGA first, the total loading of water at point C is also the same for both curves. This leads us to believe that at 100°C the adsorption and desorption of water and CO_2 occur via independent mechanisms.

Figure 3.5 shows that identical conclusions derived from 100°C can also be reached at 80°C for both 100 and 2.0 vol. % CO_2. Save for a very minor difference between the desorption curves of the 100 vol. % of CO_2 (figure 3.5-b), wherein the "in the absence of water" water being a bit faster at the beginning, both curves overlap quite well during both adsorption and desorption. However, when analyzing the results of Figure 3.5 in reference to results in figures 3.2 and 3.3, figure 3.3-b shows that a small difference between both curves between points B and C. Because of the very good agreement between the two curves in figure 3.5, it is speculated that the observed difference lies in differences on the kinetics of adsorption for water between the two curves.

At 60°C (Figure 3.6), perceivable differences between curves become noticeable. In particular, more loading in the adsorption curves are observed when water is present (figure 3.6-a, c). However, no apparent difference is seen during desorption between the two runs (figure 3.6-b, d). The almost exact overlap between the curves during desorption indicates no influence of water on CO_2 desorption dynamics. Since the desorption rate is related to the amount of loading, the identical desorption rates, as it is easily concluded from the perfect overlap of the curves, entail the presence of identical loading of CO_2 in both cases. This result leads to the conclusion that also the same amounts of CO_2 were adsorbed in both curves during adsorption and hence that the additional loadings observed in figures 3.6-a, 3.6-d were due to only to water. In other words, at this temperature, while CO_2 adsorption both in terms of thermodynamics and kinetics is still not influenced by the presence of water, the presence of CO_2 instead does influence the adsorption of water in the form of higher loadings. To further analyze the

effect of CO_2 on water adsorption, the results in figure 6 are contrasted against results in figures 3.2-c and 3.3-c. For 100 vol. % CO_2 (figure 3.2-c) the increase in loading between point B and C in the "CO_2 Before/After" curve is similar to the increase in loading between points A and B in the "H_2O Before/After" curve ($\delta_3 \approx \delta_4$), but with a slope that is clearly shallower and depicting a process still ongoing. However, this is not the case for the 2.0 vol. % CO_2 (figure 3.3-C), where the concentration of CO_2 is significantly smaller. The loading at point C is the same for both runs, and apparently already at equilibrium. Given that the adsorption of CO_2 is the same for both curves, and that further water uptake took place in BC (Figure 6), $\delta_3 > \delta_4$ in figure 3.3-c. It is clear, then, that at 60^oC, the presence of CO_2 enhances the loading of water while negatively affecting its kinetics at elevated concentrations. It must be observed, however, that this negative influence that CO_2 on the adsorption kinetics of H_2O is not so much the result of the presence of abundant amount gas CO_2 molecules but more apparently due to a phase of adsorbed CO_2 that is already in place. Figure 2-c shows how that for 100 vol. % CO_2 the "H_2O Before/After" curve between points B and C rapidly reaches a plateau evidencing quick kinetic towards thermodynamic equilibrium and yet the gas phase concentrations of CO_2 are as equally high as that the "CO_2 Before/After" curve. The difference between the two curves then lies in the fact that for the "CO_2 Before/After" curve the sample has already been exposed to CO_2 for 40 minutes and very close to if not at equilibrium. It is hypothesized that the adsorbed CO_2 serves as a hindrance to water adsorption. Such hindrance seems not to occur when water is first to adsorb as with the "H_2O Before/After" curve of when the loading of CO_2 are not due to significant concentration of CO_2, i.e., 2.0 vol. %.

At 40°C, differences between the two runs during can be observed for both adsorption and desorption (figure 3.7). A comparison of the desorption curves shows that the initial amount right before desorption and total amount of desorbed are not much different, however. Much of the observed discrepancies are in terms of kinetics. In this regard, the "in the presence of H_2O" curves showed a little higher slope, and hence fast kinetics, during the first 15 minutes of desorption, suggesting that water does show a slight positive influence on its desorption kinetics of CO_2. Aside from this, it is still apparent that even at this temperature, water does not play much role on the thermodynamics of adsorption of CO_2, i.e., no changes on the overall adsorption of CO_2 is the same in both "H_2O Before/After" and "CO_2 Before/After" curves. Because of this the same conclusions reached at 60^oC regarding the differences of loadings observed between the curves in figures 3.7-a and 3.7-c being attributed solely to water. At this temperature, however, the differences are more pronounced. However, when comparing these results in reference to those in figure 3.2-d and 3.3-d, the kinetics of adsorption for water is also affected by adsorbed CO_2 that is already in place even at 2.0 vol. %. It must be observed in figure 3.3-d how different the slope of the "CO_2 Before/After" curve between points B and C is with respect that of the "H_2O Before/After" curve between points A and B, and observed how the much faster the latter reaches equilibrium between point B and C. Indeed unlike the "H_2O Before/After" curve right before points B and C, wherein the sample seems in equilibrium, the "CO_2 Before/After" curve at point C shows that adsorption is still on going. The same is to be said with results with 100 vol. % of CO_2 but with an effect on the kinetics of adsorption of H_2O being even more important (3.2-d). While at 2.0 vol. % CO_2, both curves almost coincide at point C (figure 3.3-d), at

100 vol. % CO_2, the "CO_2 Before/After" curve remains significantly below the curve "H_2O Before/After". Because at loadings are still increasing at point C (figures 3.2-d and 3.3-d), it is not clear, if given longer time, whether both curves would overlap at equilibrium. For this reason a set of new four runs identified as "CO_2 Before-1", H_2O Before", "CO_2 Before-1", "CO_2 dry" were carried out. For these runs, the same sample was used, which was regenerated between runs. These results are shown in figure 8, which contains two graphs (one for 100 vol. % CO_2 and another for 1.7 vol. % CO_2) showing a period of 320 min divided in the following three sections:

0-A: 50 min; same for all 4 cases: pure Nitrogen

A-B: 40 min; 2.0 vol. % water in N_2 in "H_2O Before"; 100 vol. % CO_2 (figure 3.8-a)/2.0 vol. % CO_2 (figure 3.8-b) in "CO_2 Before-1", "CO_2 Before-2", and "Dry CO_2"

B-C: 230 min; 2.0 vol. % water in 100 vol. % CO_2 (figure 3.8-a)/2.0 vol. % CO_2 (figure 3.8-b) in "CO_2 Before-1", "H_2O Before", and "CO_2 Before-2"; 100 vol. % CO_2 (figure 3.8-a)/2.0 vol. % CO_2 (figure 3.8-b) in "Dry CO_2"

The almost exact overlap between "CO_2 Before-1" and "CO_2 Before-2" for the entire period of 320 min, or the overlap of between these two together with that of "Dry CO_2" between points A and B, shows the excellent repeatability of the experiments. The major differences are observed between points B and C between curves "CO_2 Before-1", "CO_2 Before-2" on one side and the curve "H_2O Before" on the other. These differences, however, become less pronounced with both time and lower concentration of CO_2. Unlike the case of 100 vol. % CO_2 (figure 3.8-a), all three curves are close to overlapping at point C with 2.0 vol. % CO_2 (figure 3.8-b). Because it has been shown that the amount adsorbed CO_2 is not influenced by the presence of water, the difference between any of

these three curves and "CO_2 dry" corresponds entirely to water. In consequence, the discrepancies between points B and C, and in particular at point C in figure 3.8-a, are due to differences in the kinetics of adsorption for water. Such differences find their explanation in the very same reasons alluded earlier when discussing results at 60 and 40^oC in figures 3.2 and 3.3: the kinetics of adsorption for water is significantly affected when samples have previously been loaded with adsorbed CO_2. The fact that there is persisting difference between "CO_2 Before-1" and "CO_2 Before-2 curves and the "H_2O Before" curve in Figure 3.8-a, is likely due sites that H_2O does not have easy access to. On the other hand, Figure 3.8 shows once again that CO_2 has a positive influence on the amount of water adsorbed: under both concentrations of CO_2, the loadings of water increased in the presence of CO_2. The loading attributable to water in the "H_2O Before" curve at point C (δ_5), is larger than the difference between points A and B for the same curve (δ_6).

3.5 Conclusions

This study was carried out to study the effect of water on adsorption and desorption of CO_2 and vice versa on silica based solid amine sorbent consisting on 40 wt% polyethylenimine physically supported on CARiACT® G10. Experiments were investigated for two concentrations of CO_2: 100 and 2.0 vol. % and one concentration of water: 2.0 vol. % at four temperatures: 100, 80, 60, and 40°C using TGA. At the conditions studied in this work, water did not have any effect on the thermodynamics of adsorption of CO_2 and barely affected its kinetics during desorption at 40^oC. On the other hand, the results showed that CO_2 has an important effect in both thermodynamics and

kinetics of adsorption of water at 60 and 40°C. No effect of CO_2 on H_2O was observed at 100 and 80°C, which strongly suggests that at these temperatures the two gases adsorbed through independent mechanisms. The impact of CO_2 on the adsorption H_2O at the two lowest temperatures is both positive and negative. On the positive side, the presence of CO_2 enhanced the adsorption of water and this was more pronounced at lower temperature. On the negative side, the pre-existence of adsorbed CO_2 had a significant role in reducing the kinetics of adsorption of water. Such impact was more significant at lower temperatures and higher preexistent loadings of CO_2 as in the latter case the detrimental effect on H_2O was more pronounced for the cases 100 vol. % was used. However, the results also show that when CO_2 is adsorbed in the presence of H_2O, CO_2 did not show any impact on the kinetics of adsorption of H_2O. Since water did show enhancement in the presence of CO_2, it is speculated that a type of reactive mechanism takes place between the two species. If such reaction did take place , it was not one that enhanced the adsorption of CO_2, contrary to what has been suggested by many aothors.[12, 14, 16, 38, 70, 73, 77, 80-81, 84-85,]. At any rate, at none of the conditions studied here, the observed effects whenever existed were significant.

3.6 Figures

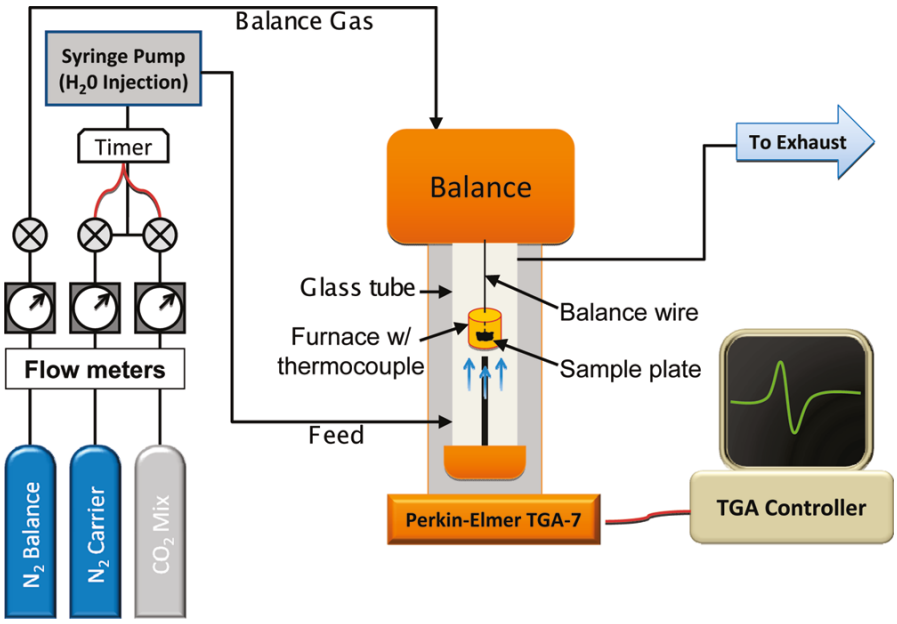

Figure 3.1 Experimental setup[3]

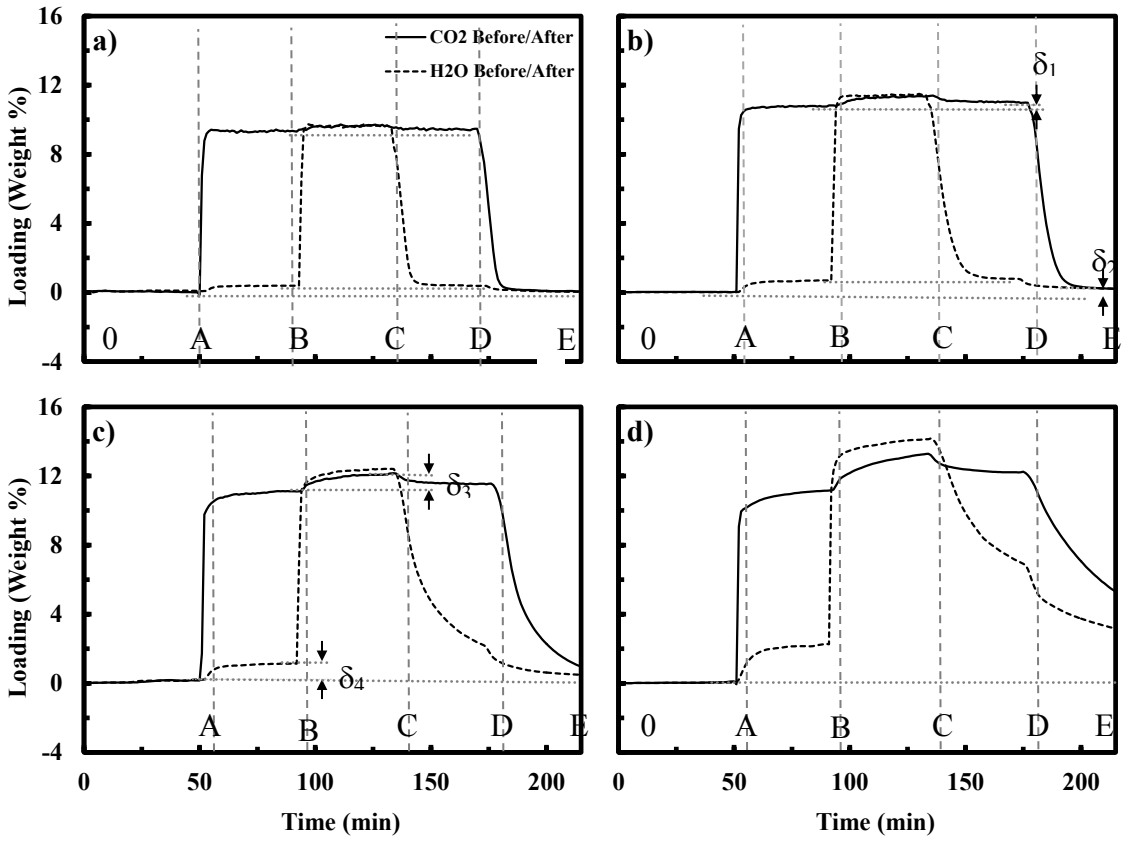

Figure 3.2- Adsorption and desorption of 2 vol. % water and 100 vol. % CO_2 in Nitrogen on CARiACT G10 solid amine sorbent at a) 100°C, b) 80°C, c) 60°C and d) 40°C

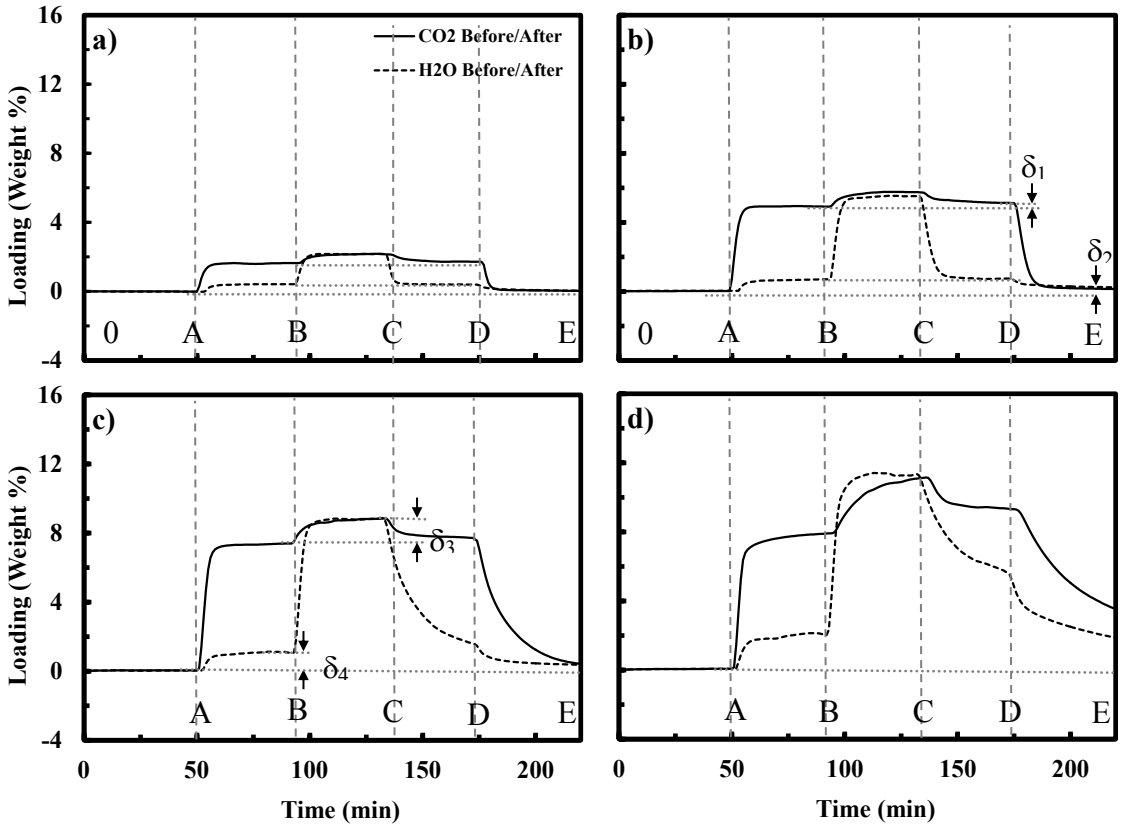

Figure 3.3 Adsorption and desorption of 2 vol. % water and a mixture of 2.0 vol. % CO_2 in Nitrogen on CARiACT G10 solid amine sorbent at a) 100°C, b) 80°C, c) 60°C and d) 40°C

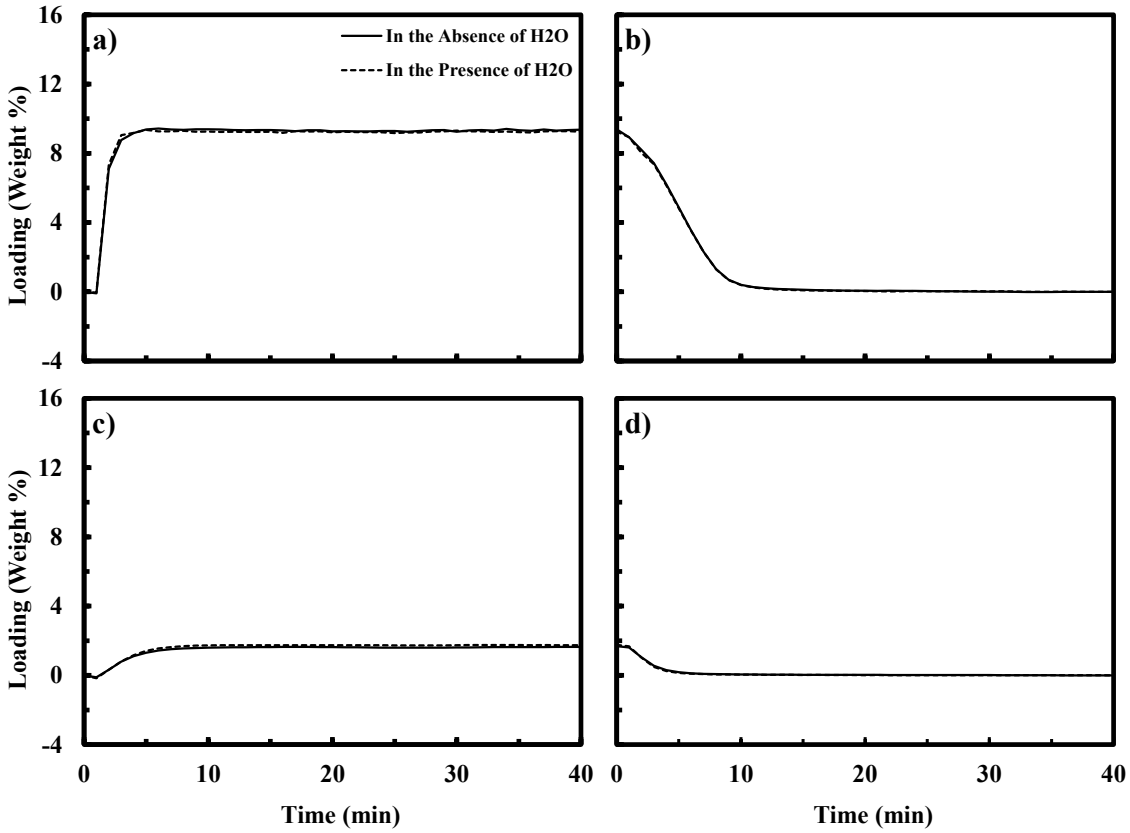

Figure 3.4 TGA Loading in the presence and absence of 2 vol. % water water at 100°C for a) adsorption of 100 vol. % CO_2, b) desorption at of 100 vol. % CO_2, c) adsorption of 2.0 vol. % CO_2, d) desorption of 2.0 vol. % CO_2 in Nitrogen

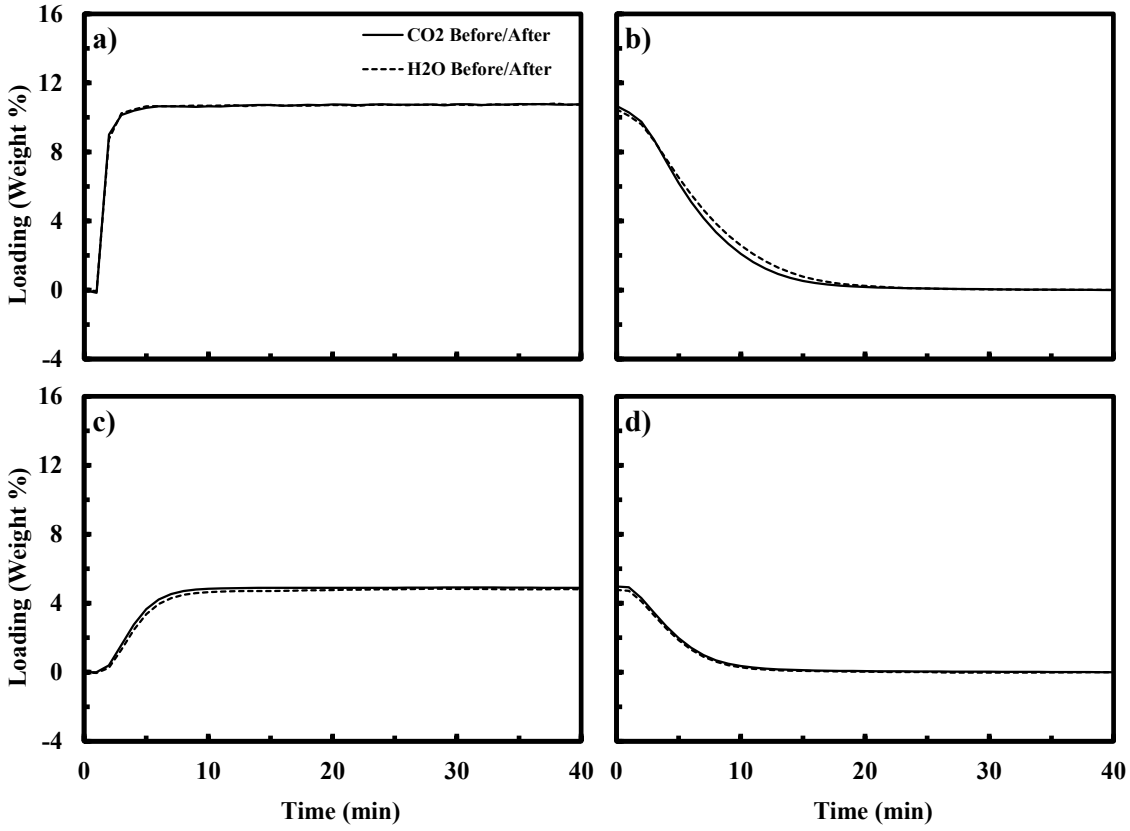

Figure 3.5 TGA Loading in the presence and absence of 2 vol. % water at 80°C for a) adsorption of 100 vol. % CO_2, b) desorption at of 100 vol. % CO_2, c) adsorption of 2.0 vol. % CO_2, d) desorption of 2.0 vol. % CO_2 in Nitrogen

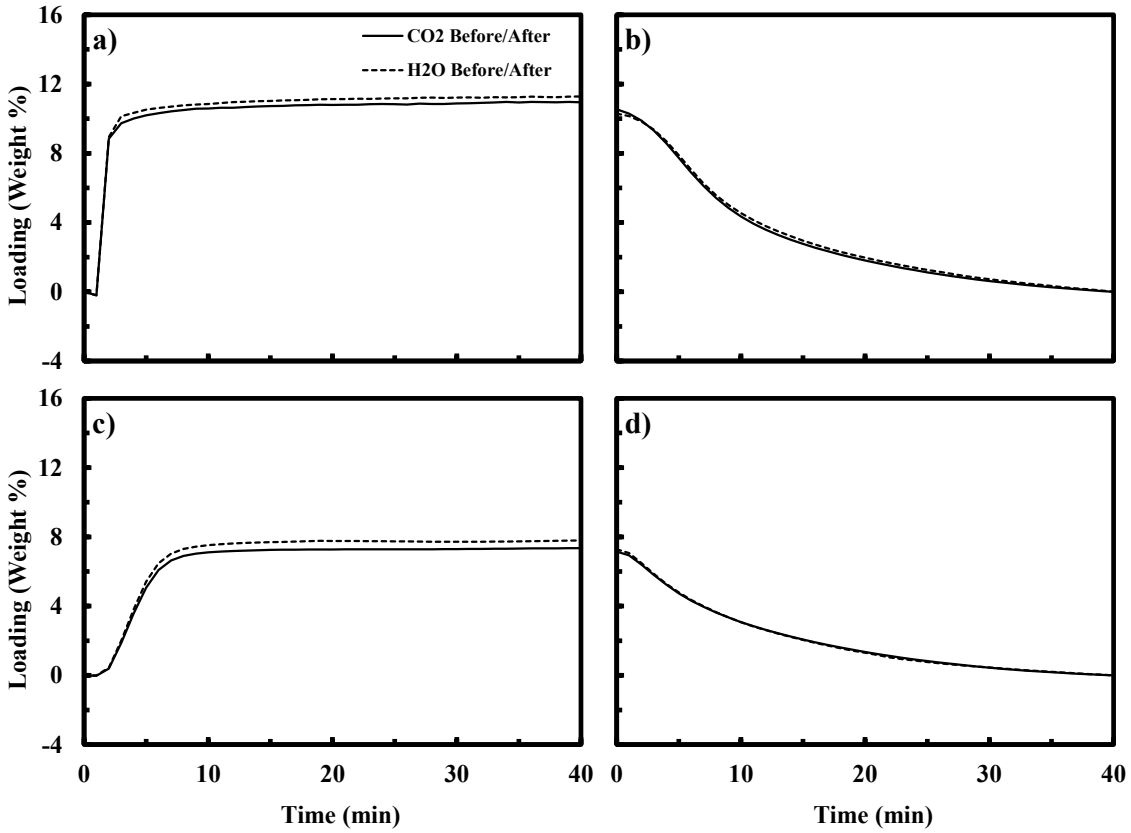

Figure 3.6- TGA Loading in the presence and absence of 2 vol. % water at 60°C for a) adsorption of 100 vol. % CO_2, b) desorption at of 100 vol. % CO_2, c) adsorption of 2.0 vol. % CO_2, d) desorption of 2.0 vol. % CO_2 in Nitrogen

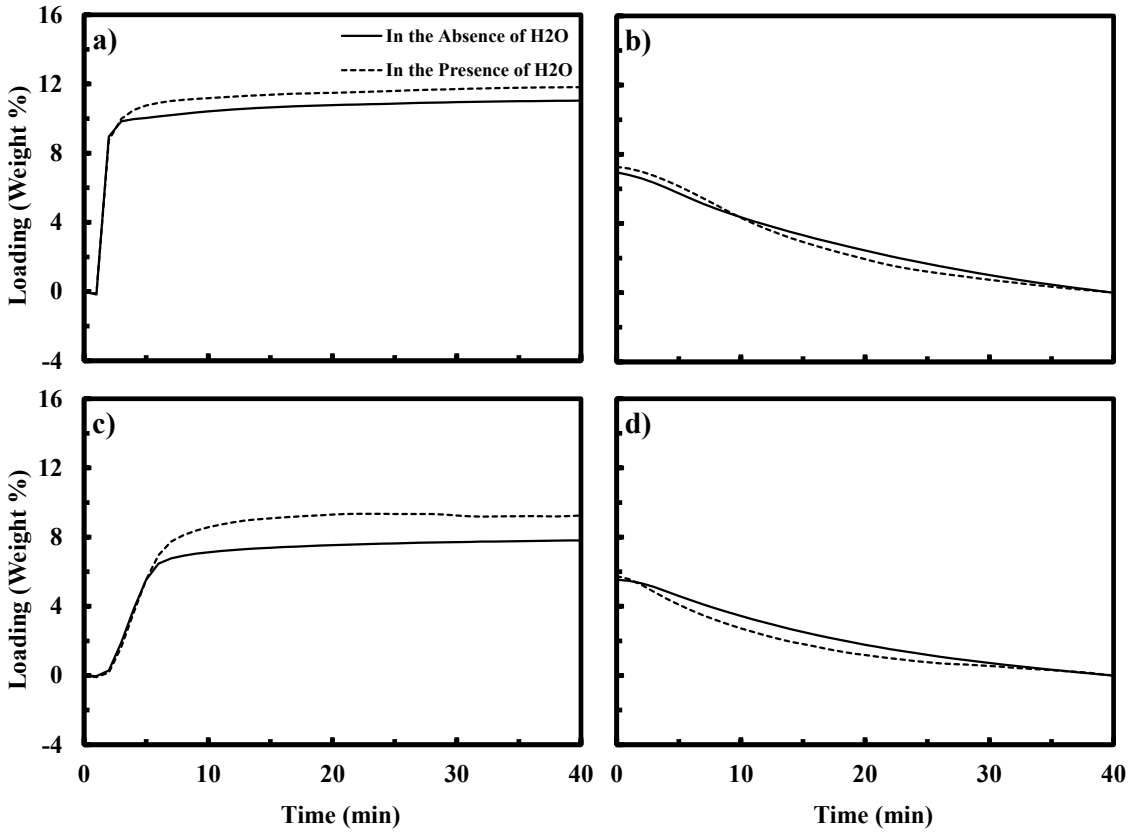

Figure 3.7 TGA Loading in the presence and absence of 2 vol. % water at 40°C for a) adsorption of 100 vol. % CO_2, b) desorption at of 100 vol. % CO_2, c) adsorption of 2.0 vol. % CO_2, d) desorption of 2.0 vol. % CO_2 in Nitrogen

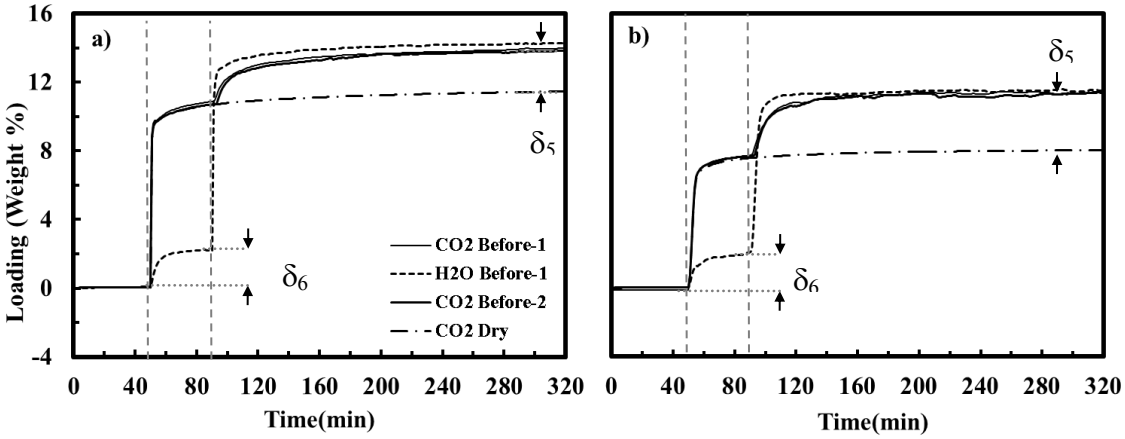

Figure 3.8 Equilibrium loading of 2 vol. % water and CO_2 on CARiACT G10 at 40°C for a) 100 vol. % CO_2 and b) 2.0 vol. % CO_2 in Nitrogen

CHAPTER 4

CO_2 CAPTURE FROM FLUE GAS BY PSA USING A SOLID AMINE SORBENT: HUMID FEED

4.1 Summary

The performance of two PSA cycles was studied for capture of CO_2 from flue gas containing CO_2, Nitrogen and water for three sorbents: a solid amine sorbent made of PEI physically immobilized on commercial silica, and two hypothetical sorbents: carbon based silica solid amine (CBSA) and hydrophobic carbon based solid amine (HCBSA). In both of these sorbents it was assumed that the support was activated carbon, instead of silica, and therefore the typical properties of activated carbon were considered for the properties of the sorbent. For CBSA, the isotherm of water was assumed to be the same as the isotherm of water on BPL activated carbon at low pressures, with the heat of adsorption calculated by using the equilibrium loadings at different temperatures and pressures. For HCBSA, all the properties were assumed to be the same as CBSA except for the water isotherm which was assumed to be the same as Nitrogen. The studies were carried out for the process conditions, that 90% recovery and 95 vol. % purity of CO_2 were achievable under dry conditions.

Simulation results for the solid amine sorbent revealed that the recovery and dry-basis purity of CO_2 was improved when water was present, although adsorption and desorption of water and CO_2 were considered to be independent. However since most of

the water leaves the bed with CO_2 in the heavy product, another separation unit is needed after the PSA unit to separate the water from the captured CO_2 resulting in more cost. Simulation results for two hypothetical sorbents with lower water capacity showed that the lower the capacity for water, the less amount of water is present in the heavy product with CO_2 which means less drying cost but on the other hand the dilution of the CO_2 in the feed gas leads to a drop in recovery and purity of CO_2.

4.2 Introduction

Pressure swing adsorption (PSA) is one of the promising technologies that have been studied for CO_2 capture from flue gas. Although flue gas may contain up to 17% water, in most of the prior studies, it was assumed that the feed gas to the PSA unit is consisted of CO_2 and Nitrogen.[51, 57-58, 65] In other words, in most of the existing studies, it has been assumed that all the water in the flue gas is being separated before the PSA unit. Only in a few studies, water in the feed has been considered.[43, 54, 62, 85] Li et al. considered a 95% relative humidity at 30°C in investigating the performance of a VSA unit for CO_2 capture from flue gas using zeolites 13X. According to their results, the presence of water led to 18.5 and 22 % reduction in recovery and productivity of CO_2 respectively.[54] In their system, 100% of the water was recovered at the heavy end of the bed with CO_2. However no results regarding the required energy for separation were provided. In a series of studies, Reynolds et al. considered 10% water in the feed, when they explored different PSA cycles for CO_2 capture form flue gas using HTLc at 302°C.[43, 62, 86] In their work, they assumed that both Nitrogen and water were inert. Yet they did not provide any

comparisons between the performance of the PSA processes for the dry and humid flue gas. Moreover all their simulations were carried out at high temperature.

At low temperatures, unlike zeolites that can easily be affected by the presence of water, solid amine sorbents have been reported to be water tolerant.[3] Although the adsorption capacity of CO_2 in a solid amine sorbents can even be enhanced in the presence of water,[14, 64] the effect of water on the performance of a PSA process is not clear. For a particular solid amine sorbent, the adsorption capacity of water, kinetics of adsorption and desorption and interplay of water and CO_2, determines how much water is recovered with CO_2 in the heavy product and how much leaves the bed with Nitrogen through the light end. With an ideal adsorbent for CO_2 capture from a wet flue gas with a PSA process, most of the water that enters the bed during the feed step will be recovered with Nitrogen, in the light product. Having most of the water in the heavy product (CO_2-enriched stream), an additional energy is needed after the PSA unit to separate the water form CO_2. However, since less Nitrogen is present in the heavy product, less amount of gas needs to be dried and thus the costs of water separation is less compared to the system in which water is removed prior to the PSA unit.

In chapter 2, it was shown that for a particular solid amine sorbent (CARiACT G10), at 100°C and for two cycle schedules (a 3 bed-8 step cycle and a 4 bed-9 step cycle), 90% CO_2 recovery with 95 vol. % purity was achievable under certain conditions. However the feed to the PSA unit was assumed to be dry. Moreover in chapter 3 it was shown that at temperatures higher than 80°C, the adsorption and desorption of CO_2 and water occurred through independent mechanisms. In this chapter, the effect of water on the performance of two PSA cycles has been explored for two concentrations of water; 2

and 17%. The PSA cycles are the same as the cycles that were explained in chapter 2. Furthermore two hypothetical sorbents are introduced with specific characteristics that can improve the simultaneous separation of water and CO_2 form flue gas. The effect of water capacity of the sorbent on the performance of the PSA process is shown via simulation results using these two hypothetical sorbents. Results obtained here can be used to improve the solid amine sorbents that being considered for CO_2 capture from flue gas.

4.3 Cycle description and mathematical model

The cycles that were described in in chapter 2 have been used to investigate the CO_2 capture from water containing flue gas using the CARiACT G10 solid amine sorbent. The simulator, mathematical model and related assumptions, initial and boundary conditions, bed and sorbent characteristics and process conditions were all the same as the ones described in chapter 2. The only difference is that in all simulations in this part, there are three components in the feed gas to the PSA unit: CO_2, Nitrogen, and water. In chapter 3 was shown before that the adsorption and desorption of CO_2 and water occurred independently at temperatures higher than 80°C. Therefore in the PSA simulations, it was assumed that there were no interactions between water and CO_2. An LDF model equation (eq. 1) and a linear isotherm (eq. 2) were considered for the loading change of water with time. In these equations k_{H2O} is the mass transfer coefficient of water, $q^*_{H_2O}$ is the loading of the water in the sorbent at equilibrium, K_{H,H_2O} is the Henry's law constant, and K_{H_0,H_2O} and E_{H,H_2O} are the Arrhenius equation constants used to describe the temperature dependency of the K_{H,H_2O}.

$$\frac{\partial q_{H_2O}}{\partial t} = k_{H_2O}\left(q^*_{H_2O} - q_{H_2O}\right) \quad \textbf{(1)}$$

$$q^*_{H_2O} = K_{H,H_2O} P y_{H_2O} \quad \textbf{(2)}$$

$$K_{H,H_2O} = K_{H_0,H_2O} \exp\left(\frac{E_{H,H_2O}}{T}\right) \quad \textbf{(3)}$$

Recovery and (dry-basis) purity of CO_2 were calculated from the same equations that were used previously in chapter 2. Recovery and purity of water in the heavy product was calculated as following:

$$\text{H}_2\text{O Recovery } (\%) = \frac{\text{H}_2\text{O(moles)}\,\big|_{\text{Heavy Product}}}{\text{H}_2\text{O(moles)}\,\big|_{\text{Feed}}} \times 100 \quad \textbf{(4)}$$

$$\text{H}_2\text{O Purity } (\%) = \frac{\text{H}_2\text{O (moles)}\,\big|_{\text{Heavy Product}}}{\text{CO}_2\text{(moles)}\,\big|_{\text{Heavy Product}} + \text{H}_2\text{O (moles)}\,\big|_{\text{Heavy Product}} + \text{N}_2\text{(moles)}\,\big|_{\text{Heavy Product}}} \times 100 \quad \textbf{(5)}$$

Two hypothetical sorbents that were explored are labeled as CBSA (Carbon Based Solid Amine) and HCBSA (Hydrophobic Carbon Based Solid Amine). It was assumed that the support of the solid amine was activated carbon and completely hydrophobic carbon instead of silica. It was further assumed that the adsorption and desorption of CO_2, and Nitrogen on this sorbent were the same as the CARiACT G10 solid amine sorbent (chapter 2). The mass transfer coefficient of water in these two hypothetical was assumed to be equal to the value used for CARiACT G10 solid amine sorbent.The isotherm of water on CBSA was obtained by fitting equation 2 to equilibrium loadings of water on BPL activated carbon at low pressures. For HCBSA, all the properties were assumed to be the same as CBSA, except for the isotherm; for this

sorbent it was assumed that the loading of water at equilibrium was equal to the loading of Nitrogen so the same two process Langmuir isotherm (eq. 6) that was used for Nitrogen previously, was considered for water in this work**.**

$$q^*_{H_2O} = q^s_{1,H_2O}\frac{b_{1,H_2O}Py_{H_2O}}{1+b_{1,N_2}Py_{N_2}} + q^s_{2,H_2O}\frac{b_{2,H_2O}Py_{H_2O}}{1+b_{2,H_2O}Py_{H_2O}} \quad \textbf{(6)}$$

$$b_{1,H_2O} = b^0_{1,H_2O}exp\left(\frac{B_{1,H_2O}}{T}\right) \quad \textbf{(7)}$$

$$b_{2,H_2O} = b^0_{2,H_2O}exp\left(\frac{B_{2,H_2O}}{T}\right) \quad \textbf{(8)}$$

In equation 6, q^s_{1,H_2O}, q^s_{2,H_2O}, b_{1,H_2O}, and b_{2,H_2O} are the parameters for Dual Process Langmuir isotherm for N_2/water in HCBSA. b^0_{1,H_2O}, b^0_{2,H_2O}, B_{1,H_2O} and B_{2,H_2O} in equations 7 and 8 are the constants in the Arrhenius equations describing temperature dependency of b_1 and b_2; pre-exponential and energy parameters respectively. Sorbent characteristics and the parameters for isotherm of water are shown in table 4.1.

In order to investigate the effect of water on the performance of the PSA cycles, 12 runs were carried out. The process conditions are shown in table 4.2. Cycles I and II are same as the cycles described in chapter 2. It was shown that under the process conditions in all these runs the 90% CO_2 recovery and 95 vol. % CO_2 purity was achievable for a dry feed by using CARiACT G10 solid amine. Each run was carried out for three different throughputs and two concentrations of water: 2 and 17 mol. %. For each condition, for a particular throughput the amount of CO_2 and Nitrogen that entered

the system per cycle per kg of the sorbent was kept constant; the dry-basis throughput was the same for both dry and wet flue gas.

4.4 Results and discussions

4.4.1 PSA simulation results for G10-CARiACT solid amine

Simulation results for runs 1-4 are shown in figures 4.1-4.5. Each graph also includes the results for the case with similar conditions but with no water. Figure 4.1 shows the purity and recovery of CO_2 and also the avoided energy needed for the process. Both of these runs are with the 3 bed-8 step cycle. It is clear from this figure, that although water and CO_2 are adsorbed and desorbed through independent mechanisms, the performance of the PSA cycle is affected by the presence of the water. The recovery of CO_2 is slightly higher when there is water in the feed gas while the dry-basis purity is significantly improved. The effect on the recovery, in the presence of 17% becomes less significant as throughput increases whereas in the runs with 2% water the increase in the purity and recovery of CO_2 is similar at all throughputs. Water in the solid phase that desorbs during the CnD/LR steps, causes the partial pressure of CO_2 to drop and hence the desorption of CO_2 is improved leading to more recovery of the CO_2. However the more CO_2 present in the bed, the less pronounced is the effect on the partial pressure, thus at higher throughputs the change in the CO_2 recovery is not that significant. It should be noted that the purities reported here are dry basis, and on this basis purities are higher when more water is present. The avoided energy increases as the water concentration increases, which are due to the need of the compression of a larger amount of gas. In figure 4.1 the dashed lines show the goal for recovery and purity that needs to be

achieved in the CO_2 capture from flue gas. For this specific cycle, the separation goal can be achieved in both runs; however run 2 provides higher throughputs and lower avoided energy.

Figure 4.2 shows the results for runs 1 and 2 in terms of recovery and purity of water that were calculated using equations 4 and 5. From this figure it is clear that at 17% water, in both runs recovery and purity of water is higher at lower throughputs. At 2% water, although both recovery and purity of water increase as the throughput decreases, the change in purity is not that significant. For 2% water, in run 1, depending on the throughput 40-65% of the water is recovered with CO_2 in heavy product. This amount is even higher in run 2; 50-75%. The recovery of water becomes lower at higher throughputs which is due to the breakthrough of the water from the light end of the bed with Nitrogen.

Simulation results for runs 3 and 4 are shown in figure 4 and 5. In these runs the purity of CO_2 does not change significantly in the presence of water while the recovery of CO_2 is improved; depending on the throughput in run 3, by adding 17% water, the recovery of CO_2 changed from 80.44-90.69% to 87.55-95.25% while in run 4 the recovery of CO_2 increased from 80.99-91.35% to 87.74-95.49%. Overall the dry-basis purity is slightly higher in run 3 because the light reflux ratio is higher in run 4 (0.01) compared to run 3 (0.009). At a specific throughput recovery increases from run 3 to run 4 while the dry basis purity drops. However at 17% water the change in recovery is almost zero. In these runs similar to the runs explained before the effect of water on the recovery and purity of CO_2 is via the dilution of the CO_2 in the gas phase. Similar to prior runs, in these runs also the process becomes more expensive by increasing the amount of

water in the feed (figure 4.3). The more water enters the bed, the more gas needs to be compressed and thus more energy is required. In the runs with 17% water the only difference seen between the two runs in figure 4 is the dry-basis purity that is lower in run 4. For both of these runs, more than 50% of the water in the feed gas ends up with the CO_2 in the heavy product (figure 4.4).

Comparing the performance of runs 3 and 4 with runs 1 and 2, it becomes apparent that when water is present, in run 2 the separation goal is achievable for higher throughputs (448.94 (L(STP)/kg/hr)), but on the other hand in runs 3 and 4, the separation can be carried out at a much lower cost; 55-60 (kJ/mol) compared to run 2: 80-106 (kJ/mol), yet at slightly lower throughputs (less than 448.94 (L(STP)/kg/hr)). Run 1, on the other hand is the run with the lowest recoveries of water (40-60%) which means the less drying cost of the heavy product.

Overall with this particular sorbent, it is possible to capture CO_2 and water without needing a dryer prior to the PSA unit or a layered bed. However the presence of the water not only adds to the cost of separation, but also for the runs with lower operating cost (runs 3 and 4), since more than 50% of the water leaves the PSA unit with CO_2, there will be an additional water separation cost after the PSA unit. In order to determine the best conditions for this type of sorbent, and also to compare this sorbent with commercial sorbents like zeolite 13X, the cost of every and all of the units including the both the PSA and drying unit should be calculated and compared.

4.4.2 PSA simulation results for Hypothetical sorbents

Figures 4.5-4.8 and 4.9-4.12 show the simulation results for the hypothetical sorbents; carbon based solid amine (CBSA), and the completely hydrophobic carbon based solid amine (HCBSA) respectively. Process conditions in runs 5 and 6 (figure 4.5) are similar to runs and 1 and 2 (figure 4.1) respectively. Comparing the results for this hypothetical sorbent (figure 4.5) with the silica bases solid amine (figure 4.1), it becomes apparent that even though the throughputs for which the goal for recovery and purity is obtainable are lower with CBSA as the sorbent, the process can be done at much lower operating cost; the avoided energy required for runs 5 and 6 are 61.20-71.13 and 52.47-62.05 (kJ/mol) respectively that are lower compared to the avoided energies in runs 1 and 2: 100.73-138.27 and 80.74-105.07 (kJ/mol) respectively. The lower energy requirement can be explained by the results shown in figure 4.6. It can be seen that with this sorbent, less than 30% of the water is recovered in the heavy product and thus more than 70% of the bed leaves the bed with Nitrogen. Having most of the water in the light product reduces the cost of compression of the gas leaving the bed through the heavy end during the CnD and LR steps. Although the cost of separation is less if compared to runs 1 and 2, the energy needed for separation is still higher than the conditions where the feed is dry (figure 4.7).

In runs 7 and 8 shown in figure 8 and 9, the process conditions are similar to runs 3 and 4 shown in figures 4.3 and 4.4. For these runs as well as the previous thus, when this hypothetical sorbent is utilized, the throughputs at which the goal of recovery and purity is obtainable is lower. For the original sorbent, the separation target can be met for throughputs larger than 336.71 but smaller than 448.94 (L(STP)/kg/hr) while with this

sorbent the throughputs cannot be larger than 336.71 (L(STP)/kg/hr). However by changing the adsorbent the avoided energy needed for the process (figure 4.7) and the recovery and purity of the water in the heavy product (figure 4.8) drop. Under the same conditions, the operating cost for the PSA process with the hypothetical sorbent is (figure 8) lower than the original sorbent (figure 4.3). More over the recovery of water in this sorbent (figure 4.8) is much lower: 20-40% than the original one (figure 4.4): 50-80%. Although some differences can be seen between runs 7 and 8 in terms of purity when there is no water in the feed or when there is 2% water, no differences is between the recoveries in these two runs. However for all the conditions, dry basis purity of CO_2 is lower in run 8.

Runs 9-10 and 11-12 are the runs with process conditions similar to runs 1-2 and 3-4 and subsequently similar to runs 5-6 and 7-8 respectively but with HCBSA sorbent. In the presence of 17% water, in neither of the runs with this sorbent (figure 4.9 and 4.10) the goal of 90% recovery and 95 vol. % purity is achievable. At 2% water on the other hand, the goal was reached, for runs 9, 11 and 12. Comparison of figure 10, with figures 2 and 6, it becomes apparent that using this sorbent reduces the cost of separation. The avoided energy for runs 9-10 is lower than runs 1-2 and also runs 5-6. Similarly in runs 11 and 12 the avoided energy at each throughput is lower compared to the corresponded throughputs in runs 3-4 and 7-8.

Figures 4.10 and 4.12 clearly indicate that for this sorbent, most of the water leave the bed with Nitrogen in the light end which means that there is a very small amount of water that should be separated after the PSA unit. In these four runs (9-12), less than 1.5 % of the water leaves the bed with Nitrogen (figures 4.10 and 4.12). For this hypothetical

sorbent, there is almost no cost regarding the drying and the CO_2 and water can be captured with one PSA unit which will significantly reduce the cost for CO_2 capture. But on the other hand since the water acts like Nitrogen, having water in the feed is like having a more dilute CO_2 at higher velocities, thus at the same process conditions the recovery and purity of CO_2 drops. Since the performance of PSA cycle is strongly dependent on the isotherm and kinetics of the gases on the sorbent that is being used, the exact equilibrium and kinetic data is required in order to design an efficient PSA process. However the results here show that, even if water and CO_2 adsorb through independent mechanisms on a sorbent, the presence of water can affect the PSA performance in terms of recovery and purity of CO_2 and the separation cost. In an ideal sorbent not only water does not affect the adsorption and desorption of CO_2, but also the capacity of water is very low.

4.5 Conclusions:

Simulation results showed that for the solid amine studied in this work, under the conditions that 90% recovery and 95 vol. % purity of CO_2 was achievable under dry conditions, the presence of water improved the recovery and purity of CO_2. However most of the water was recovered with the CO_2 in the heavy products that needed to be separated after the PSA unit, and thus adding to the cost of separation. However, having the drying unit after the PSA unit will be cheaper compared to having one prior to the PSA unit, because the amount of the gas that needs to be processed is smaller. Simulation results for two hypothetical sorbents with lower water capacity for water showed that the lower the capacity for water, the less amount of water is present in the heavy product

with CO_2 which means less drying cost but on the other hand, for a hydrophobic solid amine sorbent, the only effect of the presence of water will be the dilution of the CO_2 in the feed gas, and thus the separation becomes more difficult leading to lower recovery with higher cost.

The results obtained here are preliminary results shedding some light on the effect of adsorption capacity of water of a solid amine sorbent on the performance of a PSA unit for CO_2 capture from flue gas. More studies have to be carried out in order to determine the best material for this purpose, by considering all the cost involved in the separation process including drying cost if needed before/after the PSA unit, costs regarding the sorbent itself considering the chemical and thermal stability, and the cost for the PSA process itself.

4.6 Tables

Table 4.1 Bed and adsorbent characteristics, gas properties and process conditions

Adsorbent characteristics-CARiACT G10 solid amine	
Pellet density (kg/m^3)	1093.0
Pellet heat capacity (kJ/kg/K)	0.921
Adsorbent characteristics-CBSA/HCBSA	
Pellet density (kg/m^3)	800.0
Pellet heat capacity (kJ/kg/K)	0.709
Species properties-Water on CARiACT G10 solid amine	
K_{H_0,H_2O} (kPa^{-1})	7.0402×10^{-6}
E_{H,H_2O} (K)	3468.4418
ΔH (kJ/mol)	-28.83
k_{H_2O} (s^{-1})	0.0059
Species properties-Water on CBSA	
K_{H_0,H_2O} (kPa^{-1})	2.6125×10^{-10}
E_{H,H_2O} (K)	6780.8519
ΔH (kJ/mol)	-56.37
k_{H_2O} (s^{-1})	0.0059
Species properties-Water on HCBSA	
B_{1,H_2O} (K)	2029.24
B_{2,H_2O} (K)	0.09084
b^0_{1,H_2O} (kPa^{-1})	5.7564×10^{-7}
b^0_{2,H_2O} (kPa^{-1})	7.6048×10^{-6}
q^s_{1,H_2O} (mol/kg)	0.8952
q^s_{2,H_2O} (mol/kg)	7.2146
ΔH (kJ/mol)	-56.37
k_i (s^{-1})	0.0059
Process Conditions	
CO_2 feed mole fraction(%)-dry feed	15.900
CO_2 feed mole fraction(%)-2% water	15.582
CO_2 feed mole fraction(%)-17% water	13.197

Table 4.2 Adsorbent type and process conditions for simulation runs 1-12; CGSA:CARiACT G10 solid amine, CBSA: carbon based solid amine, HCBSA: hydrophobic carbon solid amine.

Run	Throughput (L(SLP)/kg/hr)	Sorbent	Cycle	LR-Ratio(ω)	H-Ratio(λ)	P_{CoD} (kPa)
1	224.47, 336.71, 448.95	CGSA	I	0.018	1.00	30.0
2	224.47, 336.71, 448.95	CGSA	I	0.036	0.75	30.0
3	224.47, 336.71, 448.95	CGSA	II	0.009	1.00	10.0
4	224.47, 336.71, 448.95	CGSA	II	0.010	1.00	10.0
5	224.47, 336.71, 448.95	CBSA	I	0.018	1.00	30.0
6	224.47, 336.71, 448.95	CBSA	I	0.036	0.75	30.0
7	224.47, 336.71, 448.95	CBSA	II	0.009	1.00	10.0
8	224.47, 336.71, 448.95	CBSA	II	0.010	1.00	10.0
9	224.47, 336.71, 448.95	HCBSA	I	0.018	1.00	30.0
10	224.47, 336.71, 448.95	HCBSA	I	0.036	0.75	30.0
11	224.47, 336.71, 448.95	HCBSA	II	0.009	1.00	10.0
12	224.47, 336.71, 448.95	HCBSA	II	0.010	1.00	10.0

4.7 Figures

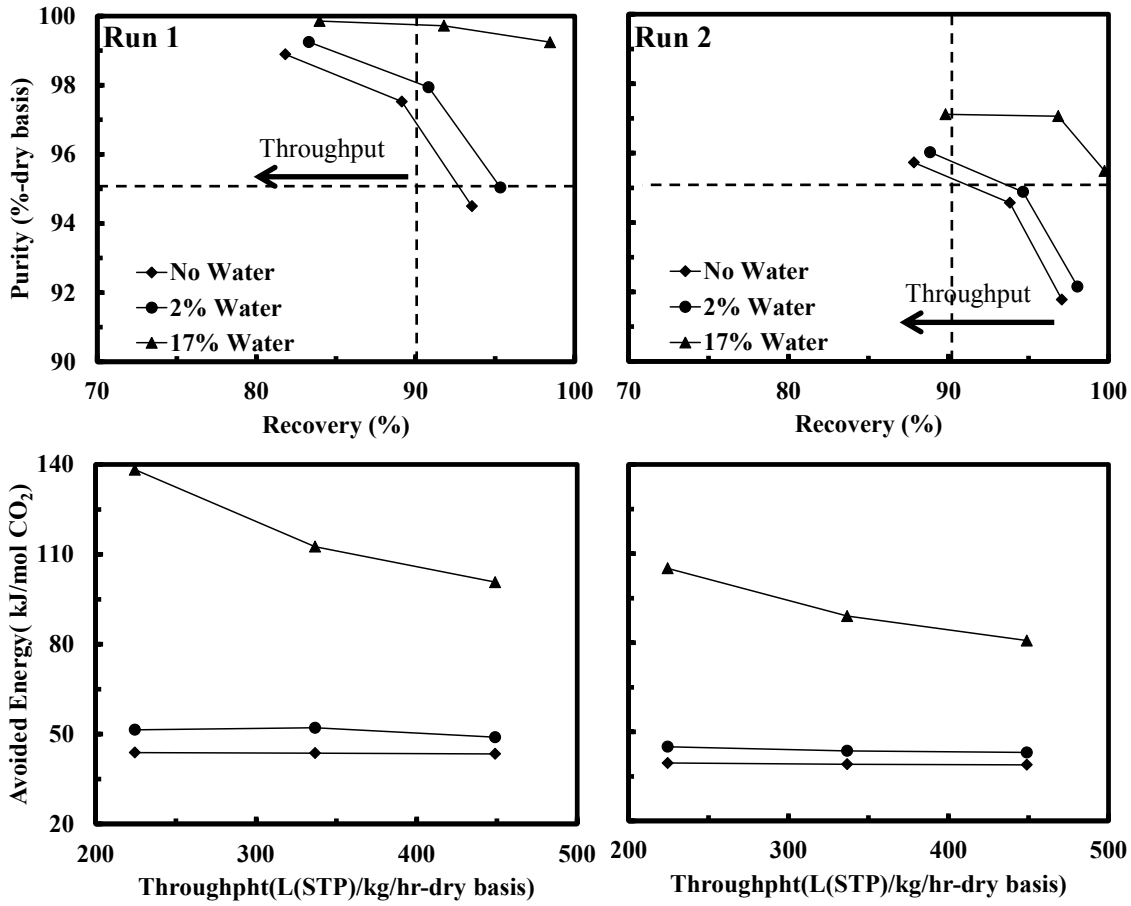

Figure 4.1 Simulation results for runs 1 and 2 with silica-based solid amine sorbent (G10 CARiACT-solid amine), in terms of CO_2 recovery (%), purity (%-dry basis) in the heavy product and avoided energy (kJ/mol CO_2) at different throughputs and for three different feed water contents: no water, 2% and 17% water. In recovery vs. purity figures, feed throughput increases from right to left.

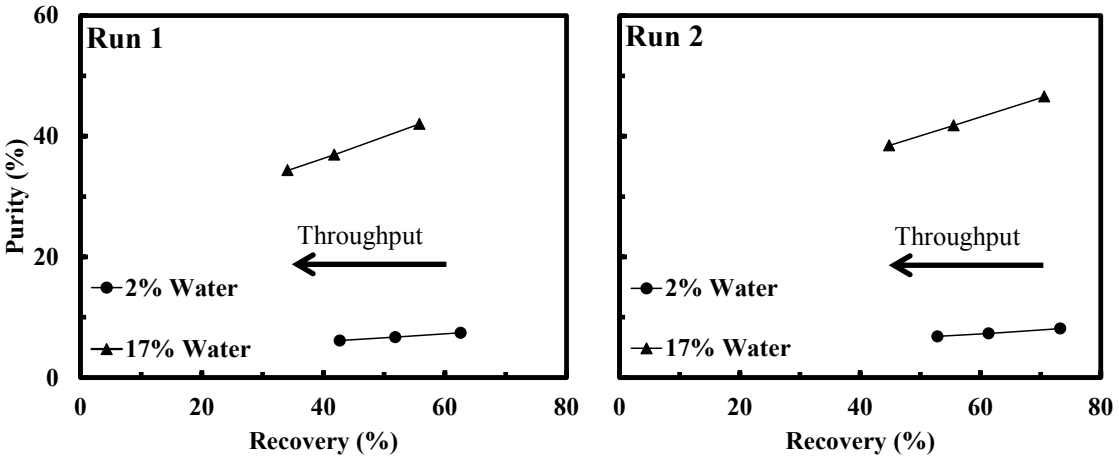

Figure 4.2 Simulation results for cycle I with silica-based solid amine sorbent (G10 CARiACT-solid amine), in terms of water recovery (%), purity (%) in the heavy product at different throughputs and for three different feed water contents: no water, 2% and 17% water. Feed throughput increases from right to left.

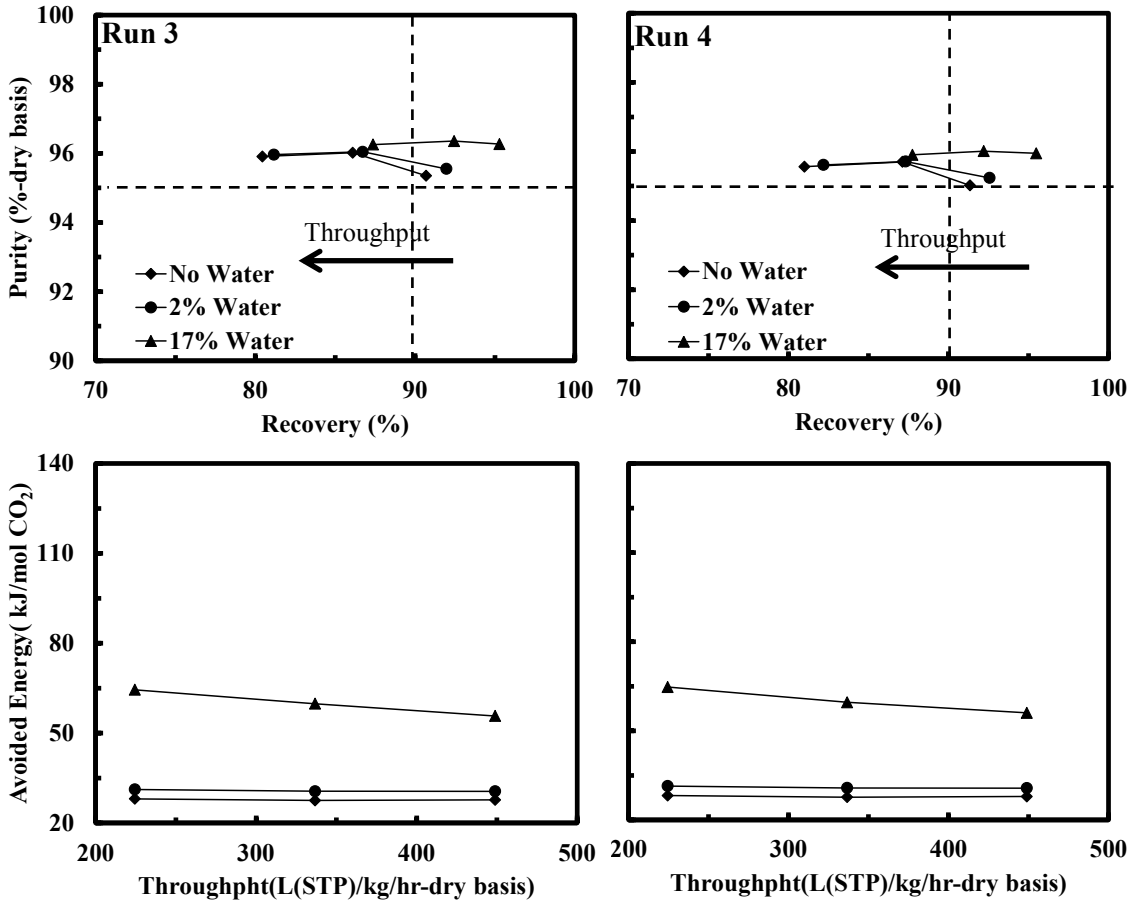

Figure 4.3 Simulation results for cycle II with silica-based solid amine sorbent, in terms of CO_2 recovery (%), purity (%-dry basis) in the heavy product and avoided energy (kJ/mol CO_2) at different throughputs and for three different feed water contents: no water, 2% and 17% water. In recovery vs. purity figures, feed throughput increases from right to left.

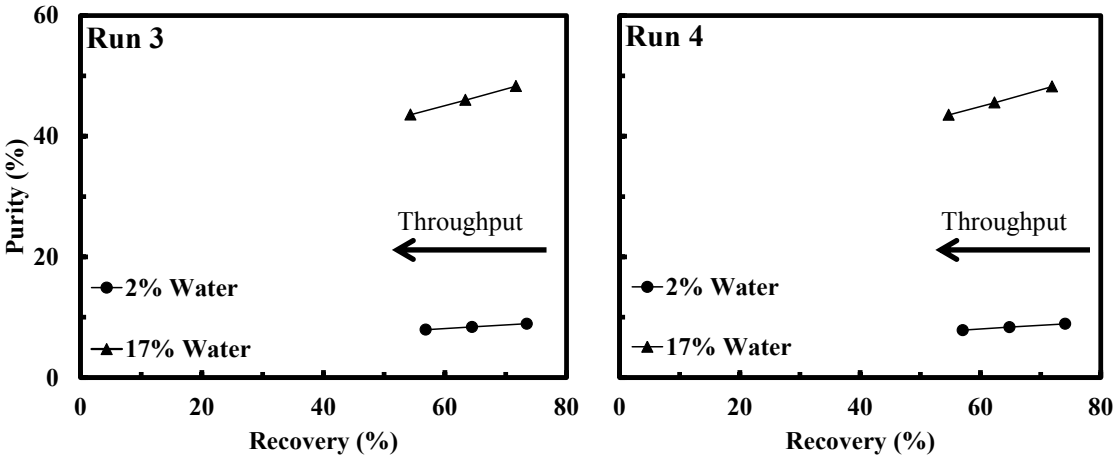

Figure 4.4 Simulation results for cycle II with silica-based solid amine sorbent, in terms of water recovery (%), purity (%) in the heavy product at different throughputs and for three different feed water contents: no water, 2% and 17% water. Feed throughput increases from right to left.

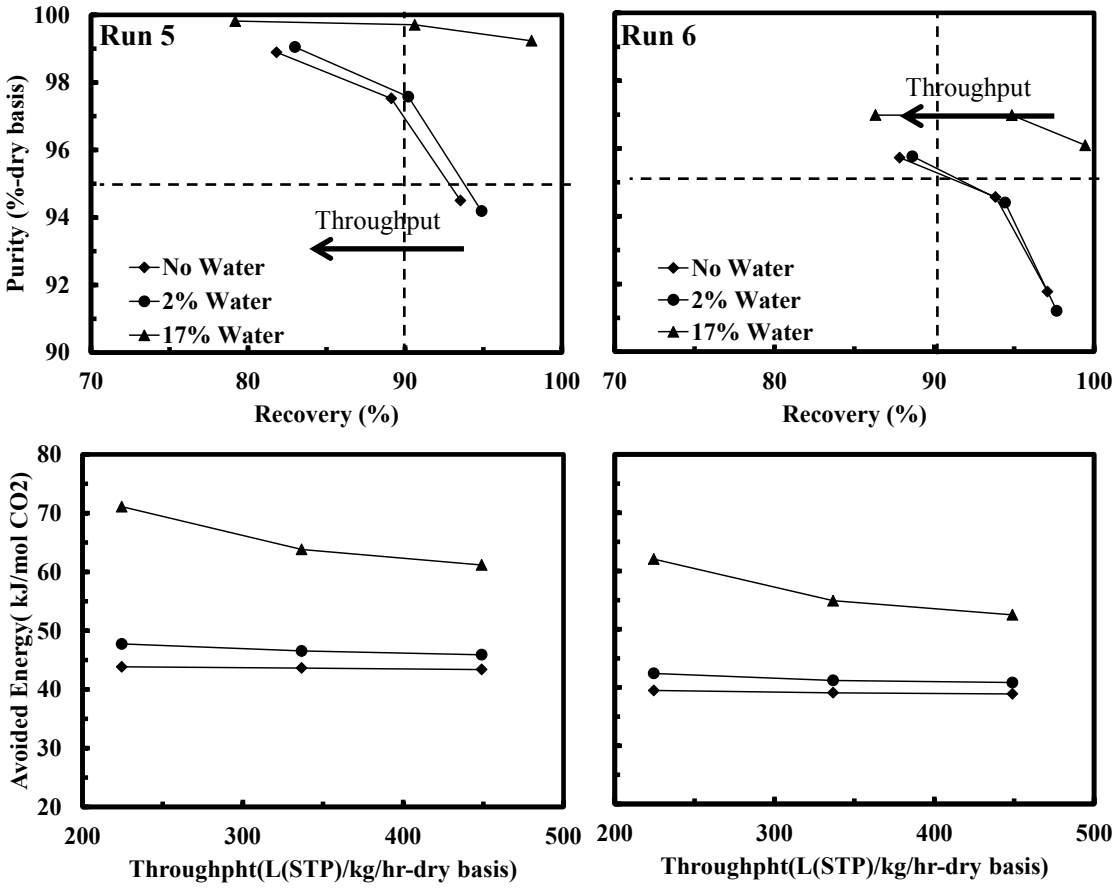

Figure 4.5 Simulation results for cycle I with carbon-based solid amine sorbent (CBSA), in terms of CO_2 recovery (%), purity (%-dry basis) in the heavy product and avoided energy (kJ/mol CO_2) at different throughputs and for three different feed water contents: no water, 2% and 17% water. In recovery vs. purity figures, feed throughput increases from right to left.

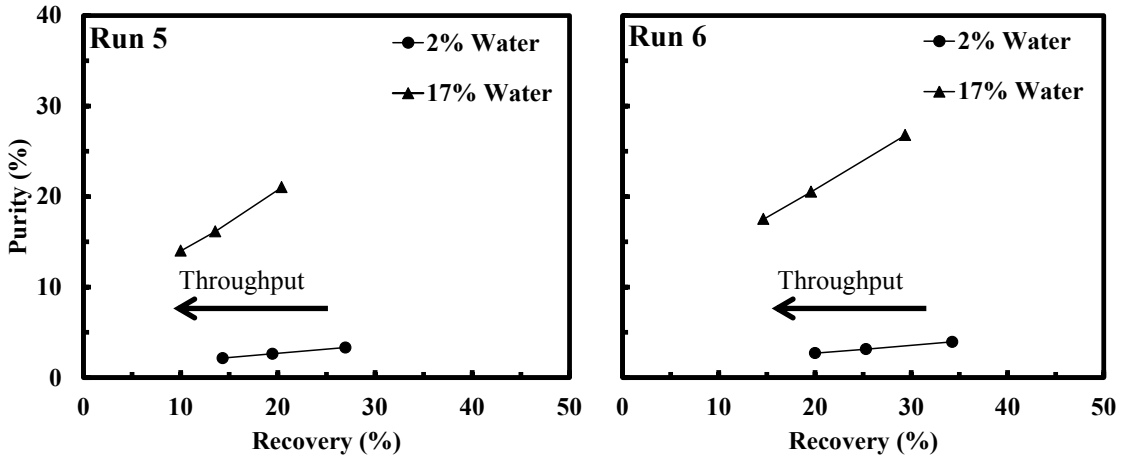

Figure 4.6 Simulation results for cycle I with carbon-based solid amine sorbent (CBSA), in terms of water recovery (%), purity (%) in the heavy product at different throughputs and for three different feed water contents: no water, 2% and 17% water. Feed throughput increases from right to left.

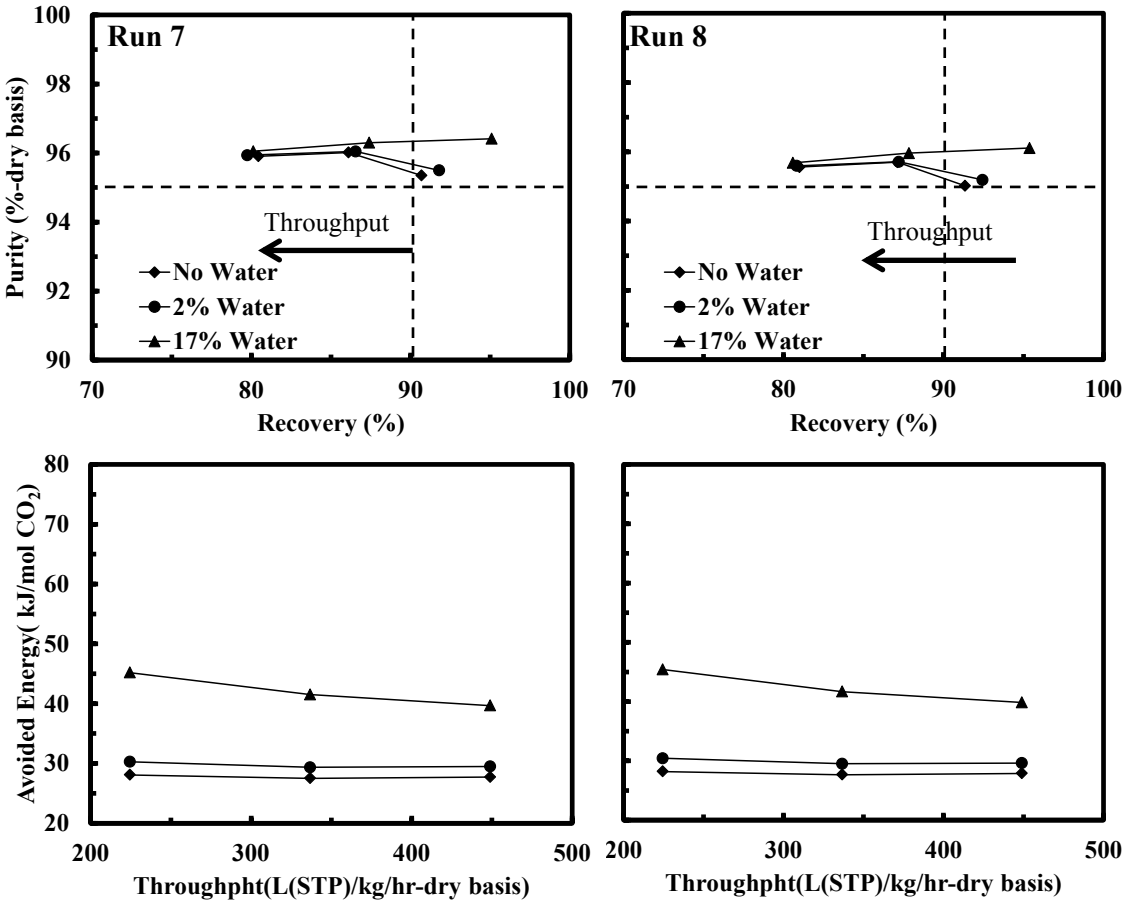

Figure 4.7 Simulation results for cycle II with carbon-based solid amine sorbent (CBSA), in terms of CO_2 recovery (%), purity (%-dry basis) in the heavy product and avoided energy (kJ/mol CO_2) at different throughputs and for three different feed water contents: no water, 2% and 17% water. In recovery vs. purity figures, feed throughput increases from right to left

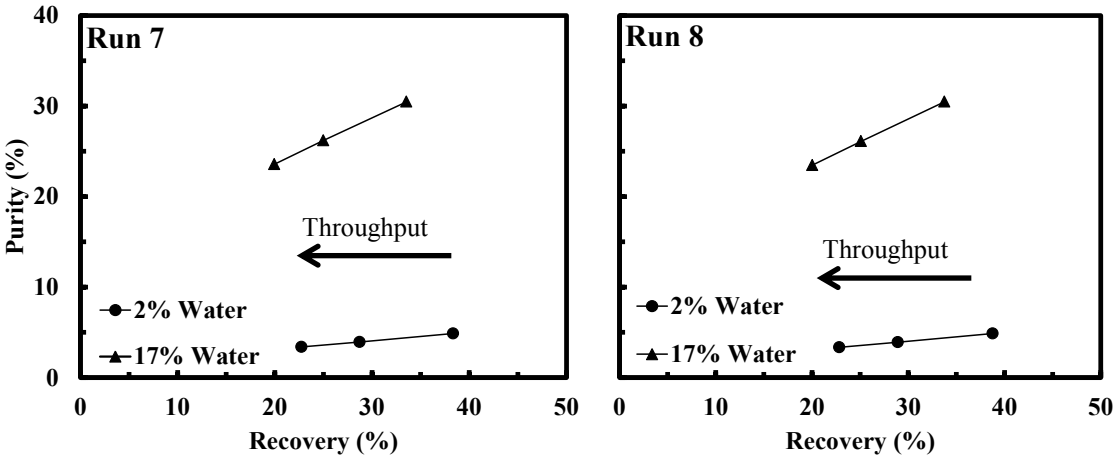

Figure 4.8 Simulation results for cycle II with carbon-based solid amine sorbent (CBSA), in terms of water recovery (%), purity (%) in the heavy product at different throughputs and for three different feed water contents: no water, 2% and 17% water. Feed throughput increases from right to left.

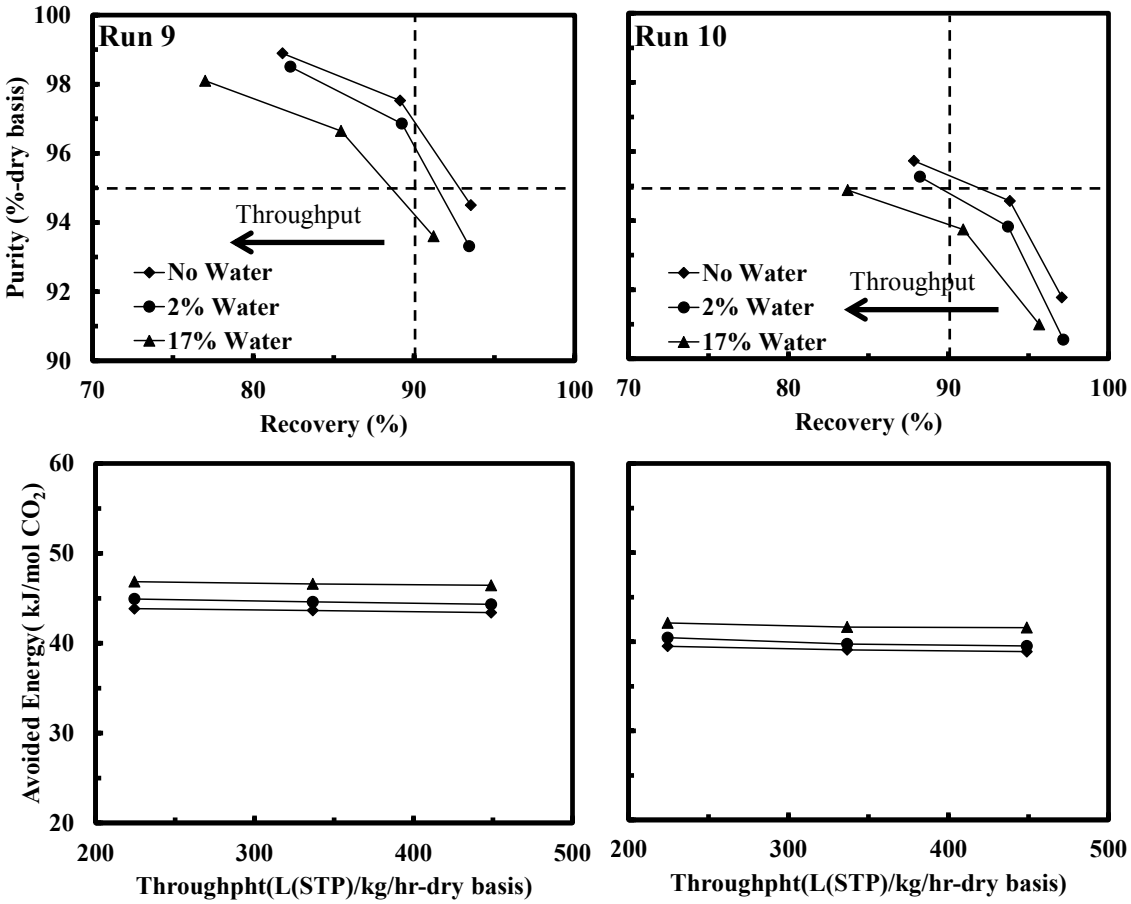

Figure 4.9 Simulation results for cycle I with hydrophobic carbon-based solid amine sorbent (HCBSA) in terms of CO_2 recovery (%), purity (%-dry basis) in the heavy product and avoided energy (kJ/mol CO_2) at different throughputs and for three different feed water contents: no water, 2% and 17% water. In recovery vs. purity figures, feed throughput increases from right to left.

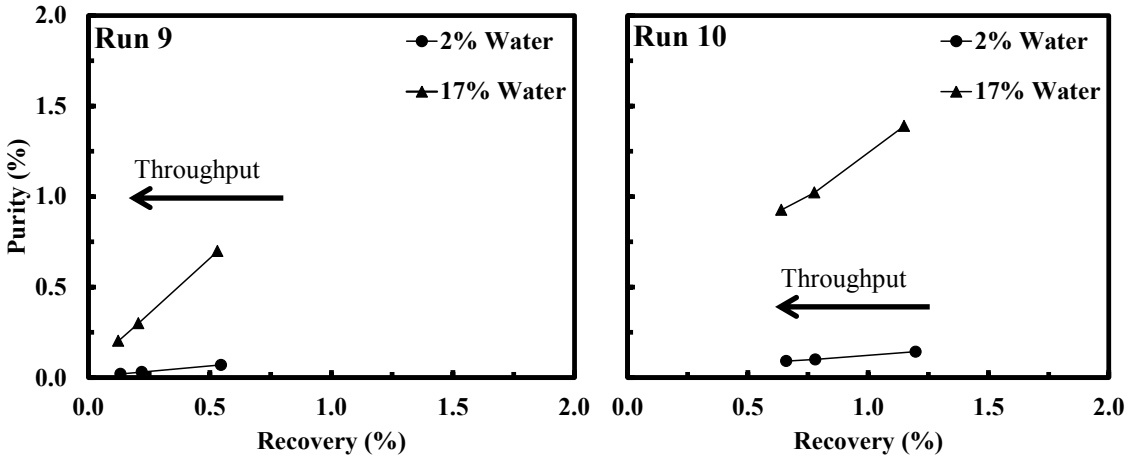

Figure 4.10 Simulation results for cycle I with hydrophobic carbon-based solid amine sorbent (HCBSA), in terms of water recovery (%), purity (%) in the heavy product at different throughputs and for three different feed water contents: no water, 2% and 17% water. Feed throughput increases from right to left.

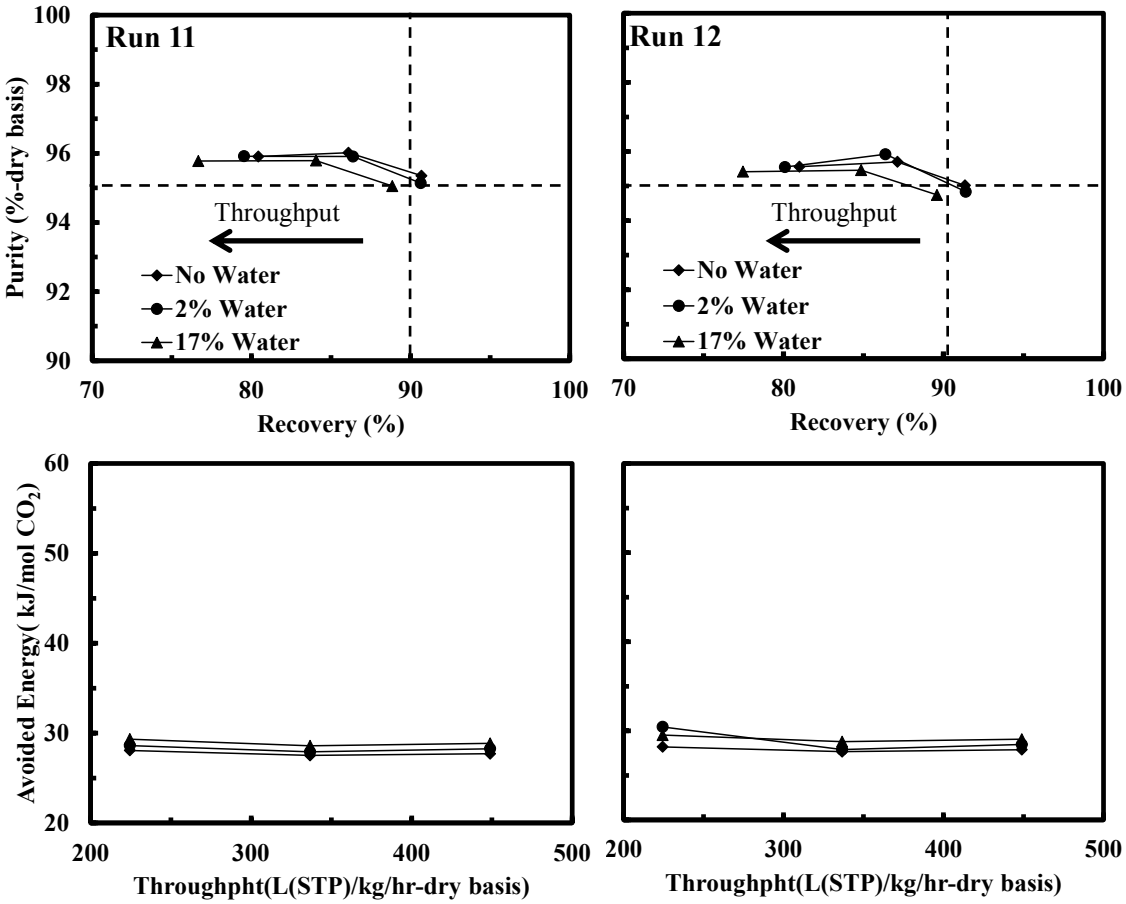

Figure 4.11- Simulation results for cycle II with hydrophobic carbon-based solid amine sorbent (HCBSA), in terms of CO_2 recovery (%), purity (%-dry basis) in the heavy product and avoided energy (kJ/mol CO_2) at different throughputs and for three different feed water contents: no water, 2% and 17% water. In recovery vs. purity figures, feed throughput increases from right to left.

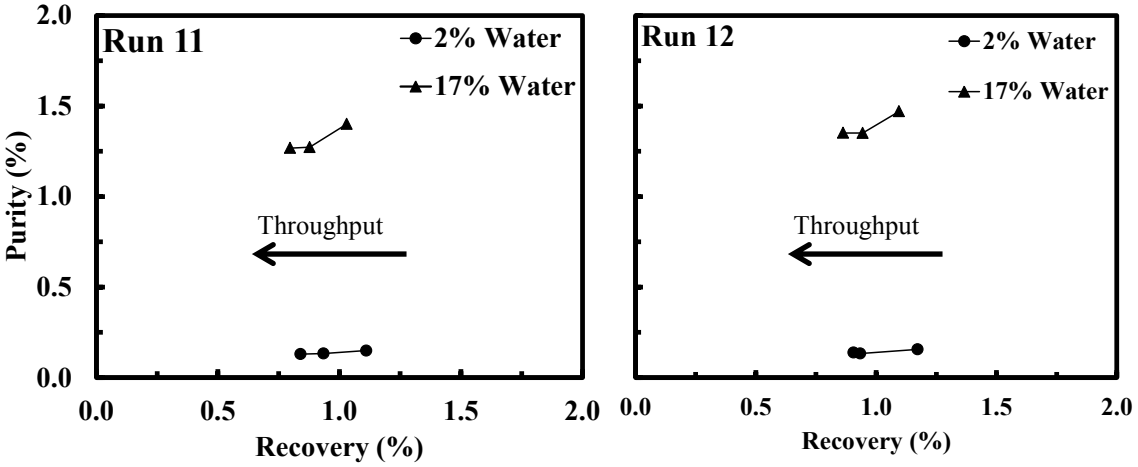

Figure 4.12 Simulation results for cycle II with hydrophobic carbon-based solid amine sorbent (HCBSA), in terms of water recovery (%), purity (%) in the heavy product at different throughputs and for three different feed water contents: no water, 2% and 17% water. Feed throughput increases from right to left.

REFERENCES

1. Secretariat of the Commission for Environmental Cooperation. The North American Mosaic: An Overview of Key Environmental Issues, Climate Change. http://www.cec.org/soe/files/en/SOE_Climate_en.pdf.
2. Ebner, A. D.; Ritter, J. A. State-of-the-art Adsoprtion and Membrane separation Processes for Carbon Dioxide Production from Carbon Dioxide Emitting Industries. *Sep. Sci. Technol*. **2009**, 44, 1273.
3. Ebner, A. D.; Gray, M. L.; Chisholm, N. G.; Black, Q. T.; Mumford, D. D.; Nicholson, M. A.; Ritter, J. A. Suitability of a Solid Amine Sorbent for CO_2 Capture by Pressure Swing Adsorption. *Ind. Eng. Chem. Res*. **2011**, *50*, 5634.
4. Belmabkhout, Y.; Sayari, A. Isothermal versus Non-isothermal Adsorption-Desorption Cycling of Triamine-Grafted Pore-Expanded MCM-41 Mesoporous Silica for CO_2 Capture from Flue Gas. *Energy Fuels.* **2010**, *24*, 5273.
5. Belmabkhout, Y.; Sayari, A. Effect of Pore Expansion and Amine Functionalization of Mesoporous Silica on CO_2 Adsorption over a Wide Range of Conditions. *Adsorption.* **2009**, *15*, 318.
6. Belmabkhout, Y.; Serna-Guerrero, R.; Sayari, A. Adsorption of CO_2 from Dry Gases on MCM-41 Silica at Ambient Temperature and High Pressure. 1: Pure CO_2 Adsorption *Chem. Eng. Sci.* **2009**, *64*, 3721.

7. Serna-Guerrero, R.; Belmabkhout, Y.; Sayari, A. Modeling CO_2 Adsorption on Amine-Functionalized Mesoporous Silica: 1. A Semi-Empirical Equilibrium Model *Chem. Eng. J.* **2010**, *161*, 173.
8. Serna-Guerrero, R.; Sayari, A. Modeling *Adsorption* of CO_2 on Amine-Functionalized Mesoporous Silica. 2: Kinetics and Breakthrough Curves *Chem. Eng. J.* **2010**, *161*, 182.
9. Birbara, P. J.; Filburn, T.P.; Nalette, T. A. Regenerable Solid Amine Sorbent. US Patent 5,876,488 (1999).
10. Birbaram, P. J.; Nalette T. A. Regenerable Supported Amine-Polyol Sorbent. US Patent 5,492,683 (1996).
11. Gray, M. L.; Hoffman, J. S.; Hreha, D. C.; Fauth, D. J.; Hedges, S. W.; Champagne, K. J.; Pennline, H. W. Parametric Study of Solid Amine Sorbents for the Capture of Carbon Dioxide. *Energy Fuels*. **2009**, *23*, 4840.
12. Wang, X.; Schwartz V.; Clark, J. C.; Ma X.; Overbury, S. H.; Xu, X.; Song, C. Infrared Study of CO_2 Sorption over "Molelcuar Basket" Sorbent Consisting of Polyethylenimine-Modified Mesoporous Molecular Sieve. *J. Phys. Chem*. C **2009**, *113*, 7260.
13. Zhang, Z.; Ma X.; Wang, D.; Song, C.; Wang, Y. Development of Silica-Gel-Supported Polyethylenimine Sorbents for CO_2 Capture from Flue Gas. *AIChE J.* **2012**, *58*, 2495.
14. Satyapal, S.; Filburn, T.; Trela, J.; Strange, J. Performance and properties of a solid amine sorbent for carbon dioxide removal in space life support applications. *Energy Fuels.* **2001**, *15*, 250.

15. Gray, M. L.; Champagne, K. J.; Fauth, D.; Baltrus, J. P.; Pennline, H. Performance of Immobilized Tertiary Amine Solid Sorbents for the Capture of Carbon Dioxide. *Int. J. Greenhouse Gas Control*. **2008**, *2*, 3.

16. Belmabkhout, Y.; Serna-Guerrero, R.; Sayari, A. Amine-Bearing Mesoporous Silica for CO_2 Removal from Dry and Humid Air. *Chem. Eng. Sci.* **2010**, *65*, 3695.

17. Belmabkhout, Y.; Serna-Guerrero, R.; Sayari, A. Adsorption of CO_2-Containing Gas Mixtures over Amine-Bearing Pore-Expanded MCM-41 Silica: Application for Gas Purification. *Ind. Eng. Chem. Res*. **2010**, 49, 359.

18. Sayari, A.; Belmabkhout, Y. Stabilization of Amine-Containing CO_2 Adsorbents: Dramatic Effect of Water Vapor. *J. Am. Chem. Soc.* **2010**, *132*, 6312.

19. Serna-Guerrero, R.; Belmabkhout, Y.; Sayari, A. Further Investigations of CO_2 Capture Using Triamine-Grafted Pore-Expanded Mesoporous Silica. *Chem. Eng. J.* **2010**, *158*, 513.

20. Drese, J. H.; Choi, S.; Lively, R. P.; Koros, W. J.; Fauth, D. J.; Gray, M. L.; Jones, C. W. Synthesis-Structure-Property Relationships for Hyperbranched Aminosilica CO_2 Adsorbents. *Adv. Funct. Mater.* **2009**, *19*, 3821.

21. Serna-Guerrero, R.; Da'na, E.; Sayari, A. New Insights into the Interactions of CO_2 with Amine-Functionalized Silica. *Ind. Eng. Chem. Res*. **2008**, *47*, 9406.

22. Khatri, R. A.; Chuang, S. S. C.; Soong, Y., Gray, M. Carbon Dioxide Capture by Diamine-Grafted SBA-15: A Combined Fourier Transform Infrared and Mass Spectrometry Study. *Ind. Eng. Chem. Res*. **2005**, *44*, 3702.

23. Belmabkhout, Y.; Weireld, G. D.; Sayari, A. Amine-Bearing Mesoporous Silica for CO_2 and H_2S Removal from Natural Gas and Biogas. *Langmuir* **2009**, *25*, 13275.

24. Tsuda, T.; Fujiwara, T. Polyethyleneimine and Macrocyclic Polyamine Silica-Gels Acting as Carbon-Dioxide Absorbents. *J. Chem. Soc., Chem. Commun*. **1992**, *22*, 1659.

25. Li, W.; Bollini, P.; Didas, S. A.; Choi, S.; Drese, J. H.; Jones, C. W. Structural Changes of Silica Mesocellular Foam Supported Amine-Functionalized CO_2 Adsorbents Upon Exposure to Steam. ACS Appl. Mater. Interfaces **2010**, *2*, 3363.

26. Li, W.; Choi, S.; Drese, J. H.; Hornbostel, M.; Krishnan, G.; Eisenberger, P. M.; Jones, C. W. Steam-Stripping for Regeneration of Supported Amine-Based CO_2 Adsorbents. *Chem. Sus. Chem*. **2010**, *3*, 899.

27. Hicks, J. C.; Drese, J. H.; Fauth, D. J.; Gray, M. L.; Qi, G.; Jones, C. W. Designing Adsorbents for CO_2 Capture from Flue Gas-Hyperbranched Aminosilicas Capable,of Capturing CO_2 Reversibly *J. Am. Chem. Soc.* **2008**, *130*, 2902.

28. Lee, S.; Filburn, T. P.; Gray, M.; Park, J.; Song, H. Screening Test of Solid Amine Sorbents for CO_2 Capture. *Ind. Eng. Chem. Res*. **2008**, *19*, 7419.

29. Khatri, R. A.; Chuang, S. S. C.; Soong, Y.; Gray, M. Thermal and Chemical Stability of Regenerable Solid Amine Sorbent for CO_2 Capture. *Energy Fuels*. **2006**, *20*, 1514.

30. Gray, M. L.; Soong, Y.; Champagne, K. J.; Pennline, H., Baltrus, J. P., Stevens, R. W.; Khatri, R.; Chuang, S. S. C. Filburn T. Improved Immobilized Carbon Dioxide Capture Sorbents. *Fuel. Process. Technol.* **2005**, *86*, 1449.

31. Serna-Guerrero, R.; Belmabkhout, Y.; Sayari, A. Influence of Regeneration Conditions on the Cyclic Performance of Amine- Grafted Mesoporous Silica for CO_2 Capture: An Experimental and Statistical Study. *Chem. Eng. Sci.* **2010**, *65*, 4166.

32. Franchi, R. S.; Haung, P. J. E.; Sayari, A. Applications of Pore-Expanded Mesoporous silica. 2. Development of a High-Capacity, Water-Tolerant Adsorbent for CO_2. *Ind. Eng. Chem. Res*. **2005**, *44*, 8007.

33. Hicks, J. C.; Dabestani, R.; Buchanan III, A. C.; Jones C. W. Assessing Site-Isolation of Amine Groups on Aminopropyl-Functionalized SBA-15 Silica Materials via Spectroscopic and Reactivity Probes. *Inorg. Chim. Acta***. 2008**, *361*, 3024.

34. Hicks, J. C.; Dabestani, R.; Buchanan III, A. C.; Jones C. W. Spacing and Site Isolation of Amine Groups in 3-Aminopropyl-Grafted Silica Materials: The Role of Protecting Groups. *Chem. Mater.* **2006**, *18*, 5022.

35. Choi, S; Drese, J. H; Jones, C. W. Adsorbent Materials for Carbon Dioxide Capture from Large Anthropogenic Point Sources. *Chem. Sus. Chem*. **2009**, *2*, 796.

36. Drage, T. C.; Arenillas, A.; Smith, K. M.; Snape, C. E. Thermal Stability of Polyethylenimine Based Carbon Dioxide Adsorbents and Its Influence on Selection of Regeneration Strategies. *Micropor Mesopor Mat*. **2008,** *116*, 504.

37. Pinto, M. L.; Mafra, L.; Guil, J. M.; Pires, J.; Rocha, J. Adsorption and Activation of CO_2 by Amin-Modified Nanoporous Materials Studied by Solid State NMR and CO_2 Adsorption. *Chem. Mater*. 2011, *23*, 1387.

38. Vaidya, P.D.; Kenig, E. Y. CO_2-Alkanolamine Reaction Kinetics: A Review of Recent Studies, *Chem. Eng. Technol*. **2007**, *30*, 1467.

39. Planas, N.; Dzubak, A. L.; Poloni, R.; Lin, L.; McManus, A.; McDonald, T.; Neaton, J. B.; Long, J. R.; Smit, B.; Gagliardi, L. The Mechanism of Carbon Dioxide Adsorption in An Alkylamine-Functionalized Metal-Organic Framework*, J. Am. Chem. Soc.* **2013***, 135*, 7402.

40. Du, H.; Ebner, A. D. ; Ritter, J. A. Temperature Dependence of the Nonequilibruim Kinetic Model that Describes the Adsorption and Desorption Behavior of CO_2 in K-Promoted HTlc. *Ind. Eng. Chem. Res.* **2010**, *49*, 3328.

41. Wei, J. Adsorption and Cracking of the N-Alkanes over zsm-5: Negative Activation Energy of Reaction, *Chem. Eng. Sci.* **1996,** *51***,** 2995.

42. Siriwardane, R.; Robinson, C. Liquid-Impregnated Clay Solid Sorbents for CO_2 Removal from Postcombustion Gas Streams, *J. Environ. Eng*-ASCE **2009**, *135*, 378.

43. Reynolds S. P.; Mehrotra A.; Ebner A. D.; Ritter J. A. Heavy Reflux PSA Cycles for CO_2 Recovery from Flue Gas: Part I. Performance Evaluation, *Adsorption*, **2008**, *14*, 399

44. DOE/NETL, DOE/NETL Carbon Dioxide Capture and Storage RD&D Roadmap, Dec. **2010.**

45. Zhang J.; Webley P. A.; Xiao P. Effect of Process Parameters on Power Rquirements of Vacuum Swing Adsorption Technology for CO_2 Capture from Flue Gas. *Energ Convers Manage.* **2008**, *49*, 346

46. Ho M. T.; Allinson G. W.; Wiley D. E.; Reducing the Cost of CO_2 Capture from Flue Gases Using Pressure Swing Adsorption. *Ind. Eng. Chem. Res.* **2008***, 47*, 4883.

47. Aaron D.; Tsouris C. Separation of CO_2 from Flue Gas: A Review. *Separ. sci. technol.* **2005**, 40, 321.

48. Inui T.; Okugawa Y.; Yasuda M. Relationship between Properties of Various Zeolites and Their CO_2-Adsorption Behaviors in Pressure Swing Adsorption Operation. *Ind. Eng. Chem. Res*. **1988**, *27*, 1103

49. Kikkinides E. S.; Yang R. T. Concentration and Recovery of CO_2 by Pressure Swing Adsorption. *Ind. Eng. Chem. Res*. **1993**, *32*, 2714.

50. Na B.; Lee H.; Koo K.; Song H. K. Effect of Rinse and Recycle Methods on the Pressure Swing Adsorption Process to Recover CO_2 from Power Plant Flue Gas Using Activated Carbon. *Ind. Eng. Chem. Res.* **2002**, *41,* 5498.

51. Chue K. T.; Kim J. N.; Yoo Y. J.; Cho S. H. Comparison of Activated Carbon and Zeolite 13X for CO_2 Recovery From Flue Gas by Pressure Swing Adsorption . *Ind. Eng. Chem. Res.* **1995**, *34*, 591

52. Liu Z.; Wang L.; Kong X.; Li P.; Yu J.; Rodrigues A. E. Onsite CO_2 Capture from Flue Gas by an Adsorption Process in a Coal-Fired Power Plant. *Ind. Eng. Chem. Res*. **2012**, *51*, 7355

53. Zhang J.; Webley P. A.; Cycle Development and Design for CO_2 Capture from Flue Gas by Vacuum Swing Adsorption. *Environ. Sci. Technol.* **2008**, *42,* 563.

54. Li G.; Xiao P.; Webley P.; Zhang J.; Singh R.; Marshall M. Capture of CO_2 from High Humidity Flue Gas by Vacuum Swing Adsorption with Zeolite 13X. *Adsorption*. **2008**, *14*, 415.

55. Xiao P.; Zhang J.; ·Webley P.; Li G.; Singh R.; Todd R. Capture of CO2 from Flue Gas streams with Zeolite 13X by Vacuum-Pressure Swing Adsorption . *Adsorption*, **2008**, *14*, 575.

56. Chaffee A. L.; Knowles G. P.; Liang Z.; Zhang J.; Xiao P.; Paul A. Webley P. A. CO_2 capture by Adsorption: Materials and Process Development. *Int J Green Energy*, **2007**, *1*, 11-18

57. Choi W., Kwon T.; Yeong-Koo Yeo Y.; Lee H., Song H. K.; Byung-Ki Na B. Optimal Operation of the Pressure Swing Adsorption (PSA) Process for CO_2 Recovery. *Korean J. Chem. Eng*. **2003**, *20*, 617

58. Chou C.; Chen C. Carbon Dioxide Recovery by Vacuum Swing Adsorption. *Sep Purif Technol*. **2004**, *39*, 51

59. Gomes V. G.; Yee K. W. K. Pressure Swing Adsorption for Carbon Dioxide Sequestration from Exhaust Gases. *Sep Purif Technol*. **2002**, *28*, 161

60. Ishibashi M.; Ota H.; Akutsu N.; Umeda S.; Tajika M. Technology for Removing Carbon Dioxide from Power Plant Flue Gas by the Physical Adsorption Method. *Energ Convers Manage*. **1996**, *37*, 929

61. Yong Z.; Mata V.; Rodrigues A. E. Adsorption of Carbon Dioxide at High Temperature-a Review. *Sep Purif Technol*. **2002**, *26*, 195

62. Reynolds S. R.; Ebner A. D.; Ritter J. A. Stripping PSA cycles for CO_2 Recovery from Flue Gas at High Temperature Using a Hydrotalcite-like Adsorbent. *Ind. Eng. Chem. Res.* **2006**, *45,* 4278

63. Haung H. Y.; Yang R. T. Amine-Grafted MCM-48 and Silica Xerogel as Superior Sorbents for Acidic Gas Removal from Natural Gas. *Ind. Eng. Chem. Res.* **2003**, *42*, 2427

64. Ko D.; Siriwardane R.; Biegler L. T. Optimization of Pressure Swing Adsorption and Fractionated Vacuum Pressure Swing Adsorption Processes for CO_2 Capture. *Ind. Eng. Chem. Res.* **2005**, *44,* 8084.

65. Ko D.; Siriwardane R.; Biegler L. T. Optimization of a Pressure-Swing Adsorption Process Using Zeolite 13X for CO_2 Sequestration. *Ind. Eng. Chem. Res.* **2003**, *42,* 339.

66. Park J.; Beum H.; Kim J.; Cho S. Numerical Analysis on the Power Consumption of the PSA Process for Recovering CO_2 from Flue Gas. *Ind. Eng. Chem. Res.* **2002**, *41,* 4122.

67. Takamura Y.; Narita S.; Aoki J.; Hironaka S.; Uchida S. Evaluation of dual-bed Pressure Swing Adsorption for CO_2 Recovery from boiler exhaust Gas. *Sep Purif Technol*. **2001**, *24*, 519.

68. Agarwal A.; Biegler L. T.; Zitney S. E. A Superstructure-Based Optimal Synthesis of PSA Cycles for Post-Combustion CO_2 Capture. *AIChE*, **2010**, *56*, 1813.

69. Brown, P. N.; Hindmarsh A. C.; Petzold L. R. Using Krylov Methods in the Solution of Large-Scale Differential-Algebric Systems, *SIAM J. Sci. Comp.* **1994**, *15*, 1467

70. Xu, X.; Song C.; Miller, B. G.; Scaroni, A. W. Influence of Moisture on CO_2 Separation from Gas Mixture by a Nanoporous Adsorbent Based on Polyethylenimine-Modified Molecular Sieve MCM-41, *Ind. Eng. Chem. Res.* **2005**, *44*, 8113

71. Xu, X.; Song, C.; Miller, B. G.; Scaroni A. W. Adsorption Separation of Carbon Dioxide from Flue Gas of Natural Fired Boiler by a Novel Nonporous "Molecular Basket" Adsorbent. *Fuel Process. Technol.* **2005**, *86*, 1457

72. Yue, M. B.; Sun, L. B.; Cao Y.; Wang, Z. J.; Wang, Y.; Yu, Q.; Zhu, J. H. Promoting the CO_2 adsoprtion in the amine-containing SBA-15 by Hydroxyl group. *Microporous Mesoporous Mater.* **2008**, *114*, 74

73. Liu, Y.; Ye Q.; Shen, M.; Shi J.; Chen, J.; Pan, H.; Shi, Y. Carbon Dioxide Capture by Functionalized Solid Amine Sorbents with Simulated Flue Gas Conditions. *Environ. Sci. Technol*. **2011**, *45*, 5710

74. Harlick, P. J. E.; Sayari, A. Applications of Pore-Expanded Mesoporous Silica. 5. Triamine Grafted Materials with Exceptional CO_2 Dynamic and Equilibrium Adsorption Performance. *Ind. Eng. Chem. Res.* **2007**, *46*, 446

75. Langeroudi, E. G.; Kleitz, F.; Iliuta, M. C.; Larachi, F. Grafted Amine/CO_2 Interactions in (Gas-) Liquid-Solid Adsorption/Absorption Equilibria. *J. Phys. Chem. C* **2009**, *113*, 21866

76. Aziz, B.; Zhao, G.; Hedin, N. Carbon Dioxide Sorbents with Propylamine Groups – Silica Functionalized with a Fractional Factorial Design Approach., *Langmuir* **2011**, *27*, 3822

77. Knowles, G. P.; Graham, J. V.; Delaney, S. W.; Chafee, A. L. Aminopropyl-Functionalized Mesoporous Silicas as CO_2 Adsorbents., *Fuel Process. Technol.* **2005**, 1435

78. Knowles, G. P.; Delaney, S. W.; Chaffee, A. L. Diethylenetriamine[propyl(silyl)-Functionalized (DT) Mesoporous Silicas as CO_2 Adsorbent., *Ind. Eng. Chem. Res.* **2006**, *45*, 2626

79. Hiyoshi, N.; Yogo, K.; Yashima, T. Adsorption Characteristics of Carbon Dioxide on Organically Functionalized SBA-15. *Microporous Mesoporous Mater.* **2005**, *84*, 357

80. Zheng, F.; Tran, D. N.; Busche, B. J.; Fryxell, G. E.; Addleman, R. S.; Zemanian T. S.; Aardahl C. L. Ethylenediamine-Modified SBA-15 as Regenerable CO_2 Sorbent. *Ind. Eng. Chem. Res.* **2005**, *44*, 3099

81. Leal, O.; Bolivar, C.; Ovalles, C.; Garcia, J. J.; Espidel, Y. Reversible Adsorption of Carbon Dioxide on Amine Surface-Bonded Silica Gel. *Inorg. Chim. Acta.* **1995**, *240*, 183

82. Hiyoshi N.; Yogo. K.; Yashima T. Adsorption of Carbon Dioxide on amine Modified SBA-15 in the Presence of Water Vapor., *Chem. Lett.* **2004**, 33, 510

83. Tsuda, T.; Fujiwara, T.; Taketani, Y.; Saegusa, T. Amino silica-gels acting as a carbon-dioxide absorbent. *Chem. Lett.* **1992**, *11*, 2161.

84. Harlick P. J. E.; Sayari A. Applications of Pore-Expanded Mesoporous Silicas. 3. Triamine Silane Grafting for Enhanced CO_2 Adsorption., *Ind. Eng. Chem. Res.* **2006**, *45*, 3248

85. Chang A. C. C.; Chuang S. S. C.; Gray M.; Soong Y. In-Situ Study of CO_2 Adsorption on SBA-15 Grafted with γ-(aminopropyl)triethoxysilane, *Energy Fuels* **2003**, *17*, 468

86. Reynolds, S. P.; Ebner, A. D.; Ritter J. A. New Pressure Swing Adsorption Cycles for Carbon Dioxide Sequestration**.** *Adsorption.* **2005**, *11*, 531